DIGITAL IMAGE ANALYSIS OF GRAIN SAMPLES FOR POTENTIAL USE IN GRAIN CLEANING

A Thesis

Submitted to the Faculty of Graduate Studies

The University of Manitoba

in partial fulfilment of the requirements for the degree of

Doctor of Philosophy

by

Jitendra Paliwal

Department of Bisosytems Engineering

University of Manitoba

Winnipeg, Canada

R3T 5V6

THE UNIVERSITY OF MANITOBA

FACULTY OF GRADUATE STUDIES

*****

COPYRIGHT PERMISSION PAGE

DIGITAL IMAGE ANALYSIS OF GRAIN SAMPLES FOR POTENTIAL USE IN GRAIN CLEANING

BY

JITENDRA PALIWAL

A Thesis/Practicum submitted to the Faculty of Graduate Studies of The University of Manitoba in partial fulfillment of the requirements of the degree of DOCTOR OF PHILOSOPHY

ABSTRACT

A database of high resolution digital images of individual kernels of five grain types (barley, Canada Western Amber Durum (CWAD) wheat, Canada Western Red Spring (CWRS) wheat, oats, and rye) collected from 23 growing locations across Western Canada, was formed. The constituents of dockage were also divided into five broad categories (broken wheat kernels, chaff, buckwheat, wheat-heads, and canola) and imaged. A total of 230 features (51 morphological, 123 color, and 56 textural) were extracted from these images and classification was done using a four layer back propagation network (BPN) and a statistical (non-parametric) classifier. Different feature models, namely, morphological, color, texture, and a combination of the three, were tested for their classification performances. The results of these classification processes were used to test the feasibility of a machine vision based grain cleaner.

For cereal grains, while using the BPN classifier, classification accuracies of over 98% were obtained for barley, CWRS wheat, oats, and rye. Because of its misclassification with CWRS wheat, CWAD wheat gave a lower classification accuracy of 91%. For the dockage fractions, because of the uniqueness in their size and/or color, broken wheat kernels, buckwheat, and canola could be classified with almost 100% accuracy. The classification accuracies of chaff and wheat-heads was low because they did not have well defined shapes.

Back propagation network outperformed the non-parametric classifier in almost all the instances of classification. None of the three feature sets, i.e., morphological, color, or texture, in themselves, were capable of giving high classification accuracies. Their

combination improved the classification significantly. But the use of all the features together did not give the best classification results as a lot of the features were redundant and did not contribute much towards the classification process. A feature set consisting of the top 20 morphological, color, and textural features each, gave the best results.

To quantify the amount of impurity in a grain sample, a relationship between the morphology and mass of the kernel (or dockage particle) was investigated. Area of a particle in a given image gave the best estimate of its mass. This relationship was tested and validated for quantifying the amount of impurity in a sample before and after passing it through a lab scale cleaner.

To automate the cleaner, it is desirable that the cleaner should have a decision support system to adjust its parameters (such as vibration rate, grain flow rate, etc.) by calculating the amount of impurity being removed from the sample. This was done by calculating the change in the ranges of morphological features of the particles before and after the sample was passed through the cleaner. The ranges of morphological features change significantly when a sample is passed through the cleaner, and thus can be used to provide a feedback to the system.

ACKNOWLEDGMENTS

I wish to express my gratitude towards Dr. D.S. Jayas for his guidance, encouragement, and support throughout the period of this study.

I am grateful to Dr. N.D.G. White for letting me use the facilities of his lab and providing me with the grain samples. I am also thankful to Dr. S.J. Symons for his valuable suggestions and comments. His help in acquiring the railcar samples is greatly appreciated. I wish to express my gratitude to Dr. Ed Shwedyk for serving on my advisory committee.

I thank Natural Sciences and Engineering Research Council of Canada, and University of Manitoba Graduate Fellowship for providing financial support and the Industry Services Division of the Canadian Grain Commission for their assistance in sample acquisition.

I also thank Neeraj Visen, Chitra Karunakaran, and Li Wang for their help and cooperation.

Thanks are also due to my family members, especially my wife Chitra, who provided the much needed emotional support during the tough times.

TABLE OF CONTENTS

LIST OF FIGURES

LIST OF TABLES

LIST OF ABBREVIATIONS

ANOVA	Analysis of Variance
CCD	Charge Coupled Device
CPS	Canada Prairie Spring
CWAD	Canada Western Amber Durum
CWRS	Canada Western Red Spring
FOV	Field of View
GLCM	Gray Level Co-occurrence Matrix
GLRM	Gray Level Run-length Matrix
HRS	Hard Red Spring
HRW	Hard Red Winter
HSI	Hue, Saturation, and Intensity
k-NN	*k*-Nearest Neighbor
LMS	Least Mean Square
MLNN	Multi-Layer Neural Network
MSE	Mean Square Error
MVS	Machine Vision Systems
NIR	Near Infra Red
NNC	Nearest Neighbor Classifier
NTSC	National Television System Committee
PC	Personal Computer
RGB	Red, Green, and Blue
SWS	Soft Winter Spring
SWW	Soft White Winter

1. INTRODUCTION

In the current grading system of Canada, grain is graded on the five factors established by the Canadian Grain Commission: test weight, varietal purity, soundness, vitreousness, and maximum limit of foreign material (excluding dockage). Of these, the latter four factors are determined visually by trained personnel, and thus, can be influenced by individual experience and human fatigue. At this point, it would be beneficial to differentiate between dockage and foreign material in food grains. Dockage is a material that is removed from the grain by using approved cleaning equipment so that the grain can be assigned the highest grade for which it qualifies. Whatever material alien to the particular grain type is left in the sample after the removal of dockage, is called the foreign material. The amount of dockage depends on the conditions during growth, harvest, storage, and transportation, due to contamination by weed seeds, stones, and other grain kernels. During cleaning, dockage is removed and this is significant for optimization of cleaners.

In a terminal elevator (grain handling facility), once the grain has been received, it goes through the cleaning process. Cleaning is necessary to meet the buyers' specifications. In some cases, if the grain is over cleaned, uncleaned or under-cleaned samples are blended in it. Cleaning performance is controlled by inspecting the grain before and after passing it through the cleaner or a battery of cleaners. Grain inspectors manually analyze the two samples and make a decision if the performance of the cleaner is satisfactory. This process of manually analyzing the samples is subjective and is influenced by the experience of the personnel and working conditions. With the advancement of computers and improvements in image analysis techniques, this inspection of grain samples before and after passing them

through the cleaner, can be automated. It is hypothesized that the variance in the features can be used as a measure to evaluate the cleaning process.

Machine vision systems (MVS) provide an alternative to manual inspection of grain samples for kernel characteristic properties and the amount of foreign material. Machine vision is a technology that has arisen from a union between camera and computer. A video camera acts as an eye to a machine vision system (Batchelor et al. 1985). Analog signals generated by the camera are digitized into a sequence of numbers and stored as an image in the computer. Image processing algorithms are used to extract a pattern from the image to represent an object. The pattern is classified by a classification algorithm which in turn can be used to generate a signal to activate an actuator to direct the object into a proper route.

Machine vision systems have gained tremendous attention for inspecting products in different industries and demands for their new applications are increasing. Here inspection refers to many industrial tasks including defect detection, measuring, locating, detecting orientation, grading, sorting, and counting. Machine vision offers many advantages over the conventional grading systems. It is compatible with other automated on-line processing tasks, can work round the clock, can take dimensional measurements more accurately and consistently than a human being, and can give an objective measure of variables such as color, projected area, and shape which an inspector could only assess subjectively (Batchelor et al. 1985). Since the inspection is done through a non-contacting procedure, it is hygienic and there is less damage to the fragile biological products when they are being inspected. The technology, however, is not being used by the grain industry at present, owing to the variation in shape, size, and color of these biological entities due to

differences in maturity and growing conditions.

Fast and accurate information on the contents of a grain sample can be used to increase the efficiency of most grain handling operations (such as grain unloading, cleaning, binning, and shipping) at terminal elevators (Shatadal et al. 1995). The important applications of machine vision to the grain industry include the design and development of an objective, fast, and reliable on-line monitoring system for grain in continuous flow at several points in a terminal elevator. This would lead to increased cleaning throughput and enhanced recovery of salvageable grains. If the grain is over cleaned (than what is required by the buyer), uncleaned and over cleaned grains of the same grade are blended to meet the buyer's requirements. Both at the cleaning and the shipping sections, the MVS can be installed to determine the cleaning performance of the cleaner (or a battery of cleaners) and the visual quality of the grain being exported (Majumdar et al. 1999), respectively.

The recent advances in hardware and software have enabled the machine vision and imaging systems to detect, process, analyze, and display a wide range of finer details of objects from their digital images in real-time situations. Thus, grain grading and identification systems based on machine vision techniques are not a distant reality. Such an MVS should be capable of identifying and grading the grain on the basis of morphology, color, and texture. Determining the potential of morphological features to classify different grain species, classes, varieties, damaged grains, and impurities using statistical pattern recognition technique has been the main focus of the published research (e.g., Segerlind and Weinberg 1972; Neuman et al. 1987; Keefe 1992; Barker et al. 1992a, 1992b, 1992c,1992d; Sapirstein and Kohler 1995; Majumdar and Jayas 2000a, 2000b, 2000c, 2000d). Some

researchers (Neuman et al. 1989a, 1989b; Luo et al. 1999a; Majumdar and Jayas 2000b) have tried to use color features for grain identification but variability in the illumination of common light sources poses a practical problem in such cases. Very little work has been done to incorporate textural features (Al-Janobi and Kranzler 1994; Majumdar et al. 1999, Majumdar and Jayas 2000c) for classification purposes. Efforts have also been made to integrate all these features in terms of a single classification vector (Paliwal et al. 1999) for grain kernel identification.

The idea of a grain monitoring system based on machine vision can be extended to design a cleaning system. The system will use an MVS to identify the amount of dockage present in a given grain sample. Over the past few years a lot of machine vision algorithms have been developed for grain identification (e.g., Neuman et al. 1987; Keefe 1992; Sapirstein and Kohler 1995; Majumdar et al. 1996; Luo et al. 1999a; Paliwal et al. 1999). As most of these algorithms extract a large number of features for classification, an optimum set of those features need to be selected to reduce computation time. This optimum feature set can be used to train an artificial neural network which would then be used as a classifier. To monitor the cleaning performance, the MVS has to analyze two samples: one before the grain goes into the cleaner and the other after the grain comes out of the cleaner. Grain samples taken before and after passing through the cleaner are presented to a camera and imaged. It is hypothesized that the differences in the ranges of the morphological features of the before and after samples, can be used for adjusting the grain flow rate or speed of the cleaner or both.

Artificial neural networks, resembling the biological nervous system, have proven

to be robust in dealing with the ambiguous data and the kind of problems that require the interpretation of large amounts of data. Neural networks, instead of sequentially performing a program of instructions, explore many competing hypotheses simultaneously using massive parallelism (Lippmann 1987). In addition, neural networks have the potential to solve problems in which some inputs and corresponding output values are known, but the relationship between the inputs and outputs is not well understood. These conditions are commonly found in agri-food industry inspection problems.

Pattern recognition has emerged as an important application of artificial neural networks. One of the most important attributes of neural network classifiers is their capability to approximate the *a posteriori* distribution of their training samples through learning and adaptation. This ability makes them unique among pattern classifiers. The application of machine vision, coupled with neural networks, seems to offer promise for inspecting agricultural products.

Grain identification using machine vision in conjunction with pattern recognition techniques, including neural networks, offers many advantages over the conventional optical or mechanical sorting devices. A digital camera can be used to gather the necessary information from the grain and send digitized images to a computer where they can be analyzed for multi-category classification. Image processing algorithms can be used to extract higher-level information from the input signals for improved classification performance. The classification parameters can be easily modified to take into account annual variations in the product. When neural networks are used as pattern classifiers, the sorting device can be equipped with a training option through which the machine can be

trained for recognizing new products.

An extensive literature search and communication with industrial sources have indicated that no pattern recognition machine or neural network based system has been used for grain cleaning. Nevertheless, enough grain classification and identification algorithms are available which can be integrated together to be used in such a system. The main objectives of this thesis were to:

1. identify an optimized set of morphological features that can be used for rapid identification of different cereal grains, e.g., Canada Western Red Spring (CWRS) wheat, Canada Western Amber Durum (CWAD) wheat, barley, oats, and rye;
2. identify an optimized set of color features that can be used for rapid identification of different cereal grains, e.g., CWRS wheat, CWAD wheat, barley, oats, and rye;
3. identify an optimized set of textural features that can be used for rapid identification of different cereal grains, e.g., CWRS wheat, CWAD wheat, barley, oats, and rye;
4. determine which combination of morphological, color, and textural features gives the best classification accuracy so that it could be used for real-time on-line cereal grain identification;
5. identify an optimized set of morphological, color, and textural features, and their combination that can be used for rapid identification of the various dockage fractions, e.g., broken wheat kernels, chaff, wild buckwheat, wheat-heads, and canola;
6. design and evaluate a machine vision based grain cleaning system which would use morphological, color, and textural features of cereal grains for optimized performance; and

7. investigate the performance of the grain cleaner when different neural network and statistical classifiers are used for classification purposes.

The material presented in this thesis is organized into six chapters. The first chapter addresses the justification, importance, and objectives of the research. Chapter II begins with the literature review of the research that has been conducted in the field of image analysis of agricultural products for their quality determination using morphological, color, and textural features. Various statistical and neural network classifiers are also discussed in detail. Chapter III discusses the materials and methods that were used in this thesis. A detailed account of the feature extraction algorithm is given in chapter IV. Results are presented in chapter V with discussions. The presentation of results follow the flow of experiments starting with classification of cereal grains using morphological, color, and textural features. Results are given for different types of features and their combinations using back propagation neural networks and a non-parametric statistical classifier. Classification results for dockage classification are also reported. Chapter V concludes with the selection of the model that can give the highest classification accuracies in quantifying the amount of dockage in the grain. Chapter VI includes the conclusions and some recommendations made for future research.

2. REVIEW OF LITERATURE

2.1 Background

There has been extensive research to apply the principle of machine vision and pattern recognition for classification of agricultural products (e.g., Al-Janobi and Kranzler 1994; Ghazanfari et al. 1997; Ng et al. 1998; Majumdar and Jayas 2000a, 2000b, 2000c, 2000d; Lu et al. 2000). The main obstacle in developing machine vision based systems for applications in the agri-food industry is the variation in size, shape, color, and texture of these biological entities (Kranzler 1985; Sarkar 1986; Tillet 1990). So far, the main focus of the research in this area has been the development of pattern recognition algorithms for classification of these objects. Most of the researchers conducted their studies using morphological and color features for classification purposes. This chapter reviews the results of the previous work in applying these classification techniques to the agri-food industry. A brief introduction to the fundamentals of artificial neural networks is also included.

2.2 Classification Features

Any image in its digital form is stored in the memory of the computer as an array of numbers that may contain over 300 000 elements depending on the size, spatial resolution, and color information of the image. Sequential processing of this information is time consuming and is not feasible for high speed on-line inspections. Therefore, image processing and analysis algorithms are applied to the images to extract some quantitative information known as *features*. These features are then used as inputs to a classification algorithm to categorize the objects in the image. A vector of such features is called a *pattern*. Pattern recognition can be done by using the morphological (defining shape and

size), color, textural (spatial distribution of color), or a combination of these features of the images.

2.2.1 Morphological features Segerlind and Weinberg (1972) first estimated grain shape by a Fourier series expansion of the radial distance from the center of gravity to the periphery of kernels. A kernel profile was traced on a grid paper to get the image. There was 1% error in separation of oats and barley versus wheat and rye based on extracted shape features. The class [e.g., hard red spring (HRS), hard red winter (HRW), amber durum, soft white spring (SWS), soft white winter (SWW), Canada prairie spring (CPS), and utility wheat are different classes of Canadian wheat] discrimination for wheat was partially successful with 11-25% error. This study is considered as one of the first attempts to classify cereal grain kernels by describing their shape using a mathematical expansion series.

A significant number of studies have been conducted since Segerlind and Weinberg (1972) to define the shape and size of different types of grain kernels (e.g., Keefe and Draper 1986, 1988; Zayas et al. 1986, 1989; ; Symons and Fulcher 1988a, 1988b; Chen et al. 1989; Keefe 1992). Most of the recent studies have focused on extraction of features from digital images of grain kernels, instead of drawing their profiles on grid papers. Because the number of such studies is very large, only a small number of related studies are briefly discussed in this section.

Neuman et al. (1987) studied the objective classification of Canadian wheat cultivars based on kernel morphology. They used 576 kernels (sound and uniform) of pedigreed seed of 14 wheat cultivars for analysis. Using transmitted light they captured silhouette images of whole wheat kernels in 'plan' (top) view and determined spatial size and shape parameters

and Fourier descriptors of kernels. Hard red spring and CWAD wheat kernels were the most easily differentiated groups while there was considerable overlap between HRW and SWS wheat classes. Discriminating varieties within classes gave inconclusive results with correct classifications ranging from 15 to 96%. Unlike earlier works, random orientation of kernels was not a problem in this case.

Keefe (1992) constructed a semi-automatic image analyzer for classification of wheat grains. His algorithm took 33 measurements and derived 36 more features from them. Because it was proprietary information, the details of the derived features were not provided. The instrument was evaluated using 20 varieties of United Kingdom wheat. The two major shortcomings of the algorithm were that it could analyze only one kernel per image and each kernel had to placed manually in a fixed orientation for imaging. Owing to the slow speed of processors of personal computers at that time, a sample of 50 kernels took about 5 min for feature extraction. The overall identification error was 32.9-65.8%.

Barker et al. (1992a, 1992b, 1992c, 1992d) used different sets of features for characterizing and discriminating among kernels of eight Australian wheat cultivars. The features were ray (i.e., radial distance from the centroid) parameters, slice and aspect ratio parameters, Fourier descriptors, and the Chebychev coefficient. The overall classification error ranged from 35 to 48%. Because of the complexity in feature extraction and low classification accuracies, the algorithm was not very useful.

Sapirstein and Kohler (1995) suggested an interesting alternative approach to objective wheat grading by proposing a completely new set of grading factors based on variability of size, shape, and reflectance features of kernels in a sample, which can be easily

administered by machine vision based grading. Cargo (grain being shipped out of terminal elevators) samples of CWRS grades 1, 2, and 3 were successfully classified using the mean and variance of the features as quantitative classification variables. On carlot (grain received at terminal elevator) samples, however, only grades 1 and 3 could be successfully discriminated from each other.

Ying et al. (1996) developed computer vision algorithms for automated channel catfish (*Ictalurus punctatus*) processing to detect the orientation of a catfish and to identify its head, tail, pectoral, ventral, and dorsal fins. The algorithms were invariant to translation, rotation, and scaling. Canny edge detection and a labeling and tracking algorithm were applied to locate the boundary of a catfish and a 2-stage, model-based, catfish segmentation algorithm was proposed to locate each part. A dominant point detection scheme was proposed and applied to find the points that connect each part of a catfish. Then morphological knowledge of the catfish was used to locate the feature points of each part of the catfish and to determine the cutting lines. The angle of the major axis and center of mass were used to represent the orientation of a catfish. They also claimed that with slight modifications the same algorithms can be used for other different objects. But no citation pertaining to the use of these algorithms to identify other objects has been found in the literature.

Ghazanfari et al. (1997) used digitally acquired images of individual pistachio nuts and graded them into four sets using Fourier descriptors (shape recognition features). The feature selection procedure applied to the first 15 Fourier descriptors indicated that 7 harmonics were sufficient to separate split nuts from unsplit nuts. Of the 7 selected Fourier

descriptors, 5 were from the higher order harmonics containing microscopic information more suitable for separating unsplit from split nuts. An average classification accuracy of 87.1% was obtained for the 4 grades when using a decision-tree classifier. Multilayer neural network analysis was able to successfully classify 94.8% based on the same input parameters, indicating the superiority of the technique.

Majumdar and Jayas (2000a) developed an algorithm based on morphological features to classify individual kernels of CWRS wheat, CWAD wheat, barley, oats, and rye. The algorithm extracted 23 morphological features for the discriminant analysis. The classification accuracies of individual kernels using the 10 most significant features in the morphology model were 98.9, 93.7, 96.8, 99.9, and 81.6%, respectively for CWRS wheat, CWAD wheat, barley, oats, and rye when tested on an independent data set. When the model was tested on the training data set the classification accuracies of CWRS wheat, CWAD wheat, barley, oats, and rye were 98.9, 91.6, 97.9, 100.0, and 91.6%, respectively. The problem in this case was due to the limitation of the image acquisition hardware. The images were captured in the form of rectangular pixels which were then converted to square pixels. This may have resulted in slight distortion of the originally captured optical information. The code was written using the KHOROS (Khoral Research, Inc., New Mexico) programming environment which was not platform independent.

2.2.2 Color features Color provides very important information for grain grading and inspection. Different grain types and their degrading factors can be easily identified using the color attribute. Initial research in the field of grain identification mainly emphasized the use of morphological features using monochrome images. This was mainly due to three

reasons. Firstly, the hardware for color image acquisition was expensive. Secondly, the color image files consisted of a large amount of data which required larger storage space. Storage of large image files and analysis of such huge data sets was not easy using personal computers at that time. And lastly, color information extracted from images can vary with the illumination variations that exist in common light sources. So far very limited work has been done on designing and calibrating illumination systems for color grain image analysis (Luo et al. 1997).

The use of color image analysis for identifying different wheat classes and varieties was reported by Neuman et al. (1989a, 1989b). Video colorimetry was used to distinguish kernel types according to wheat class and variety for six wheat classes grown in Western Canada. Discriminant analyses were performed based on mean red (R), green (G) and blue (B) reflectance (tristimulus) features. Average correct classification for the Canada Western Soft White Spring wheat, CWAD wheat, and CWRS wheat were 76, 76 and 62%, respectively. Relatively lower scores of 56 and 34% were achieved for the HRW and CPS wheat classes.

A field crop research was conducted by El-Faki et al. (1997) where they used color features to establish a simple weed detection method using a color machine vision system. Their system was based on the fact that stems of wheat and soyabean are green as compared to the stems of most of the weed species which are red in color. As compared to the methods using shape and texture features, the method based on color was less sensitive to canopy overlap, leaf orientation, camera focusing, and wind effects. The correct classification rate using the discriminant classifiers for weeds associated with soyabean and wheat were 54.9

and 62.2%, respectively.

Luo et al. (1999a, 1999b) used a set of morphological and color features for classification of cereal grains and obtained average classification accuracies of 98.2, 96.9, 99.0, 98.2, and 99.0% for CWRS wheat, CWAD wheat, barley, rye, and oats, respectively. They also concluded that combining morphological and color features improves the classification accuracies over using morphological or color features alone.

Ng et al. (1998) developed machine vision algorithms for measuring maize kernel mechanical damage and mold damage. Mechanical damage was determined using both single-kernel and batch analyses by extracting from kernel images the damaged area stained by green dye and by calculating the percentage of total projected kernel surface area that was stained green. Mold damage was determined using single-kernel analysis by isolating the moldy area on kernel images and by calculating the percentage of total projected kernel surface area covered by mold. Their vision system demonstrated high accuracy and consistency for both mechanical and mold damage measurements.

Other applications of color image analysis in the agri-food industry have been in detection and classification of fungal damaged soybeans (Wigger et al. 1988, Casady et al. 1992), inspection and grading of fresh market peaches (Miller and Delwiche 1989), and inspection of apples, mushrooms, and potatoes (Morrow et al. 1990).

2.2.3 Textural features Texture is a property of surfaces associated with the tactile quality they represent. In machine vision, texture refers to a closely related concept, that of a spatially repeating pattern on a surface that can be sensed visually. Texture represents the local statistics of correlated intensity variations. Texture is an important characteristic for

the analysis of many types of images. Visual texture is difficult to define, but it is commonly attributed to images containing repetitive patterns in which *elements* or *tonal primitives* are arranged according to certain *placement rules*. It has two basic dimensions - the first is for describing the tonal primitives out of which the image texture is composed, and the second dimension is for describing the spatial dependance or interaction between the primitives of an image texture. Tonal primitives are regions with tonal properties. The tonal primitives can be described in terms such as the average tone, or maximum and minimum tone of its region. The region is the maximally connected set of pixels having a given tonal property. The tonal region can be evaluated in terms of its area and shape. The tonal primitive includes both its gray tone and tonal regional properties. Image texture can be qualitatively evaluated as having one or more of the properties of fineness, coarseness, smoothness, granulation, randomness, or irregular. Each of these adjectives translates into some property of the tonal primitives and the spatial interaction between the tonal primitives (Majumdar et al. 1999).

Hayes and Han (1993) evaluated two image processing methods, linear discrimination and textural difference, using slides taken of 23 soils and 5 soil-surface cover treatments. Percent cover results from each image processing method were compared with those measured manually. Tests were purposely aimed at conditions that tend to be difficult to evaluate with machine vision because of limited visible contrast. These two image processing methods were found to provide reasonable cover estimates under conditions having bright green cover. Linear discrimination produced better estimates than did textural difference in situations with obvious color difference. Textural difference performed better

when color difference was not apparent such as brown residue with a brown soil background.

Zayas (1993) used a digital imaging technique to evaluate bread crumb grain, and the potential of image texture analysis for crumb grain assessment. Eighteen image texture features were extracted from slices of two commercially available brands (BRRA and BRDI). One hundred percent of BRRA and 97.5% of BRDI sub-images (128 x 128) from the middle area of a slice were correctly recognized. Technological factors and location of sub-images on a slice affected the value of image texture features such as crumb grain vow across a slice. Variations in the crumb grain within a slice were studied, and a ranking scale was developed for evaluating the degree of coarseness of crumb grain in boundaries of 64 x 64 pixels.

Al-Janobi and Kranzler (1994) used color and textural analysis for grading of date fruits into different classes. They compared their results with manually classified dates according to the USDA grading standards. A total of 39 features and eight models were used by applying a non-parametric discriminant analysis to each model and by incorporating subsets of the features. The classification errors for all models ranged between 0.8 and 26.4%.

Sapirstein et al. (1989) developed a system for quantitative assessment of bread crumb grain. Grain crumb features like cell area, cell density, cell wall thickness, cell total area ratio, crumb brightness, and uniformity of cell size were extracted from their digital images. Bread crumb containing oxidants was 6% brighter and had 21% more cells/cm^2, 17% smaller cell cross-sectional area, 13% thinner cell walls, and 16% more uniform grains. Time to compute the cell structure for a single bread slice (approximate size 100 mm x 100

mm) was about 10 s.

Majumdar and Jayas (2000c) used the textural features of individual kernels of CWRS wheat, CWAD wheat, barley, oats, and rye to develop algorithms for grain classification. For bulk samples, the textural features extracted from the red color band, with 256 gray levels from acquired image grouped into 32 gray levels, gave the highest classification accuracies of 92.0 % using non-parametric estimation. For individual kernels, the textural features extracted from the green color band, when 256 gray levels were grouped into 8 gray levels, gave the highest classification accuracies of 92.9% using non-parametric estimation. The classification accuracies improved significantly (as high as 100%) when textural features were combined with morphological and color features (Majumdar and Jayas 2000d). Although it was not mentioned by the authors, it is speculated that the computational time would significantly increase in the latter case.

2.2.4 Limitations of available algorithms Most of the available algorithms use the kernel size for classification purposes. Use of size can result in significant mis-classifications because the variations in kernel size depend on maturity and growing conditions. Kernel sizes are also dependent on the growing region of the crop. Because the grain at a grain handling facility is a mixture of grain coming from different farm locations, size variability can give erroneous results.

Secondly, most of the available algorithms extract a large number of features and use them for classification. Extraction and comparison of a large number of parameters increases the computation time. For any system, to be used on an industrial scale, operational speed is a constraining factor.

Paliwal et al. (1999) showed that cereal grains can be rapidly identified using a feature vector consisting of just three attributes viz. length, shape function (Fourier descriptor in polar coordinates), and color. They obtained classification accuracies of 100, 94, 93, 99, and 95% for CWRS wheat, CWAD wheat, barley, oats, and rye, respectively. A broadening of the training set to include a large number of growing regions, classification of damaged kernels, other foreign material like chaff, stone pieces, broken kernels, and other types of grains (e.g., oilseeds and speciality crops) would be required to incorporate such an algorithm in a grain classification system.

2.3 Classifiers used for pattern recognition

Classification analysis uses a decision rule, called a *classification criterion*, to classify objects into two or more known groups, called *classes*, on the basis of the quantitative features extracted from the objects. A set of features extracted from an object is called an *observation* of the object. The classification criterion is usually derived from the observations of the known classes, called the *training set*. The derived classification criterion can then be applied to classify new observations, called the *test set*.

A classification criterion partitions an observation or feature hyper-space Ω into hyper-regions Ω_i, $i = 1, 2, ..., N$, where N is the number of classes. An object is classified as coming from class ω_i if its corresponding feature vector or observation m, a point in the hyper-space Ω, belongs to the region Ω_i. Many different types of classifiers are explained in various pattern recognition books and research papers (Hand 1981; Devijver and Kittler 1982; Fukunaga 1990; Zurada 1992). To determine which classifier works best for a particular application usually involves some degree of experimentation. Although, for a

given problem most of the classifiers give comparable results, the difference might lie in their time complexity, storage requirements, and precise degree of accuracy (Hush and Horne 1993). Different classification methods and their applications are reviewed in the following section.

2.3.1 Statistical methods The statistical methods are based on the Bayes minimum error rule (Duda and Hart 1973):

$$m \in \Omega_k \text{ if } P(w_k \mid m) > P(w_j \mid m) \qquad \forall j \neq k \tag{2.1}$$

where $P(w_i \mid m)$ is the posterior probability, by which an object with a feature vector m belongs to class w_i. The rule states that to minimize the average probability of error, an object should be classified as belonging to a class w_i that maximizes the posterior probability $P(w_i \mid m)$.

By applying the Bayes' theorem:

$$P(w_i \mid m) = P(w_i)\, p(m \mid w_i)/p(m) \tag{2.2}$$

a more practical formulation of the rule can be obtained as

$$m \in \Omega_k \text{ if } P(w_k)\, p(m \mid w_k) > P(w_j)\, p(m \mid w_j) \qquad \forall j \neq k \tag{2.3}$$

where: $P(w_i)$ is the prior probability by which an object comes from class w_i; $p(m)$ is the probability density function for m; and $p(m \mid w_i)$ is the class-conditional probability density function for m.

In most of the practical applications, the posterior probabilities or the class-conditional probability density functions are unknown, and thus, need to be estimated. There are two ways of doing this.

2.3.1.1 Parametric approach The parametric approach is based on the assumption that the class-conditional probability density function for m, $p(m \mid w_i)$, has a form of multivariate normal distribution:

$$p(m \mid w_i) = (2\pi)^{-d/2} |\Sigma_i|^{-1/2} \exp[-0.5\ (m-\mu_i)`\ \Sigma_i^{-1}\ (m-\mu_i)] \qquad (2.4)$$

where: d is the dimension of the feature vector; μ_i is the d-dimensional vector containing feature means in a class w_i, Σ_i is the covariance matrix, and ` means transpose.

So to estimate the probability density, one needs to estimate the parameters μ_i and Σ_i. The parameters, μ_i and Σ_i, can be estimated from the training data set using different parameter estimation methods (Hand 1981). The prior probability $P(w_i)$ can also be estimated from the training data set. Then the classification criterion, Eq. 2.2 or 2.3, can be determined in an analytical form.

2.3.1.2 Non-parametric approach The non-parametric approach calculates the posterior probability $P(w_i \mid m)$ directly from the training data set without any assumption of the underlying probability density. There are several different methods of estimating $P(w_i \mid m)$ such as the histogram, the kernel method, the nearest neighbour method, and the series method (Hand 1981). The most popular of them is the nearest neighbour method which is described briefly in the following section.

Nearest neighbor classifiers The nearest neighbour classifier (NNC) makes use of the correspondence between similarity and distance, i.e., the smaller the Euclidian distance between classes the more similar they are. The nearest neighbour decision rule assigns an unknown U to the class of its nearest neighbour X:

$$U \in class(i) \text{ if } d(U,X_i) = \min d(U,X_j), \text{ for } k \neq j;\ k, j = 1,2,.....C \qquad (2.5)$$

where $d(U,X)$ is a distance measure between U and X and C is the number of classes.

The underlying idea behind the nearest neighbor rule is that samples which fall close together in feature space are likely to belong to the same class. The NNC stores a number of patterns for each class. Then the unknown is compared to all of the stored patterns and assigned to the class of the patterns which is most similar with the unknown. The decision surface created by NNC is piecewise linear.

The k-nearest neighbour classifier (k-NN) is an extension of NNC. The k-NN rule classifies X by assigning it the class most frequently represented among the k nearest samples. In other words, a decision is made by examining the labels on the k nearest neighbours and taking a vote.

2.3.1.3 Parametric versus non-parametric methods The parametric approach has the advantage that the derived classification criterion is of an analytical form which can be easily transferred into a computer classification program. The assumption of the multivariate normal distribution, however, made for the class-conditional probability density function in deriving the classification criterion, could be incorrect or insufficient in many applications and may lead to significant classification error. The k-NN approach avoids the subjective assumption by directly estimating the posterior probability $P(w_i \mid m)$ from the training data set. A disadvantage of this approach is that the derived classification criterion cannot be expressed analytically. All of the training data must be retained - the distance from a new observation to each of the training set points must be determined to choose the k nearest points. This means a large amount of computer memory and a slow classification process. In addition, the estimation of the posterior probability is biased (Rosenblatt 1958) towards

larger values.

2.3.2 Neural network classifiers Artificial neural networks are synthetic networks inspired by the biological system found in living organisms. Due to the limited knowledge available about the human nervous system, the correspondence between this system and artificial neural networks is still rather weak. Based on our present understanding of the neuron function, different models have been developed to simulate functioning of the nervous system. A typical mathematical model of a neuron is presented in Fig. 2.1. The model consists of a processing element with a number of input connections (x_1, x_2, ..., x_n) and a single output. The flow and the process of input signals are considered to be unidirectional as indicated by the arrows.

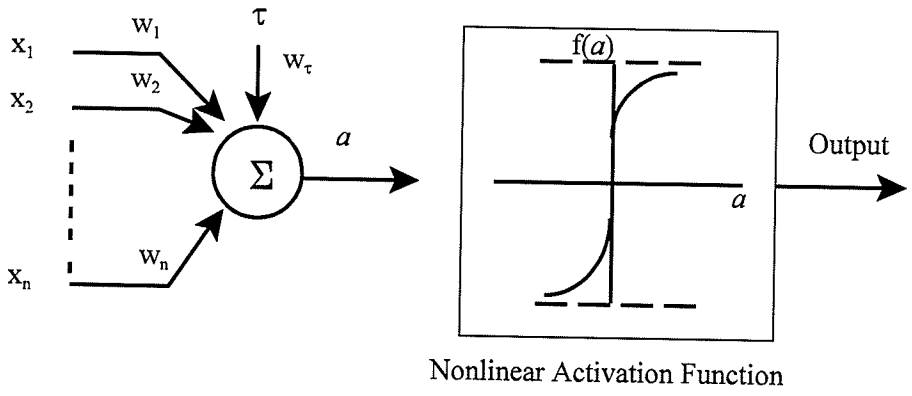

Fig. 2.1 A mathematical model of a neuron

The neuron receives a weighted sum of the inputs. Then a threshold, τ, is added to the weighted sum which results in the activation value a for the neuron. The threshold usually has a constant value equal to -1 (Zurada 1992). The activation value of the neuron

is computed using:

$$a = \sum_{i=1}^{n} (w_i x_i + \tau w_\tau) \tag{2.6}$$

where n is the number of inputs, and w_i the weight of the connection i of the neuron. The activation value of the neuron is passed through a non-linear activation function (sigmoid) which generates the output of the neuron. Typical neuron activation functions are:

$$f(a) = \frac{2}{1 + \exp(-\lambda a)} - 1 \tag{2.7}$$

and

$$f(a) = \begin{cases} +1, a > 0 \\ -1, a < 0 \end{cases} \tag{2.8}$$

Equation 2.7 is a bipolar sigmoid function (Fig. 2.2a) which provides a neuron with a continuous value between -1.0 and +1.0. In this equation λ is a positive constant proportional to the neuron gain. Equation 2.8 is a bipolar binary function (Fig. 2.2b) which provides a neuron with binary outputs of -1.0 and +1.0. The original neuron model used the binary function, sometimes called hard-limiting, as its activation function (Zurada 1992). Later, because of their differentiability, different forms of continuous functions became the dominant neuron activation functions (Zurada 1992; Jou et al. 1994; Mehrotra et al. 1996).

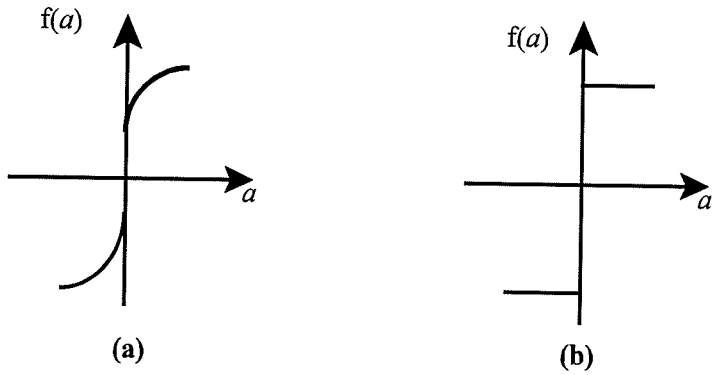

Fig. 2.2 Typical activation functions for neurons: a) sigmoid and b) hard-limiting

In a neural network system, a number of neurons are interconnected such that each neuron output is an input to some or all other neurons and possibly to itself. Lag-free neurons accomplish their tasks in parallel, thus providing a high speed information processing tool. Parallel processing of information through many processing elements with primarily local connections provides a great degree of robustness or fault tolerance. Depending on the application, these networks may have different connection types such as forward or backward with time delay, thus providing potential for application in many different areas.

Neural networks learn to perform a specific task. Learning in a neural network is accomplished by a systematic procedure for altering the connection weights to reduce the network errors. Learning is performed in either supervised or unsupervised mode. In supervised learning the desired response for an input is provided to the *teacher*. The teacher implements a reward-and-punishment scheme to adapt the network weights. In unsupervised learning, the desired response is not known and the network must discover any possible

existing patterns, regularities, and separating properties among its inputs.

Different neural network classifiers have been applied to different classification problems. In supervised mode, Hopfield net and Hamming net are normally used with binary inputs while the single layer perceptron and multi-layer neural network use continuous-valued inputs (Zurada 1992; Mehrotra et al. 1996). Because of the use of continuous-valued inputs, only single-layer and multi-layer neural networks (Villiers and Barnard 1992) are discussed in this thesis. For further information on other networks the interested reader is referred to Mehrotra et al. (1996).

2.3.2.1 Single layer perceptrons One of the original models of a neuron was proposed by Rosenblatt (1958). The model is referred to as the *perceptron* and it is presented in Fig. 2.3. The perceptron forms a weighted sum of the n-dimensional input vectors (Eq. 2.6) and adds a bias value to it. The result is passed through a hard-limiting activation function, i.e., Eq. 2.8. Due to its binary output, the perceptron can be considered as a dichotomizer which divides its input patterns into two classes separated by a decision boundary in the form of a hyperplane.

To achieve the correct classification result, the connection weight and the threshold in a perceptron can be adapted using a number of different learning rules. The perceptron learning rule (Rosenblatt 1958) was originally developed for training a perceptron. In this rule, the weight adjustment, ΔW, is proportional to the product of input vector X and the difference between the neuron's actual output o and the desired output d:

$$\Delta W = c\,(d-o)X \tag{2.9}$$

where c is a learning step. In the perceptron learning rule, if the classes are not separable or

overlap exists between them, the decision boundary between the two classes may oscillate contiguously (Lippmann 1987).

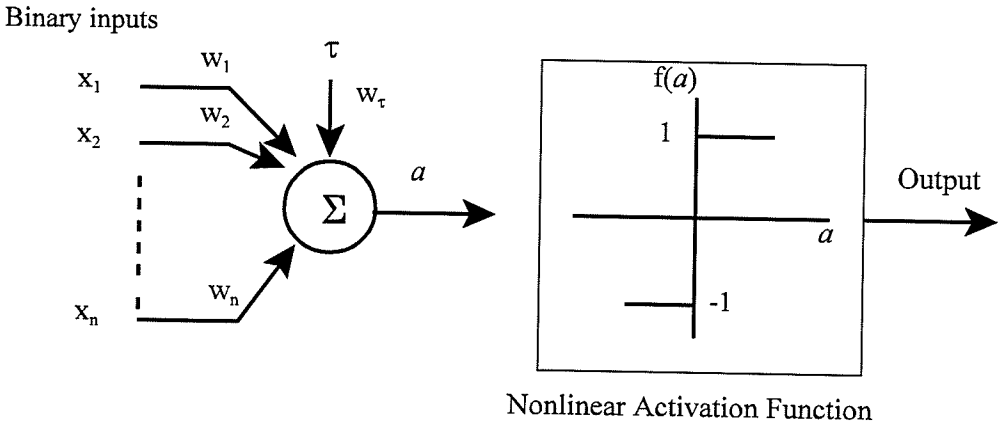

Fig. 2.3 A mathematical model of a perceptron

Least mean square (LMS) (Widrow and Hoff 1960) is another widely used algorithm for training perceptrons. This algorithm minimizes the squared error between the desired output and the activation value of the neuron. The weight increment is therefore proportional to the product of this squared error and the input vector:

$$\Delta W = c\,(d - W^t X)^2 X \tag{2.10}$$

The weight adaptation through LMS algorithm is independent of the activation function used by the neurons.

Perceptrons can be arranged in a layer to accomplish multi-category classification when the classes are linearly pairwise separable (Zurada 1992). A multi-category classifier using discrete perceptrons is shown in Fig. 2.4. In this classifier, there is one perceptron for each class. Each perceptron is trained to have an output, O, of +1 for one class and -1 for other classes.

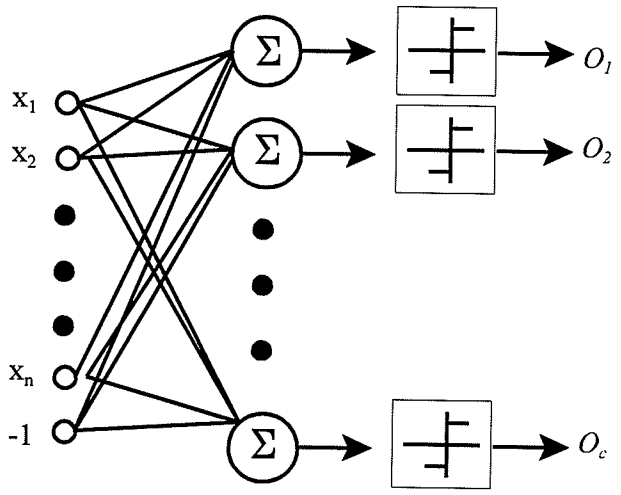

Fig. 2.4 A multi-category classifier using *c* discrete perceptrons

2.3.2.2 Multi-layer neural networks The perceptron was criticized for its inability to implement the exclusive-or (XOR) function (Minsky and Papert 1969). Furthermore, the decision regions formed by perceptrons are hyperplanes similar to those formed by maximum likelihood Gaussian classifiers (Lippmann 1987). There are many problems, however, that require nonlinear decision boundaries. Some deficiencies of perceptrons are overcome by implementation of multi-layer neural networks (MLNN).

Multi-layer neural networks are created by cascading neurons in layers. Continuous activation functions such as sigmoids are used in the neurons. The advantages of using a sigmoid function include its differentiability and its continuous-valued outputs. Differentiability is of great interest in minimization of errors using a gradient search. Continuous-valued outputs are important, in particular, in classification problems because outputs between -1 and +1 or between 0 and +1 may be interpreted as probability estimates.

In an MLNN, the input vector feeds into each of the neurons in the second layer (first hidden layer). The outputs of the second layer feed the third layer neurons and so on. Often the neurons are fully interconnected between the layers and flow of information is from the inputs toward the outputs. The MLNN with this type of unidirectional information flow are called feedforward networks.

A typical four-layer feedforward neural network is shown in Fig. 2.5. The illustrated network has a three dimensional input vector. The most common terminology used for referring to the layers of a feedforward network is as follows. *Input layer:* The layer to which the input patterns are fed and the outputs are passed on to the subsequent hidden layer. *Hidden layer*: The layer whose outputs are fed to its following layer. *Output layer*: The last layer of neurons whose inputs are the output of the last hidden layer and its outputs are the output of the network. Therefore, Fig. 2.5 represents a four-layer network consisting of two hidden layers and one output layer. It has been demonstrated that three-layer feedforward networks are capable of forming a close approximation to any nonlinear decision boundary (Makhoul et al. 1989). Many problems, however, are solved more efficiently using four-layer networks (Chester 1990, Mehrotra et al. 1996).

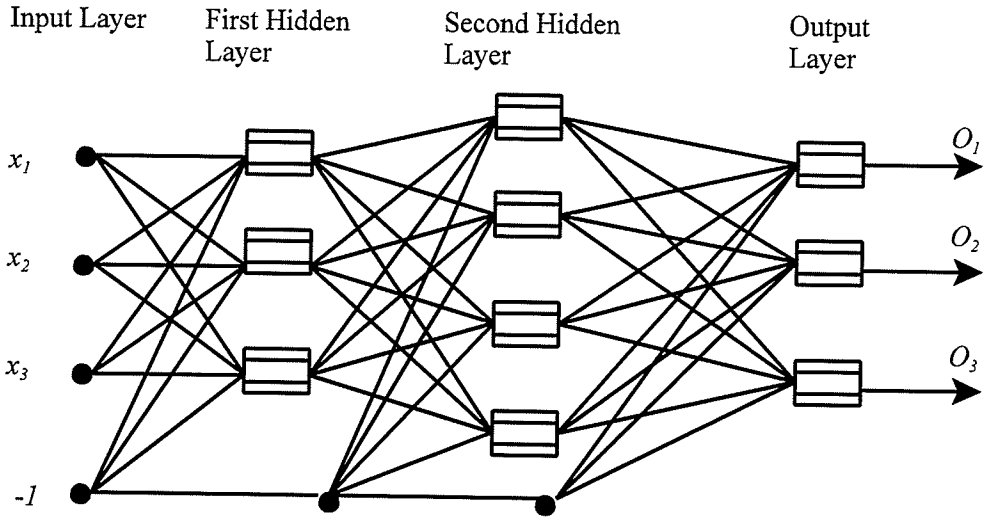

Fig. 2.5 A typical four-layer neural network

2.4 Issues on multi-layer neural networks

Multi-layer neural networks have been established as robust and extremely powerful pattern classifiers. These classifiers are used in recognition and classification problems and usually have multiple inputs corresponding to the number of features used for object representation and multiple outputs corresponding to the number of classes. These networks are trained to give a desired output vector for a particular input pattern within a predetermined error. Typically, because feedforward networks do not take advantage of predefined relationships between the input and output, they require a large number of training passes. Even after extensive training with a large training set, they usually result in only 80-90% recognition accuracy (Spirkovska and Reid 1993).

Choosing a proper size of network for a particular application is an unsolved issue in neural network studies. A small network may never converge, while a large network converges fast but lacks the generalization power (Hush and Horne 1993). Besides a suitable network size, there are many other questions that need to be answered to use a network for a particular problem. Learning step, proper training procedure, number of layers, network initialization, value of gain, and the number of neurons in each layer are some of the MLNN issues which have been investigated by different researchers, reviewed in the following sections.

2.4.1 Number of layers Makhoul et al. (1989) have shown that MLNN with one hidden layer can form arbitrarily close approximation to any nonlinear decision boundary. This does not necessarily imply that there is no benefit of using more than one hidden layer. Chester (1990) demonstrated that a small three-layer network was more capable than a large two-layer network. Lippmann (1987) stated that for any classification problem, no more than two hidden layers (i.e., a four-layer network) would be needed. Villiers and Barnard (1992) compared the performance of three-hidden layer networks with two-hidden layer networks. They indicated that three-hidden layer networks were more prone to fall into local minima, but they performed similarly in all other aspects.

The above work indicates that even though MLNN with one-hidden layer can perform most of the classification tasks, it is better to use a two-hidden layer network. More than two-hidden layers may also be used, but it does not increase the efficiency. On the other hand, using more than two-hidden layers may result in a lower accuracy because these networks are more prone to fall into a local minimum.

2.4.2 Number of neurons in each layer Determining the optimum number of neurons in the hidden layers is still an unsolved issue. In general, the number of neurons that should be used for a given problem is not known. Most researchers have selected the number of neurons in the first hidden layer to be equal to the number of elements in the input patterns (Emmerson and Damper 1993, Jou et al. 1994). The number of neurons in the output layer is usually taken to be equal to the number of classes (Mehrotra et al. 1996).

While there are some guidelines for selecting the number of neurons in the output and the first hidden layer, there is no clear method for selecting the number of neurons for the second or subsequent hidden layers. Most researchers use a trial-and-error method to find a suitable number. Emmerson and Damper (1993) randomly chose the number of neurons in the second hidden layer. Gupta and Upadhye (1991) empirically determined the number of neurons for the second hidden layer. Jou et al. (1994) started with a large number of neurons and used a pruning algorithm to decrease it to a suitable size.

2.4.3 Neuron gain and learning rate The neuron gain, λ in Eq. 2.7, determines the steepness of the sigmoid function in the transition region. Although any value can be used for λ, most often it is taken to be 1.0 (Zurada 1992, Hush and Horne 1993). This gain provides a moderate steepness for the sigmoid function. The learning rate (η) determines the size of the step for weight adjustment. The effectiveness and convergence of a network during training depends significantly on this parameter. Like most of the other factors, the value of η depends on the problem being solved. Larger values of η will result in more rapid convergence, but if it is too large, the result is instability in network learning. A small value of η should be chosen to avoid overshooting and to have a smooth convergence. A value of

η that might be suitable during the initial phase of training might not be suitable during the final stages. Values between 0.001 to 10 have been reported in different technical publications (Chester 1990, Villiers and Barnard 1992, Jou et al. 1994). So the value of η for any particular application must be determined empirically.

2.4.4 Momentum in learning The back propagation of error based on the gradient descent method is generally a slow learning process. A momentum term is sometimes added to the weight adjustment to accelerate the convergence of the networks. In this method a fraction of the previous weight change is added to the current weight adjustment in the following form:

$$\Delta W(t) = - \eta \nabla E(t) + a \ \Delta W(t\text{-}1) \qquad (2.11)$$

where the arguments t and t-1 are used to indicate the current and the most recent weight adjustments. The user defined parameter a is a positive constant with a recommended value between 0.1 and 0.9 (Zurada 1992). In Eq. 2.11, the second term on the right hand side is called the *momentum term*. The momentum term typically helps to speed up the convergence process and it is recommended for problems with convergence that occur too slowly or for the cases where learning is difficult to achieve.

Silva and Almedia (1990) showed that training a network using regular back propagation required 10 367 training cycles. The same network trained with two momentum values of 0.5 and 0.9 required 5180 and 1007 training cycles, respectively. Emerson and Damper (1993) used a constant momentum value of 0.8 for training different networks. In general, incorporating a momentum term will reduce the number of training cycles for a network to reach some predefined error.

2.5 Multi-layer Neural Network Classifiers Versus Statistical Classifiers

Various studies have been conducted to compare the performance and the classification procedures of MLNN classifiers with statistical classifiers (Khotanzad and Lu 1991, Sethi 1991, Luo et al. 1999b, Jayas et al. 2000). As discussed earlier, most of the statistical classifiers are based on the Bayes decision rule. The Bayes decision rule performance is optimal for a given set of features in the way that it minimizes the probability of error and the conditional risk. Although the Bayes decision rule is very simple, it is difficult to apply in practice because the posterior probabilities are usually unknown and so must be estimated from the samples (Hush and Horne 1993).

Multi-layer neural network classifiers learn the class knowledge directly from the training data set and, therefore, it is unnecessary to make any assumptions regarding the underlying probability density functions. Information about *a priori* probability can be adjusted after training (Hush and Horne 1993), or by increasing the number of training patterns. After training (learning), the MLNN classifier is specified by a set of processing elements which are arranged in a certain topological structure and interconnected with fixed connections (weights). There is no need for retaining the training data and no extensive computation is involved in the classification of unknown patterns.

The problem in designing an MLNN, however, is that there is no theoretical method available to optimally determine the network structure, the number of hidden layers, and the node numbers in each hidden layer, which control the learning and classifying ability of the MLNN. Although, it has been shown that an MLNN with two hidden layers can form any discriminant surface (Pao 1989), MLNNs with three or more hidden layers are also used for

their efficiency and speed in learning (Keppler et al. 1996). An MLNN with a small and simple hidden layer structure may not grasp sufficient class knowledge for classification, while an MLNN with a large and complex hidden layer structure may tend to memorize the specific patterns in the training data set rather than learn the general class information. The best way for structure design is to start with a small number of hidden layers and processing nodes. The network complexity can be gradually increased until the network is trained sufficiently. Multi-layer neural networks using the gradient descent technique and back-propagation learning rule can get trapped in a local minimum and consequently result in lower classification rates. To reduce the risk of local minima it is suggested to use extra hidden nodes, smaller learning rates, and train the network with different initial weight values.

Khotanzad and Lu (1991) compared the performance of MLNN with nearest neighbour classifiers for character recognition. Both the classifiers were similar in their performance. The time taken by the MLNN classifier, however, was much less than the nearest neighbour classifier. In general, *k*-NN classifiers are not very effective for high dimensional discrimination problems (Lippmann 1987).

The use of sigmoid functions in the MLNN allows perturbations in the feature values to be tolerated. Moreover, the use of soft limiting functions in MLNNs provide smoother boundaries between different classes and this subsequently offers more flexible decision models than the conventional decision trees. The issue of missing features is also less crucial in the neural networks implementation because of the parallel nature and graceful degradation property of the neural networks (Sethi 1991).

2.6 Application of MLNN Classifiers in Agri-Food Research

Neural network classifiers have been considered and applied for quality inspection of different agricultural products. Thai and Shewfelt (1991) compared statistical regression techniques and neural networks to evaluate the external color for tomato and peach. Both techniques provided the same answers regarding the selection of the factors to be included in the final mathematical equations. Statistical methods gave slightly better results as compared to neural network methods. They, however, recommended the use of neural networks because of fewer steps in the analysis phase.

Bochereau et al. (1992) presented a general purpose method for approximating an arbitrary continuous function on a compact set from a given set of observations. The method consisted of constructing a model based on a feedforward MLNN, embedding both classical data analysis techniques and neural network techniques. The model construction was divided into three steps: (1) principal components analyses was first applied to reduce the number of input variables and to decorrelate them, (2) multiple regression analysis was used to derive the best linear estimator, and (3) multilayer neural networks were trained to extract the non-linear components of the function. The model was applied to reflectance data of the sugar content obtained using NIR spectroscopy to determine the quality of apples. The results of the experiments were used to derive a model for predicting apple quality from near infra-red spectra. The model gave an error of 5%.

Murase et al. (1992) developed a neural network model to estimate the maximum hoop stress produced in the skin of tomato fruit in the cracking process. A three-layer neural network was used with gradient descent back propagation as the training algorithm. The

inputs were physical and mechanical properties of the tomatoes generated by a finite element model capable of describing their cracking behavior. They inferred that crack occurrence in tomato can be easily estimated using their neural network model.

Patel et al. (1995) used machine vision in conjunction with an MLNN for detecting defective eggs with dirt stains and blood spots. The gray level histogram data extracted from the images of the eggs were used as input to the network. An accuracy of 83.3% was reported for detecting the dirt stains and the accuracy for blood spot detection was 91.7%. The authors indicated that a coupled neural network and computer vision system was an attractive and feasible method for egg defect detection.

Romaniuk et al. (1993) used a technique developed by Zahn and Roskies (1972) and obtained the first 20 Fourier descriptors for different cultivars of barley. The Fourier descriptors were used as inputs to an MLNN classifier. Their neural network was able to recognize different varieties of barley seeds with about 80% accuracy. In this research no attempt was made to reduce the number of features. The trained networks had only one neuron in the output layer and this approach to MLNN classification makes the task of classification very difficult.

Dowell (1993) used a feedforward neural network for classification of damaged and undamaged peanut kernels. The spectrum reflectance from 400 nm to 700 nm in 10 nm intervals was used as the recognition feature. The author indicated classification was best when the network had 20 or more hidden neurons. The author tested the network with 1 to 20 and then to 40 neurons in the hidden layer without any systematic approach to select the number of neurons. Indicating "20 or more" is a rather weak conclusion because in this case

"more" can be considered any number between 20 and 40. Using an excessive number of neurons in the hidden layer decreases the generalization power of networks.

Park and Chen (1994) applied different neural network models to develop an accurate, reliable, and economical sensor for on-line inspection of cadavers and detecting infected carcasses at poultry processing units. They used spectral reflectance data obtained by a diode array spectrophotometer as the discrimination feature. The networks compared were feedforward back propagation, self organization map with back propagation, and counter propagation. They found that feedforward back propagation network was the most suitable network for this application. This network was also compared with other classification discrimination methods such as multiple linear regression, closest cluster mean, *k*-nearest neighbor, and principal component analysis with Mahalanobis distance. The Feedforward back propagation network was also superior to these classical classifiers.

Chen et al. (1995) used the feedforward backpropagation neural networks with near-infrared (NIR) diffuse reflectance spectra of ground kernels as input to classify hard red, winter, and spring wheats. Networks with and without hidden layers were used with various subsets of the full spectral region as inputs. Using samples from the 1987-1989 crop years, the best neural network models yielded 97.0 and 96.8% accuracies for calibration and validation sets, respectively, utilizing the full wavelength range. When applied to the 1990 crop year, the prediction accuracies of the full and abbreviated wavelength range models were 95.1 and 95.6%, respectively. These models performed better than a previously reported principal component analysis with Mahalanobis distance classifier.

Sayeed et al. (1995) used a feedforward neural network to develop a methodology to evaluate the quality of a snack product through non-destructive analysis. Input to the network included visual texture and morphological characteristics. They used step-wise linear regression to reduce the number of features. The neural network was shown to predict the sensory attribute of the snack with a reasonable degree of accuracy. The network, however, performed better when trained and tested with the whole set of data than with a reduced one. This indicates that either the procedure followed for feature selection was not suitable or the features could not be reduced. The proposed algorithm seems to be computationally expensive because of the large network size, large number of features, and the pre-processing time required for extracting the features.

A method for evaluating tomato ripeness, utilizing its surface color, was developed by Shibata et al. (1996) using a machine vision system with color image processing capability and an MLNN-based software system. The tomato ripeness was classified into 4 categories according to the standard commercial classification for manual sorting. Three color specification values were calculated from the RGB gray levels of a captured color digital image of a tomato by an on-line image processing system. The authors suggest that only 0.2-0.5% of the total surface area of a fruit is needed for color image sensing. A 3-layer back-propagation neural network with 4 hidden nodes gave a satisfactory performance. The total processing time from image capture to output for a single fruit was 0.45 s. The recognition rate for the ripeness classification using this method was as high as 93%. A recognition rate of only 77% was obtained by the multiple regression model tested. This work provides another example to strengthen the area of application of neural networks,

machine vision systems, and robotics for post-harvest processing of agricultural products.

Luo et al. (1999b) applied and empirically compared two statistical and one neural network classifier for the classification of cereal grain kernels (e.g., CWRS wheat, CWAD wheat, barley, rye, and oats) and for the classification of one healthy and 6 types of damaged (e.g., broken, grass-green/green-frosted, black-point/smudge, mildewed, heated, and bin/fire-burnt) CWRS wheat kernels, using selected morphological and color features extracted from the grain sample images. The classification of cereal grain kernels and the classification of healthy and damaged CWRS wheat kernels using a non-parametric (*k*-nearest neighbor) statistical classifier and the MLNN classifier gave similar and the best classification results. Using an MLNN classifier with a selected set of 15 morphological and 13 color features, the average classification accuracies were 98.2, 96.9, 99.0, 98.2, and 99.0% for CWRS wheat, CWAD wheat, barley, rye, and oats, respectively, when trained and tested with 3 different training and testing data sets. The classification accuracies achieved using a parametric classifier were lower than the classification accuracies achieved using both the non-parametric and the MLNN classifiers.

Ghazanfari et al. (1998) used a machine vision system to classify unshelled pistachio nuts based on United States Department of Agriculture grades. The gray-level histogram data obtained from the gray scale image of the nuts were analyzed to select a set of suitable recognition features. Based on the analyses, the mean of the gray-level histogram over the 50-60 gray-level range and the area of each nut (the integral of its gray-level histogram) were selected as the recognition features. The selected features were used as input to 3 classification schemes: a Gaussian, a decision tree, and an MLNN. The MLNN classifier

resulted in slightly higher performance with more uniform classification accuracy than the other two classifiers.

To quantify single wheat kernel color, Wang et al. (1999) used an optical radiation measurement system which measured reflectance spectra from 400 to 2000 nm. Six classes of wheat were used for this study. A neural network using input data dimension reduction by divergence feature selection and by principal component analysis was used to determine single wheat kernel color class. The highest classification accuracy was 98.8% when the divergence feature selection method was used to reduce the number of inputs. The highest classification accuracy was 98% when the principal component analysis method was used to reduce the number of inputs.

3. MATERIALS AND METHODS

3.1 Imaging Hardware

For image acquisition a 3-chip charge coupled device (CCD) color camera (DXC-3000A, SONY) was used. The camera was fitted with a zoom lens (VCL-1012 BY, SONY) of 10-120 mm focal length. To provide rigid stable support and easy vertical movement, the camera was mounted on a stand (m3, Bencher Inc., Chicago, IL). The camera was connected to a camera control unit (CCU-M3, SONY). The iris was selectable to manual or automatic mode. The option of the manual iris control was used to achieve repeatability in the experiments. The automatic gain control of the camera was disabled. Before each imaging session, the camera was white balanced. Figure 3.1 shows the camera set up.

The image acquisition procedure was controlled using a personal computer (PC) (PIII 450 MHz) which was fitted with a color frame grabbing board (Matrox Meteor-II multi-channel, Matrox Electronic Systems Ltd., Montreal, PQ). The National Television System Committee (NTSC) composite color signal from the camera was converted by the camera control unit at a speed of 30 frames per second into three parallel analog video signals, namely red (R), green (G), and blue (B), corresponding to the three NTSC color primaries, and a synchronous signal. The frame grabber digitized the RGB analog video signals from the camera control unit to a 24 bit 640 x 480 color digital image. The image resolutions were approximately 0.064 mm/pixel in the horizontal and vertical directions (see Table 3.1). The programs to control the frame grabber were provided by the Matrox imaging library, supplied by the manufacturer of the frame grabbing board. The digital images were then sent to the computer monitor for on-line display and transferred to the hard disk for storage.

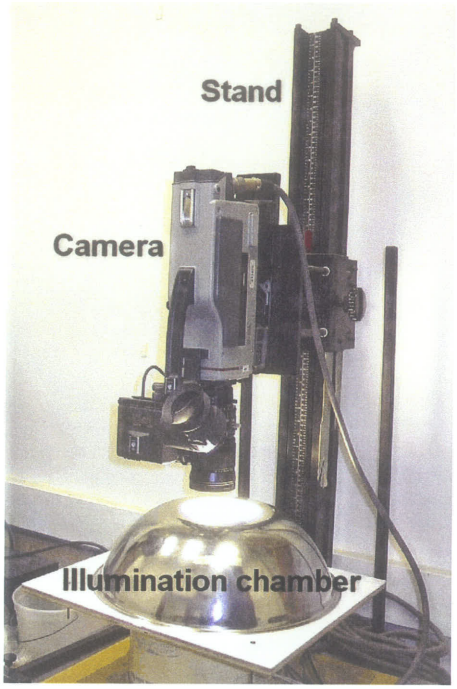

Fig. 3.1 The image acquisition system

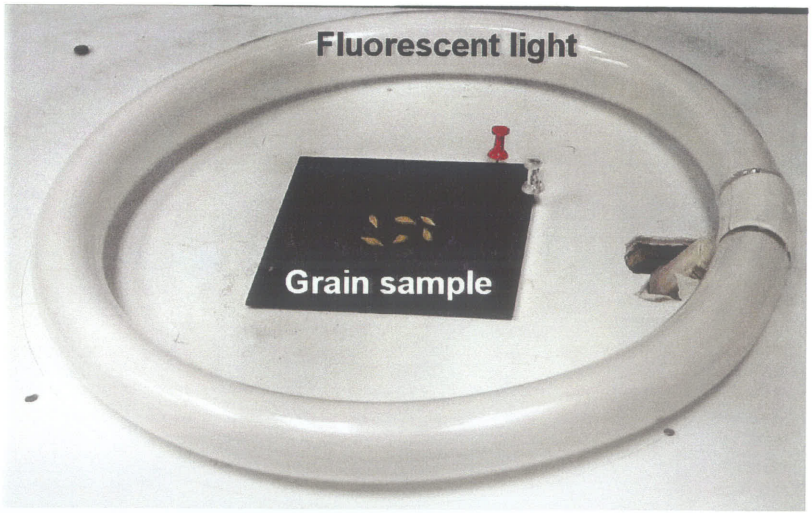

Fig. 3.2 The illumination setup for image acquisition

3.2 Sample Illumination

Illumination plays a very important role in image acquisition. An ideal illumination source should provide uniform light distribution over the field of view (FOV), should be consistent over time, and should eliminate any shadows of the objects. It is impractical to meet all these conditions in an industrial imaging system but a careful selection and arrangement of light sources can minimize the inconsistencies due to changes in power voltage, ambient temperature, and lamp deterioration. Luo et al. (1997) evaluated incandescent, halogen, and flourescent lamps for their sensitivity to lamp voltage variations, stability with time, and uniformity over FOV. They suggested that a flourescent lighting is best suited for the system that was used for this thesis.

A flourescent tube with a 305 mm diameter 32-W circular lamp (FC12T9/CW, GE Lighting, USA) with a rated voltage of 120 V was placed around and just below the surface level of the sample placement platform of the light chamber (Fig 3.2). A light diffuser, a semi spherical steel bowl of 390 mm diameter, covered the light bulb and the object plane such that the object plane was only exposed to the diffused light. The inner side of the bowl was painted white and smoked with magnesium oxide. A 125 mm diameter opening at the top of the bowl facilitated the camera to view the FOV.

A voltage regulator (CVS, Sola Canada Inc., Toronto, ON) supplied stable AC power (±0.5 V) to the light sources and the voltage to the lamps was adjusted by a variac. A light controller (FX0648-2/120, Mercron, Richardson, TX) fitted with a photodiode light sensor was used with the flourescent lamp. The light controller automatically detected the illumination level in the light chamber and adjusted the AC frequency of the lamp to

maintain a stable level of illumination. The frequency of the AC power output of the controller varied between 140 kHz at the minimum light levels to 60 kHz at full power.

3.3 Illumination Standardization

A Kodak white card with 90% reflectance (E152-7795, Eastman Kodak Co., Rochester, NY) was used as a white reference to standardize the illumination level. The lamp voltage was set to the rated 120 V. The image of the white card was acquired and over a small central area of 50 x 50 pixels the mean gray level values of the R, G, and B bands were computed and used as the illumination level indicators. By manually adjusting the iris control and performing the white balance with the camera control unit, all three values (R, G, and B) were adjusted to 250 ± 1.

3.4 Spatial Calibration

All the morphological features were calculated in pixels. To convert these pixel dimensions into real-world measurement units, the spatial resolution of pixels was calculated. This was done by taking the image of a Canadian 10 cent coin, counting the number of pixels in its diameter, and then measuring it with a micrometer (No. 961, Moore and Wright, Sheffield, England). Table 3.1 shows the results of the spatial calibration. The spatial resolution of the images was 6.38×10^{-2} mm/pixel. The camera was adjusted to this resolution prior to taking images every time.

Table 3.1 Spatial calibration results for a Canadian 10 cent coin

Image number	Diameter of coin (pixels)	Diameter of coin (mm)	Spatial resolution (mm/pixel)
1	281	17.95	6.39×10^{-2}
2	281	17.96	6.39×10^{-2}
3	282	17.96	6.37×10^{-2}
4	281	17.96	6.37×10^{-2}
5	282	17.95	6.37×10^{-2}
	Average resolution		**6.38×10^{-2}**

3.5 Grain Samples

The grain samples for this study were obtained from the Industry Services Division of the Canadian Grain Commission (Winnipeg, MB). For the 1998 growing year, clean grain samples of CWRS wheat (Grade 1, 2, and 3), CWAD wheat (Grade 1, 2, and 3), barley (Special Select Malt Barley), rye (Grade 1), and oats (Grade 1) were used in color image analysis of grain samples for content identification and cleaner performance determination. Samples were collected from eight locations in Manitoba, nine locations in Saskatchewan, and six locations in Alberta (Fig. 3.3). These locations were chosen using the climatic subdivisions of the Canadian Prairies (Putnam and Putnam 1970). The selected locations represent five sample locations from the humid prairie, seven locations from the sub-boreal region, six locations from the sub-humid prairie, and five locations from the semi-arid region.

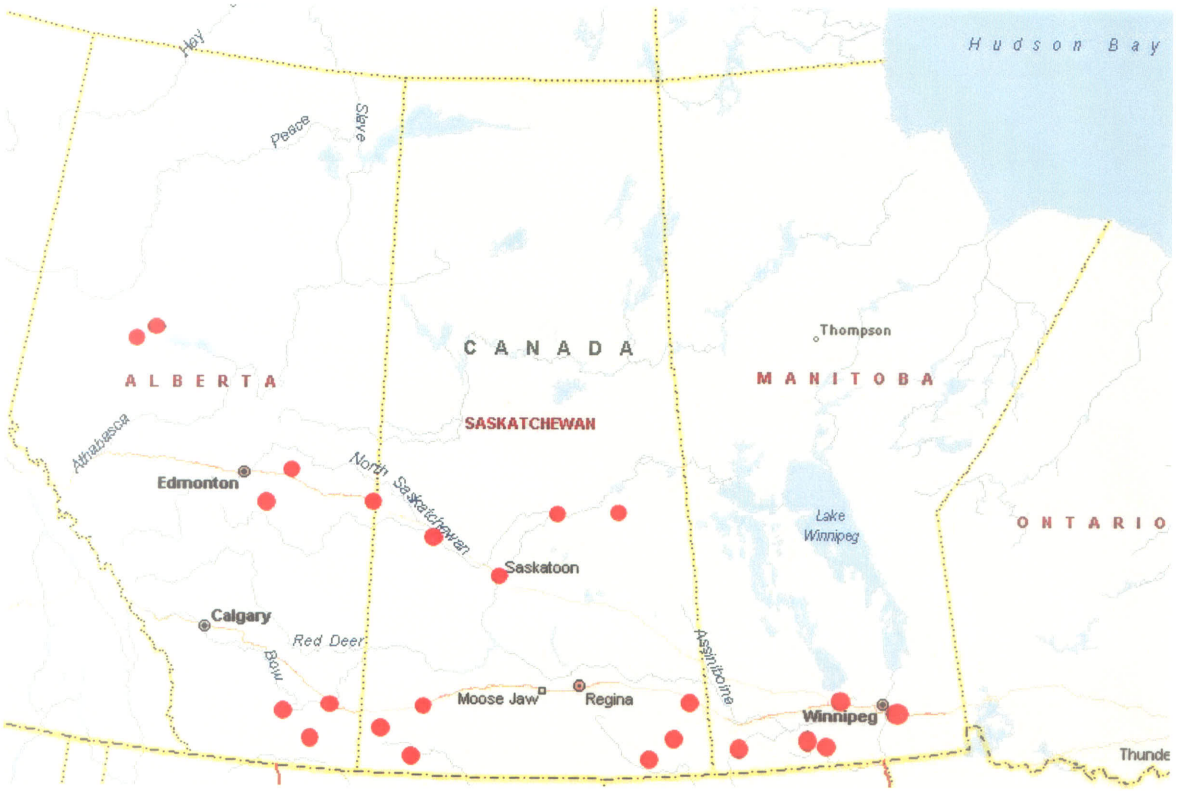

Fig. 3.3 A map of Canadian prairies showing the various locations from where the grain samples were collected, many representing different climatic regions

3.6 Image Acquisition

For its stabilization, the image acquisition system was switched on 30 min prior to acquiring images. The gray level calibration (white balance) of the FOV was done after that using a Kodak white card. The spatial calibration was done with an object of known dimension (a Canadian 10 cent coin).

For each grain type and growing region sample, about 500 g of grain was poured into a large plastic bag and shaken thoroughly. A scoop was used to take out approximately 1000 kernels from the plastic bag. Six kernels were then taken one at a time and placed in the FOV of the camera in a non-touching fashion. A black background was used to image the grain kernels. One hundred such images were taken for each grain type from every growing region (i.e., 600 kernels of each grain type were imaged for every growing region).

For imaging the dockage fractions, standard dockage samples were obtained from the Industry Services Division of the Canadian Grain Commission (Winnipeg, MB). Dockage samples were obtained by running uncleaned farm samples of CWRS wheat through the Carter dockage tester (Carter Day International, Minneapolis, MN). The sample was then divided into five different fractions namely, broken wheat, chaff, wild buckwheat, wheat-heads, and canola. One hundred grams of each dockage tester fraction were collected. To image these fractions, each individual component was carefully placed in the FOV of the camera using a pair of tweezers. The component was then weighed on a microbalance (Metller M3, Germany). Because the mass density of the different fractions were very different from each other, weighing them was necessary so that their mass could be correlated to their morphology. By doing so, a correlation between the morphology and the

mass of the particle was obtained for each type of dockage fraction.

3.7 Morphology Mass Relationship of Cereal Grains and Dockage

A study was conducted to quantify the mass of the grain kernels and dockage fractions from their two-dimensional images. It was hypothesized that the mass of any grain or dockage fraction is dependent on its morphology. Seven morphological features, namely, area, perimeter, maximum radius, minimum radius, mean radius, major axis length, and minor axis length were correlated to the mass of the objects. Approximately 600 kernels of each grain type and 400 particles of each class of dockage were imaged and weighed separately. A linear regression was performed to find which morphological feature best described the mass of that particular class.

3.8 Grain Cleaner

A prototype grain cleaner was designed and fabricated (Fig. 3.4). The cleaner consisted of a wooden frame which could support two screens and a similar trough of 310 mm x 605 mm dimensions. These screens were similar to the ones that are used in a Carter dockage tester. After consulting the personnel at Carter Day International and the literature on dockage testers, the sieve sizes were chosen as #8 (2.26 mm [inscribed circle] perforated double triangle) for the top sieve and #5 (1.79 mm x 11.90 mm perforated slot) for the bottom sieve. The whole assembly was mounted on a vibratory motor (15A, Eriez Manufacturing Co., Erie, PA). The screens had a slope of one in 20. The RPM of the vibrator and the slope of the screens could be varied to achieve different flow rates through the cleaner. The screens could be taken out and replaced for cleaning and minor slope adjustments.

(a)

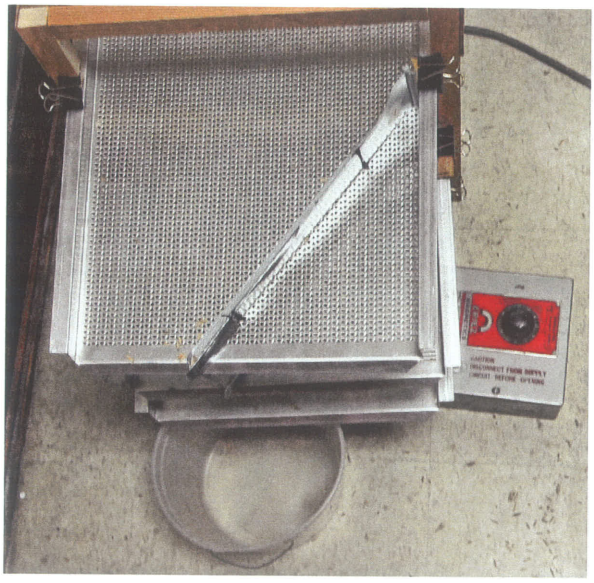

(b)

Fig. 3.4 The lab scale grain cleaner: (a) side view and (b) top view

3.8.1 Grain cleaner testing The grain cleaner was tested at three different flow rates of 4 kg/h, 8 kg/h, and 12 kg/h. The flow rates of 4 kg/h and 8 kg/h were obtained by adjusting the vibrator rpm, keeping the slope of the screens at 0.05. To achieve a flow rate of 12 kg/h, the slope was increased to 0.08. Table 3.2 shows the slope and vibrator frequencies for the tested flow rates for different grain types.

One hundred grams of clean grain sample were taken and the kernels were imaged by placing them in the field of view of the camera in a non-touching fashion. Using the regression equation, the mass of that sample was calculated. Five grams of dockage was then added to it to create an impurity level of 5%. Prior to mixing the clean grain with dockage, the dockage particles were also imaged and analyzed for the mass of their constituents using the regression equations. The clean grain and dockage were mixed thoroughly in a plastic bag and passed through the grain cleaner. The clean grain obtained from the cleaner was taken and foreign material was manually removed from it. The clean grain and foreign material were separately weighed and imaged again. Their masses were estimated using the regression equations. Three replicates at each flow rate were done for all the grain types.

Seven morphological features, namely, area, perimeter, maximum radius, minimum radius, mean radius, major axis length, and minor axis length of grain and dockage mixture were calculated. The range of these features was compared to the range of the corresponding features after the grain had been passed through the cleaner. This change in the range of these features was studied to investigate if it could serve as a feedback to control the cleaning process.

Table 3.2 The vibrator rpm and slope of sieves used to obtain the test flow rates for different grain types

Flow rate	Barley		CWAD wheat		CWRS wheat		Oats		Rye	
(kg/h)	Vibrator rpm	Slope of sieves	Vibrator rpm	Slope of sieves	Vibrator rpm	Slope of sieves	Vibrator rpm	Slope of sieves	Vibrator rpm	Slope of sieves
4	1350	0.05	2000	0.05	1350	0.05	2000	0.05	2000	0.05
8	2500	0.05	4000	0.05	2500	0.05	4000	0.05	4000	0.05
12	4500	0.08	5500	0.08	4500	0.08	5500	0.08	5500	0.08

3.9 Data Analysis

For the cereal grain classification part, images of 1500 kernels of each grain type were taken to form a set of 7500 kernels (1500 kernels of each of the five grain types). This set was divided into five groups of 1500 kernels each (now each group had 300 kernels of each of the five grain types). One group (i.e., 1500 kernels) was then used as a training set and another group was used as a test set. Validation was then done on the remaining three groups, i.e., 4500 kernels. This replication was done five times so that each group was used as a training and testing set once.

For cereal grain and dockage classification, 600 objects of each type (cereal grain and dockage categories) were taken to form a set of 6000 objects (600 of each category). The complete set was divided into five groups of 1200 objects (now each group had 120 objects of each type). One group (i.e., 1200 objects) was used as a training set and another was used as a test set. Validation was done on the remaining three groups, i.e., 3600 objects. Again the replication was done five times so that each group was used as a training and testing set once.

Data analysis was done using a four-layer BPN and a non-parametric statistical classifier and the results of the two were compared.

3.9.1 Neural network training Neural networks were designed and implemented using the software package NeuroShell 2 (Ward Systems Group, Frederick, MD). Jayas et al. (2000) indicated that a BPN network is best suited and thus is the most popular choice for classification of agricultural produce. A four-layer BPN was used for cereal grain and dockage classification. To begin with, the number of nodes n in the hidden layer was

calculated using the formula:

$$n = (I + O)/2 + y^{0.5} \tag{3.1}$$

where: I is the number of inputs; O is the number of outputs; and y is the number of input patterns in the training set (Ward Systems Group 1998). The number of nodes was varied to see any significant improvement in performance. If no improvement was observed, the number of nodes calculated by the formula was used to train the network. Because two hidden layers were used in this thesis, the number of nodes calculated by the formula was equally divided between them. The network training was done on one group (1500 kernels) and while training, another group was used as a test set. The three remaining groups were used for validation after the network was trained.

While training, the weights and thresholds for each neuron were adjusted to minimize the mean square error (MSE) between the predicted and observed outputs. For all the connections, logistic activation functions (also called *sigmoid, semi-linear*, or *soft-limiting* functions) were used. Logistic activation functions provide a balance between linear and non-linear (hard-limiting) activation functions and are considered to be the closest to biological neurons. Linear activation functions cannot suppress noise and have limited learning capabilities whereas non-linear functions may introduce network instability and risk computational and analytical intractability (Mehrotra et al. 1996). The number of hidden nodes were varied until the best results were obtained. Training was stopped after 1000 epochs. An epoch is defined as the time during which a network is trained by presenting each pattern in the training set exactly once. In a preliminary study it was found that 1000 epochs were more than enough for the network to train as the coefficient of multiple

determination (R^2) became constant well before 1000 epochs (Paliwal et al. 2001). To avoid over-training, the trained network was saved every time it reached a new minimum average error for the test set. Time taken by each network to train was also determined to compare the computational speeds of various networks.

The network also gives the contribution of each input feature to the network's classification performance. For every input feature it gives a number which is indicative of the percent contribution that the particular feature made towards the classification process. These percent contributions for individual features were averaged for different replicates to rank the contribution for every feature. After ranking, the top 10 and top 20 features were taken for further analyses and the rest of the features were eliminated.

3.9.2 Non-parametric statistical classifier As described in section 2.3, the selection of a statistical classifier depends on the class-conditional probability density function of the input features. Because the distribution of features in feature space cannot be assumed to be normal, a non-parametric statistical classifier was used. This was implemented using procedure DISCRIM of SAS (SAS 1990). The DISCRIM procedure uses Bayes' theorem to determine the probability of an observation belonging to a particular group by assuming the prior probabilities of its group membership and the group-specific densities. The ranking of features was done using procedure STEPDISC of SAS.

4. ALGORITHM DEVELOPMENT FOR IMAGE ANALYSIS

The algorithm development for this thesis was done on an IBM compatible (Pentium III, 450 MHz) computer in Microsoft Visual C++ (Version 6.0) programming language. The algorithm was complete in the sense that it could do all the analyses on the image, starting from reading the image to thresholding, region labeling, extraction of various features, and writing those features to a text file. The algorithm was capable of sequentially analyzing multiple files. A description of the C++ code is given in Appendix A and an electronic copy can be obtained from Dr. D.S. Jayas. The various operations that the algorithm performed are described in this chapter.

4.1 Thresholding

Conversion of a multi level gray level image to a binary image so as to distinguish the objects from the background is called thresholding. It can either be done manually or automatically. In manual thresholding, a threshold value is specified by the user and the pixels whose gray levels are less than the threshold value are set to background (0) and the remaining pixels are set to object (1). Manual thresholding is time consuming as the thresholded image has to be displayed for every threshold value specified by the user to visually examine the thresholded image and to decide the final threshold value.

In this study, automatic thresholding (Parker 1994) was used. In automatic thresholding, the threshold value is decided by the algorithm. The threshold value was calculated by the principle of iterative selection. The blue band was used for thresholding the image (Luo et al. 1999a). The number of pixels for each gray level of the blue band were multiplied with the gray level value and summed. The sum was divided by the total number

of pixels to obtain the first threshold value, X_1. The same iteration was done for the two parts i.e., 0 to X_1 and X_1+1 to 255 (assuming that there are 255 gray level values of the blue band in the image), to generate two more numbers P_1 and P_2. The mean of P_1 and P_2 gave the second threshold value X_2. Now the iterative process was done for values from 0 to X_2 and X_2+1 to 255, to generate P_3 and P_4. Taking the mean of P_3 and P_4 gave the new threshold X_3. This process was repeated until X_n equals X_{n+1}. This stabilized value of X was taken as the threshold for the image. The maximum number of iterations was set to 40 to reduce the runtime of the algorithm.

4.2 Region Labeling

Region labeling was done to assign a unique label or identifier to each object in the binary image. The region labeling algorithm scanned the binary image once from the top left to the bottom right. The first encountered unlabeled object pixel was assigned a unique label. Then from that pixel the region was expanded and the same label value was propagated by following 8-neighbors connectivity (Gonzalez and Woods 1992). The propagation of the same label value continued until no more neighboring pixels of the objects could be found. The scanning of the binary image was resumed and the same process was continued until all the objects were labeled with their unique label. After labeling there could be some pixels in the object region with the background gray level value (called *hole*) or some pixels in the background with the object gray levels (called *extra region*). In practical applications, certain bright spots on the surface of the objects may appear as holes, and dusts, dirty background spots, or small pieces of grain shell may result in small false regions in the thresholded image. It is very important to change the values of these pixels

to the right values for the accurate measurement of the morphological features. Therefore, a hole filling and region deleting subroutine was used to solve this problem (Luo et al. 1999a). Starting from a background pixel, the whole background region was connected by following the 8-neighbor connectivity. The left out pixels whose gray levels were that of the background were changed to the respective object label value. For the cereal grains, any region with less than 200 pixels (0.72 mm^2) was deleted and for the dockage, regions smaller than 50 pixels (0.18 mm^2) were deleted.

4.3 Feature Extraction

Once the objects of interest in the image have been clearly segmented, the next step is to measure individual features of each object. Features of unknown objects are compared to those of known objects to do the classification. As a rule of thumb, the features that are simplest to measure and contribute substantially towards the classification are the best to use. A total of 51 morphological, 123 color, and 56 textural features were extracted by the algorithm.

4.3.1 Morphological features The features defining the physical dimensions that characterize the appearance of an object are called morphological features. A list of the 51 morphological features extracted from an individual grain kernel is given in Table B1 (Appendix B). The morphological features that the algorithm extracted are described below.

Area The pixel area of the interior of an object is defined as area. It is computed as the total number of pixels inside, and including, the object boundary.

$$A = \sum_{i}^{n} \sum_{j}^{m} X(i, j) \tag{4.1}$$

where $X(i, j) = 1$, in a binary image and n and m define the horizontal and vertical size of the image.

Perimeter The pixel distance around the circumference of an object is defined as perimeter. It is a measure of the boundary length of the object. Generally, the perimeter of a region is calculated by adding the number of pixels on the boundary. But a pixel represents an area not a linear distance. Boundary pixels can be identified using the 4-neighbor or 8-neighbor connectivity methods. In the 4-neighbor connectivity method, the gray level of each pixel relative to its four neighbors is examined. A pixel $X(i, j)$ is considered a boundary pixel if $X(i, j+1)$ or $X(i, j-1)$ and $X(i+1, j)$ or $X(i-1, j)$ is a background pixel (gray level 0). In the 8-neighbor connectivity method in addition to the 4-neighbors, the four corner pixels are considered (Fig. 4.1). Perimeter length of objects is determined using the Euclidean distance principle. The distance represented by each pixel was weighted as 1 if all neighbors were horizontal or vertical, 1.414 if all neighbors were diagonal, and 1.207 if there was one diagonal and one non-diagonal pixel.

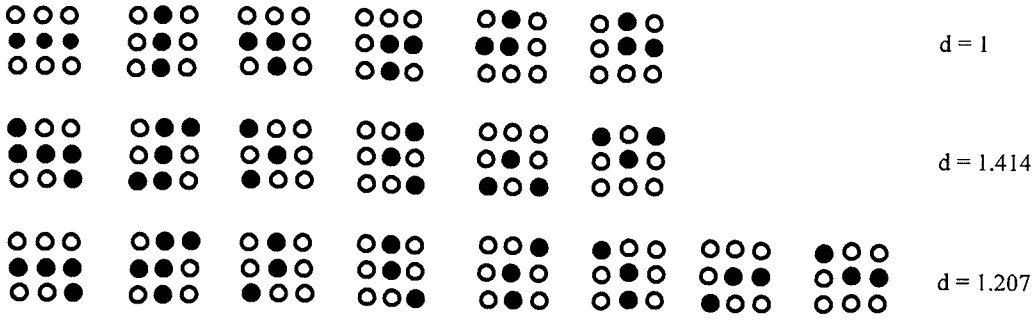

Fig. 4.1 Distance template for boundary pixels

Centre of Mass The centre of mass of an object can not be used as a feature but is required for determining major and minor axes and other features of an object. The centre of mass (x_c, y_c) of an object consisting of N pixels is determined as:

$$x_c = \frac{1}{N}\sum_{i=0}^{N-1} x_i \tag{4.2a}$$

$$y_c = \frac{1}{N}\sum_{i=0}^{N-1} y_i \tag{4.2b}$$

where x_i and y_i are the x and y coordinates of the i^{th} pixel, respectively.

Major axis length It is defined as the longest line that can be drawn through the centre of mass of an object. The candidate pixels were identified by finding the distance between each possible pair of boundary pixels which could be connected by a straight line through the centroid and the longest distance was taken as the length of the major axis.

Minor axis length The minor axis is defined as the longest line that can be drawn perpendicular to the major axis through the centre of mass.

Spatial Moments The spatial moments of an object are statistical shape measures that do not characterize the object specifically. Rather, they give statistical measures related to an object's characterizations. Moments of binary objects describe their shape and moments of gray level images describe the gray level distribution of objects. The general moments (m_{pq}) of different orders are determined as:

$$m_{pq} = \sum_i \sum_j i^p j^q X(i, j) \tag{4.3}$$

where $p, q = 0, 1, 2, \ldots$ is the order of the moment and $X(i, j)$ is the gray level of the object at coordinate (i, j).

In binary images the gray level of the object, $X(i, j)$ is 1 for all pixels. For monochrome and color images, the gray scale or R, G, and B gray values are substituted for the value of $X(i, j)$.

The zero-order spatial moment (m_{00}) is computed as the sum of the brightness values in an object. In the case of a binary image, this is simply the number of pixels in the object, because every pixel in the object is equal to 1 (white). Therefore, the zero-order spatial moment of a binary object is its area. For a gray level image, an object's zero-order spatial moment is the sum of the brightness of pixels and is related to the object's energy.

The first-order spatial moments (m_{10} and m_{01}) of an object contain two independent components, x and y. They are the x and y sums of the pixel brightness in the object, each multiplied by its respective x or y coordinate in the image. In the case of a binary image, the first-order x spatial moment is just the sum of the x coordinates of the object's pixels, because every object pixel is equal to 1. Similarly, the y spatial moment is the sum of the y coordinates of the object's pixels. The second order moments m_{20} and m_{02} represent the moment of inertia.

The moments m_{pq} are dependent on the position of the object in the image and therefore, were not used as features. For comparison and identification of objects, the moments have to be independent of position and orientation in the image and size of the

objects. The central moments μ_{pq} that are invariant to translation (position of the object in a given image) and normalized central moments η_{pq} (Gonzalez and Woods 1992) that are invariant to translation and size of the object are given by:

$$\mu_{pq} = \sum_i \sum_j (i - x_c)^p (j - y_c)^q X(i, j) \tag{4.4}$$

$$\eta_{pq} = \frac{\mu_{pq}}{\mu_{00}^{\gamma}} \tag{4.5}$$

where

$$\gamma = \frac{(p + q)}{2} + 1 \tag{4.6}$$

From the second and third normalized central moments, a set of measurements that are invariant to translation, rotation, and scaling of the object (Gonzalez and Woods 1992) were derived as follows:

$$\phi_1 = \eta_{20} + \eta_{02} \tag{4.7}$$

$$\phi_2 = (\eta_{20} - \eta_{02})^2 + 4(\eta_{11})^2 \tag{4.8}$$

$$\phi_3 = (\eta_{30} - 3\,\eta_{12})^2 + (\eta_{21} - \eta_{03})^2 \tag{4.9}$$

$$\phi_4 = (\eta_{30} + \eta_{12})^2 + (\eta_{21} + \eta_{03})^2 \tag{4.10}$$

Fourier Descriptors Fourier descriptors are shape recognition features based on the Fourier series expansion of periodic functions. The general idea is to represent the boundary of an object as a periodic function with a period of 2π. The obtained periodic function is then expanded in a Fourier series and its coefficients are calculated.

Consider an object with an N-point digital boundary in the xy plane. Starting at an arbitrary point (x_0, y_0), coordinate pairs (x_0, y_0), (x_1, y_1), (x_2, y_2),.... (x_{N-1}, y_{N-1}) are encountered in traversing the boundary, say, counter-clockwise. These coordinates can be expressed in the form $x(k) = x_k$ and $y(k) = y_k$. Now, the boundary can be represented as the sequence of coordinates $f(k) = [x(k), y(k)]$, for $k = 0,1,2...., N-1$. Each coordinate pair can be treated as a complex number so that $f(k) = x(k) + j\, y(k)$ for $k = 0,1,2,....N-1$, i.e., the x axis is treated as the real axis and the y axis is treated as the imaginary axis of sequence of a complex numbers. The discrete Fourier transform of $f(k)$ is:

$$F(u) = \frac{1}{N}\sum_{k=0}^{N-1} f(k) e^{-j2\pi uk/N} \tag{4.11}$$

for $u = 0, 1, 2,...., N-1$. The complex coefficients $F(u)$ are called the Fourier descriptors of the boundary. The inverse Fourier transform of the $F(u)$ restores the $f(k)$, i.e.,

$$f(k) = \frac{1}{N}\sum_{k=0}^{N-1} F(u) e^{j2\pi uk/N} \tag{4.12}$$

for $k = 0, 1, 2,...., N-1$. Because these features were extracted by taking the Fourier transform of the coordinates along the boundary of the kernel, they were called *boundary Fourier descriptors*.

The magnitude of $F(u)$ is the square root of sum of squares of its real and imaginary values. Fourier transforms determined from the radius of the boundary pixels is given by:

$$F(u) = \frac{1}{N} \sum_{k=0}^{N-1} r(k) e^{-j2\pi uk/N} \tag{4.13}$$

where *r(k)* is the radius of the boundary pixel *k*. These features were called *radial Fourier descriptors*.

Slow variations or smooth boundaries are represented by the low harmonic components and complex variations along a boundary are represented by the high harmonic components of the Fourier descriptors (Tao et al. 1995). Therefore, for both the boundary and radial Fourier descriptors, ten lower harmonics and ten higher order harmonics were taken.

4.2.2 Color Features

4.2.2.1 Measurements derived from RGB model The most commonly used color feature model in image processing is the RGB color model. In the RGB model, an image consists of three independent image planes, one in each of the primary colors, red, green, and blue. A particular color is specified by the amount of each of the primary components present. Figure 4.2 shows the geometry of the RGB color model for specifying colors using a Cartesian coordinate system. The gray scale spectrum, i.e. those colors made from equal amounts of each primary, lies on the line joining the black and white vertices.

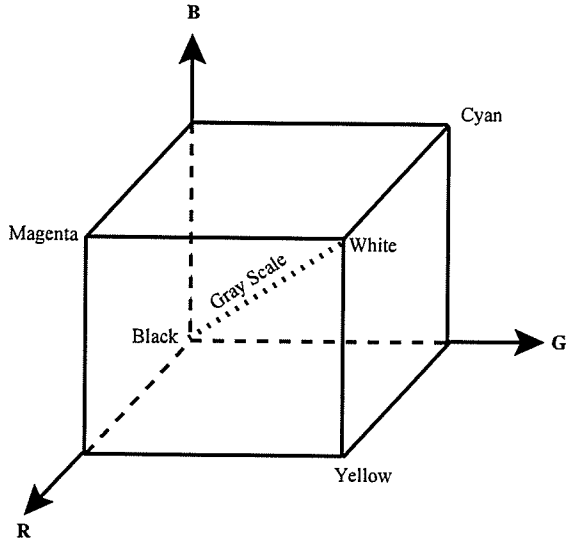

Fig. 4.2 The RGB color cube. The gray scale spectrum lies along the line joining the black and white vertices (Gonzalez and Woods 1992)

This is an additive model, i.e. the colors present in the light add to form new colors, and is appropriate for the mixing of colored light for example. The RGB model is used for color monitors and most video cameras.

The normalized RGB signals, $r(x,y)$, $g(x,y)$, and $b(x,y)$ were computed from each of

its three color band signals, *R(x,y)*, *G(x,y)*, and *B(x,y)*, respectively, using the following equations:

$$r = \frac{R}{R+G+B} \tag{4.14a}$$

$$g = \frac{G}{R+G+B} \tag{4.14b}$$

and

$$b = \frac{B}{R+G+B} \tag{4.14c}$$

The following measurements were derived from the normalized RGB signals of a kernel region Ω which consisted of N pixels.

Mean normalized RGB signals

$$\bar{r} = \frac{1}{N}\sum_{\Omega} r(x,y) \qquad \bar{g} = \frac{1}{N}\sum_{\Omega} g(x,y) \qquad \bar{b} = \frac{1}{N}\sum_{\Omega} b(x,y) \tag{4.15}$$

Variances of normalized RGB signals

$$\sigma_r^2 = \frac{1}{N-1}\left(\sum_{\Omega} r^2(x,y) - N\bar{r}^2\right) \tag{4.16a}$$

$$\sigma_g^2 = \frac{1}{N-1}\left(\sum_{\Omega} g^2(x,y) - N\bar{g}^2\right) \tag{4.16b}$$

and

$$\sigma_b^2 = \frac{1}{N-1}\left(\sum_{\Omega} b^2(x,y) - N\bar{b}^2\right) \tag{4.16c}$$

Ranges of normalized RGB signals

$$\Delta r = r_{\max} - r_{\min} = \max_{\Omega}[r(x,y)] - \min_{\Omega}[r(x,y)] \tag{4.17a}$$

$$\Delta g = g_{\max} - g_{\min} = \max_{\Omega}[g(x,y)] - \min_{\Omega}[g(x,y)] \tag{4.17b}$$

and

$$\Delta b = b_{\max} - b_{\min} = \max_{\Omega}[b(x,y)] - \min_{\Omega}[b(x,y)] \tag{4.17c}$$

4.2.2.2 Measurements derived from HSI model In this model three independent quantities are used to describe any particular color. The *hue* (*H*) is determined by the dominant wavelength. The *saturation* (*S*) is determined by the excitation purity, and depends on the amount of white light mixed with the hue. A pure hue is fully saturated, i.e. no white light mixed in. Hue and saturation together determine the *chromaticity* for a given color. Finally, the *intensity* (*I*) is determined by the actual amount of light, with more light corresponding to more intense colors. The entire space of colors that may be specified in this way is shown in Fig. 4.3. Figure 4.3a shows the HSI solid and Fig. 4.3b shows the HSI triangle formed by taking a horizontal slice through the HSI solid at a particular intensity. Hue is measured from red, and saturation is given by distance from the axis. Colors on the surface of the solid are

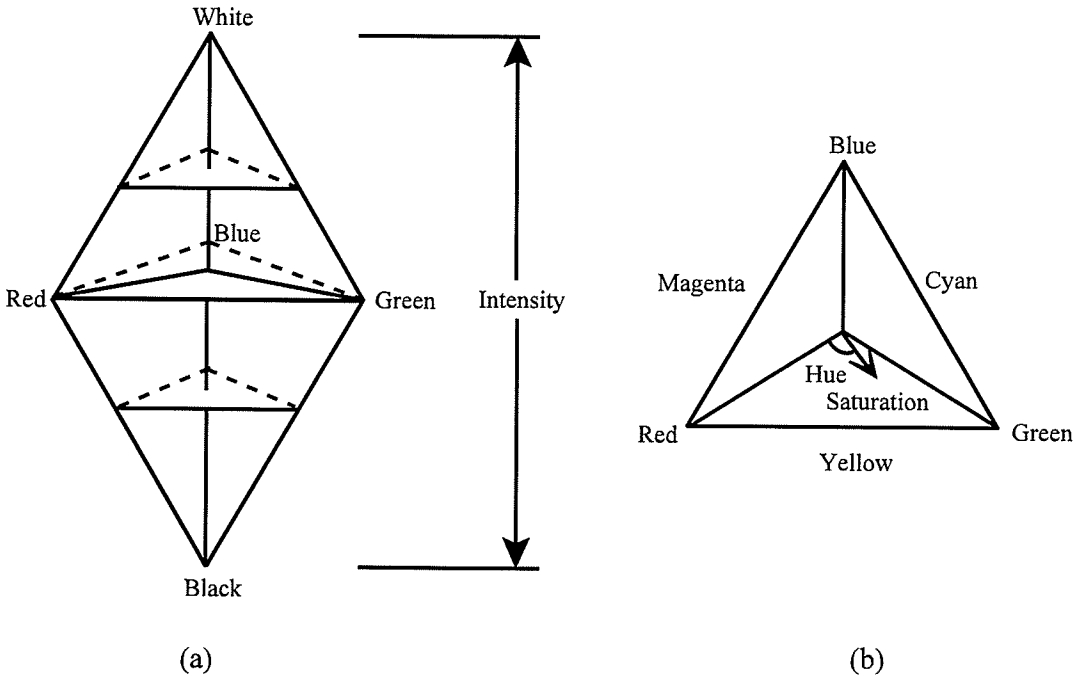

Fig. 4.3 The HSI model. (a) HSI solid depiction (b) HSI triangle formed by taking a horizontal slice of HSI solid at any given intensity

fully saturated, i.e. pure colors, and the gray scale spectrum is on the axis of the solid. For these colors, hue is undefined.

The H, S, and I attributes can be derived from the normalized RGB values, r, g, and b, by (Gonzalez and Woods 1992):

$$H = \cos^{-1}\left\{\frac{0.5[(r-g)+(r-b)]}{[(r-g)^2+(r-b)(g-b)]^{1/2}}\right\} \tag{4.18a}$$

$$S = 1 - \frac{3}{(r+g+b)}[\min(r,g,b)] \tag{4.18b}$$

and

$$I = \frac{1}{3}(r + g + b) \tag{4.18c}$$

The HSI signals, $H(x,y)$, $S(x,y)$, and $I(x,y)$ were computed for each image from its three color band signals, $R(x,y)$, $G(x,y)$, and $B(x,y)$ for each image using the Eqs. 4.14 and 4.18. The following measurements were derived from the HSI signals of a kernel region Ω of N pixels:

Mean normalized HSI signals

$$\overline{H} = \frac{1}{N}\sum_{\Omega} H(x,y) \qquad \overline{S} = \frac{1}{N}\sum_{\Omega} S(x,y) \qquad \overline{I} = \frac{1}{N}\sum_{\Omega} I(x,y) \tag{4.19}$$

Variances of normalized HSI signals

$$\sigma_H^2 = \frac{1}{N-1}(\sum_{\Omega} H^2(x,y) - N\overline{H}^2) \tag{4.20a}$$

$$\sigma_S^2 = \frac{1}{N-1}(\sum_{\Omega} S^2(x,y) - N\overline{S}^2) \tag{4.20b}$$

and

$$\sigma_I^2 = \frac{1}{N-1}(\sum_{\Omega} I^2(x,y) - N\overline{I}^2) \tag{4.20c}$$

Ranges of normalized HSI signals

$$\Delta H = H_{\max} - H_{\min} = \max_{\Omega}[H(x,y)] - \min_{\Omega}[H(x,y)] \tag{4.21a}$$

$$\Delta S = S_{\max} - S_{\min} = \max_{\Omega}[S(x,y)] - \min_{\Omega}[S(x,y)] \tag{4.21b}$$

and

$$\Delta I = I_{\max} - I_{\min} = \max_{\Omega}[I(x,y)] - \min_{\Omega}[I(x,y)] \tag{4.21c}$$

4.2.2.3 Color moments For bi-level grain images, the invariant moments were defined by Eqs. 4.7 to 4.10 as shape measures. Similarly the color moments were computed on each of the three normalized color bands, namely *r(x,y)*, *g(x,y)*, and *b(x,y)*, for each individual grain kernel as color measurements.

4.2.2.4 RGB histograms An M-band histogram of an object in a digital image with gray levels in the range [*0, L-1*] is defined as a discrete function $H(k) = n_k/N$, $k = 0, 1, ..., M-1$ ($1 \leq M \leq L$); where k is the band number, n_k is the number of pixels in the object region with gray levels in the *kth* band range [$k*L/M$, $(k+1)*L/M$], and N is the total number of pixels in the object region. Because a color image consists of three gray level images, namely *R*, *G*, and *B* images, correspondingly three *M*-band histograms, $H_R(k)$, $H_G(k)$, and $H_B(k)$, of an object in a color image can be obtained from the three gray level images. These histograms provide a global description of the object's color appearance. The selection of the number of bands, *M* depends on specific applications. Generally, the larger the *M*, more precise is the description of the object's color appearance. However, when the histograms are used as color features to represent color differences between different objects, this statement is not always true. In addition a larger *M* means a larger number of measurements. Luo et al.

(1999a) conducted a study to compare histograms with M = 8, 16, and 32, by examining the significance of the corresponding measurements to the classification of the different types of cereal grains. They found that the 16-band histogram gave the best measurements. Thus a value of M = 16 was used in this study.

A list of the 123 color measurements extracted from an individual grain kernel is given in Table B2 (Appendix B).

4.2.3 Textural features Texture can be defined as the distribution of color in an image with respect to the spatial coordinates. It can be qualitatively evaluated as having one or more of the properties of fineness, coarseness, smoothness, granulation, randomness, or irregular (Majumdar and Jayas 2000c). Two objects, in their digital image form, can be comprised of same number of pixels and exactly same color histograms but if the distribution of color is dissimilar, they can have totally different appearance. These two objects, if classified using simple color features, would be classified as similar objects.

There have been many statistical and structural approaches to the measurement and characterization of image texture: autocorrelation functions, autoregressive models, optical transforms, digital transforms, structural elements, spatial gray tone co-occurrence probabilities, gray level run lengths, and sum and differences histograms (Haralick 1979). In this study, gray level co-occurrence matrix (GLCM) and gray level run-length matrix (GLRM) models were used.

4.2.3.1 Gray level co-occurrence matrix model This model was first described by Haralick et al. (1973). It provides information about the distribution of gray level intensities with respect to the relative position of the pixels with equal intensities. The matrix elements M

(i, j) are the number of occurrence of pixels with gray level *i* encircled by pixels with gray level *j* at a distance *d* in 0°, 45°, 90°, and 135° directions (Fig. 4.4a). Considering a 4 x 4 image with gray levels in the range 0 to 3 (Fig. 4.4b), the co-occurrence matrices in the 0°, 45°, 90°, and 135° directions are shown in Fig. 4.4c.

The co-occurrence matrices in the four directions are combined (Fig. 4.4d) and each element was divided using a normalizing constant, *k* given by:

$$k = 2N_x(N_y - 1) + 2N_y(N_x - 1) + 4(N_x - 1)(N_y - 1) \tag{4.22}$$

where N_x and N_y are the number of pixels in the horizontal and vertical directions, respectively.

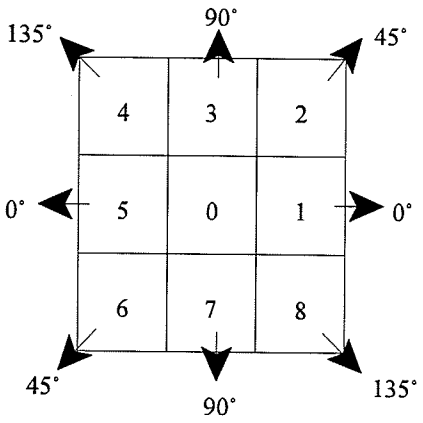

(a)

0	0	1	1
0	0	1	1
0	2	2	2
2	2	3	3

(b)

At 0°, M =
$$\begin{matrix} 4 & 2 & 1 & 0 \\ 2 & 4 & 0 & 0 \\ 1 & 0 & 6 & 1 \\ 0 & 0 & 1 & 2 \end{matrix}$$

At 90°, M =
$$\begin{matrix} 6 & 0 & 2 & 0 \\ 0 & 4 & 2 & 0 \\ 2 & 2 & 2 & 2 \\ 0 & 0 & 2 & 0 \end{matrix}$$

At 135°, M =
$$\begin{matrix} 2 & 1 & 3 & 0 \\ 1 & 2 & 1 & 0 \\ 3 & 1 & 0 & 2 \\ 0 & 0 & 2 & 0 \end{matrix}$$

At 45°, M =
$$\begin{matrix} 4 & 1 & 0 & 0 \\ 1 & 2 & 2 & 0 \\ 0 & 2 & 4 & 1 \\ 0 & 0 & 1 & 0 \end{matrix}$$

(c)

		Gray level			
		0	**1**	**2**	**3**
Gray level	**0**	16	4	6	0
	1	4	12	5	0
	2	6	5	12	6
	3	0	0	6	2

(d)

Fig. 4.4 (a) Eight nearest-neighbor resolution cells (b) A 4 x 4 image with 0 to 3 gray level values (c) Calculation of gray level co-occurrence matrices (GLCMs) in four directions (d) Final GLCM

From the normalized co-occurrence matrix, the following invariant features were calculated (Galloway 1975):

Mean

$$\mu = \sum_{i=1}^{N_g} \sum_{j=1}^{N_g} iM(i,j) \tag{4.23}$$

Variance

$$\sigma^2 = \sum_{i=1}^{N_g} \sum_{j=1}^{N_g} (i-\mu)^2 M(i,j) \tag{4.24}$$

Uniformity

$$U = \sum_{i=1}^{N_g} \sum_{j=1}^{N_g} M(i,j)^2 \tag{4.25}$$

Entropy

$$E = -\sum_{i=1}^{N_g} \sum_{j=1}^{N_g} M(i,j)\log\{M(i,j)\} \tag{4.26}$$

Inertia

$$I = \sum_{i=1}^{N_g} \sum_{j=1}^{N_g} (i-j)^2 M(i,j) \tag{4.27}$$

Correlation

$$C = \sum_{i=1}^{N_g} \sum_{j=1}^{N_g} \frac{(i-\mu)(j-\mu)}{\sigma^2} M(i,j) \tag{4.28}$$

Homogeneity

$$H = \sum_{i=1}^{N_g} \sum_{j=1}^{N_g} \frac{M(i,j)}{[1+(i-j)^2]} \tag{4.29}$$

Cluster

$$c = \sum_{i=1}^{N_g} \sum_{j=1}^{N_g} (i+j-2\mu)^3 M(i,j) \tag{4.30}$$

where N_g is the maximum gray level of the image.

4.2.3.1 Gray level run-length matrix model Gray level run length matrix (GLRM) is a representation of the occurrence of collinear and consecutive pixels of similar gray levels in an object. The matrix elements *RM(i, j)* specifies the number of times that picture contains a run of length *j*, in a given direction, consisting of points having gray level *i* (or lying in the gray level range *i*). Figure 4.5 shows the calculation of GLRMs for a 4 x 4 image consisting of three gray levels, for the four principal directions (0°, 45°, 90°, and 135°).

0	0	3	1
0	1	1	1
2	2	3	3
2	2	3	1

(a)

At 0°, RM =
$$\begin{matrix} 1 & 1 & 0 & 0 \\ 2 & 0 & 1 & 0 \\ 0 & 2 & 0 & 0 \\ 2 & 1 & 0 & 0 \end{matrix}$$

At 45°, RM =
$$\begin{matrix} 1 & 1 & 0 & 0 \\ 3 & 1 & 0 & 0 \\ 2 & 1 & 0 & 0 \\ 2 & 1 & 0 & 0 \end{matrix}$$

At 90°, RM =
$$\begin{matrix} 1 & 1 & 0 & 0 \\ 3 & 1 & 0 & 0 \\ 0 & 2 & 0 & 0 \\ 2 & 1 & 0 & 0 \end{matrix}$$

At 135°, RM =
$$\begin{matrix} 3 & 0 & 0 & 0 \\ 5 & 0 & 0 & 0 \\ 2 & 1 & 0 & 0 \\ 4 & 0 & 0 & 0 \end{matrix}$$

(b)

		Run length			
		1	**2**	**3**	**4**
Gray level	**0**	6	3	0	0
	1	13	2	1	0
	2	4	6	0	0
	3	10	3	0	0

(c)

Fig. 4.5 (a) A 4 x 4 image with 0 to 3 gray level values (b) Calculation of gray level run length matrices (GLRMs) in four directions (c) Final GLRM

The following features were extracted from all four GLRMs and their mean value and range were calculated for analyses (Galloway 1975):

Short Run

$$S = \sum_{i=1}^{N_g} \sum_{j=1}^{N_r} \frac{RM(i,j)}{j^2} R \tag{4.31}$$

Long Run

$$L = \sum_{i=1}^{N_g} \sum_{j=1}^{N_r} \frac{j^2 RM(i,j)}{R} \tag{4.32}$$

Gray level non-uniformity

$$G_{nu} = \sum_{i=1}^{N_g} \frac{\{\sum_{j=1}^{N_r} RM(i,j)\}^2}{R} \tag{4.33}$$

Run length non-uniformity

$$R_{nu} = \sum_{j=1}^{N_r} \frac{\{\sum_{i=1}^{N_g} RM(i,j)\}^2}{R} \tag{4.34}$$

Run percent

$$R_p = \frac{R}{\sum_{i=1}^{N_g} \sum_{j=1}^{N_r} jRM(i,j)} \tag{4.35}$$

Gray level entropy

$$E_{gl} = \sum_{i=1}^{N_g} \sum_{j=1}^{N_r} \frac{RM(i,j)\log\{RM(i,j)\}}{R} \tag{4.36}$$

where N_r is the maximum number of run lengths in an image, and

$$N_r = \sum_{i=1}^{N_g} \sum_{j=1}^{N_r} RM(i,j) \tag{4.37}$$

Table B3 (Appendix B) lists the 56 textural features that were extracted from each individual grain kernel.

5. RESULTS AND DISCUSSION

5.1 Gray Level Reduction for Textural Features

In applications like online monitoring of grains, computational time is of essence. Depending on the type of application, a small amount of performance can be sacrificed to reduce the computational time. In this thesis, the computational time was a direct consequence of the number of maximum gray levels in an image because the size of co-occurrence and run-length matrices depended on gray levels.

Before starting the actual analysis of data, a preliminary study was conducted to find out the number of gray levels to which the original 256 gray levels of the image can be reduced, without incurring a significant loss in the classification accuracy. Maximum gray level values of 256 were reduced to 128, 64, 32, 16, and 8 for all the three bands (i.e., red, green, and blue) in each image. All the 56 textural features were extracted for 600 kernels of every grain type (3000 kernels in total) and classification accuracies were obtained. A four-layer BPN with 56 neurons in the input layer, 30 neurons in each of the two hidden layers, and 5 neurons in the output layer, was used for classification. Training was done on 900 kernels and 600 were used for testing. The experiment was replicated three times. The network was trained until 1000 epochs were reached. Once the network was trained, it was applied to a production (validation) set consisting of the remaining 1500 kernels. The average classification accuracies of the three replicates obtained for each grain type at 256, 128, 64, 32, 16, and 8 gray levels are given in Table C1 through C6 (Appendix C). Table 5.1 shows a summary of classification accuracies. Although there was no clear pattern as the number of gray levels were increased from 8 to 256, gray levels of 32 and 64 seemed to give

slightly better results. And because 32 gray levels involved lesser computational complexity, they were chosen for extracting the textural features for further analyses of data in the thesis. At higher gray level values (e.g., 256 and 128) the image is highly textured and the tonal primitives cannot be characterized where as at lower gray levels (e.g., 16 and 8) there is too much loss of textural information from the image.

5.2 Grain Type Identification of Individual Kernels

5.2.1 Morphological feature model A complete set of 51 morphological features was used for classification of the five grain types using neural network and statistical classifiers.

5.2.1.1 Neural network classifier The BPN had 51 neurons in the input layer, 58 neurons in each of the hidden layers, and five neurons in the output layer. The network took approximately 11.5 h to train. The classification accuracies based on morphological features using a BPN classifier are shown in Table 5.2. It is evident from Table 5.2 that barley and CWRS wheat could be described better on the basis of their shape and size alone, as compared to the other grain classes. The lower classification accuracy of CWAD wheat indicates that there is little consistency in shape and size of its kernels.

The network also gave the ranking of the contribution the input features made to the classification process. Table 5.3 gives the top 20 features ranked in order of their decreasing contribution to the classification process. The contribution of the perimeter to the classification process was much higher as compared to any other feature. It was followed by mean radius and area. Although 13 of the top 20 features were independent of the size of the kernels, the top three features did however depend on the size. This means that the

size of the kernel cannot be discounted and shape alone is not the best classification parameter.

Table 5.1 Classification accuracies of cereal grains at different gray levels

Grain type	Number of Gray Levels					
	8	16	32	64	128	256
Barley	88.5	89.4	89.3	90.5	89.2	90.1
CWAD	93.2	91.0	91.7	92.1	91.4	92.5
CWRS	87.2	89.4	88.6	88.4	87.9	84.6
Oats	94.6	95.4	96.8	96.9	96.6	96.7
Rye	93.1	95.3	94.5	95.9	93.9	94.9

Table 5.2 Classification accuracies of cereal grains obtained using a BPN classifier with morphological features as inputs

Grain type	Classification accuracies for 5 validation sets, %					
	1	2	3	4	5	Mean
Barley	95.9	96.0	97.0	96.3	97.2	96.5
CWAD	90.3	88.0	90.0	88.7	90.0	89.4
CWRS	98.7	99.2	98.9	98.0	96.6	98.3
Oats	93.4	94.2	97.2	95.9	94.4	95.0
Rye	92.4	92.7	92.3	93.8	92.8	92.8

Table 5.3 The top 20 morphological, color, and textural features based on their respective contribution towards classification accuracy for cereal grains while using a BPN classifier

Rank	Feature set		
	Morphological	**Color**	**Textural**
1	Perimeter	Red moment 1	Green GLCM mean
2	Mean radius	Red moment 2	Green GLCM cluster shade
3	Area	Green moment 2	Green GLRM runpercent
4	Boundary FD 2	Blue histogram range 1	Green GLCM variance
5	Minor axis length	Red moment 3	Blue GLCM mean
6	Boundary FD 18	Blue moment 1	Green GLCM correlation
7	Radial FD 2	Hue mean	Green GLRM long run
8	Radial FD 3	Blue variance	Blue GLRM color non-uniformity
9	Shape moment 3	Saturation mean	Green GLCM entropy
10	Boundary FD 5	Blue mean	Green GLRM short run
11	Boundary FD 17	Red histogram range 9	Green GLRM run length non-uniformity
12	Shape moment 4	Green variance	Blue GLCM correlation

...continued

Table 5.3 The top 20 morphological, color, and textural features based on their respective contribution towards classification accuracy for cereal grains while using a BPN classifier

Rank	Feature set		
	Morphological	**Color**	**Textural**
13	Radial FD 5	Red variance	Blue GLRM short run
14	Minimum radius	Blue range	Red GLCM homogeneity
15	Major axis length	Red histogram range 10	Blue GLCM variance
16	Boundary FD 20	Green histogram range 1	Red GLCM variance
17	Boundary FD 1	Green moment 1	Gray GLRM run length non-uniformity
18	Boundary FD 3	Red range	Blue GLRM runpercent
19	Maximum radius	Green range	Red GLRM run length non-uniformity
20	Boundary FD 12	Red histogram range 11	Blue GLRM run length non-uniformity

5.2.1.2 Statistical classifier Classification accuracies obtained using a non-parametric statistical classifier are shown in Table 5.4. Canada Western Red Spring wheat followed by barley were classified the best using the statistical classifier. The results of the non-parametric classifier were inferior to those of the BPN classifier for all the grain types except for CWAD (Fig. 5.1).

With a minimum significant level of 0.15, procedure STEPDISC of SAS was used to find out the relative importance of the input features in the classification process. Table 5.5 shows the rankings of input features in descending order of their contribution to the discriminatory power of the model. The top 20 features had 14 shape and 6 size features. However the ranking of the features with the non-parametric classifier was different from that obtained with the BPN classifier.

Table 5.4 Classification accuracies of cereal grains obtained using a non-parametric classifier with morphological features as inputs

Grain type	Classification accuracies for five validation sets, %					
	1	2	3	4	5	Mean
Barley	93.8	94.1	92.0	92.4	93.5	93.2
CWAD	91.4	91.0	90.8	90.0	90.1	90.7
CWRS	96.2	97.4	97.5	97.0	96.8	97.0
Oats	89.4	90.1	94.4	92.1	90.9	91.4
Rye	89.6	90.6	92.0	91.9	92.7	91.4

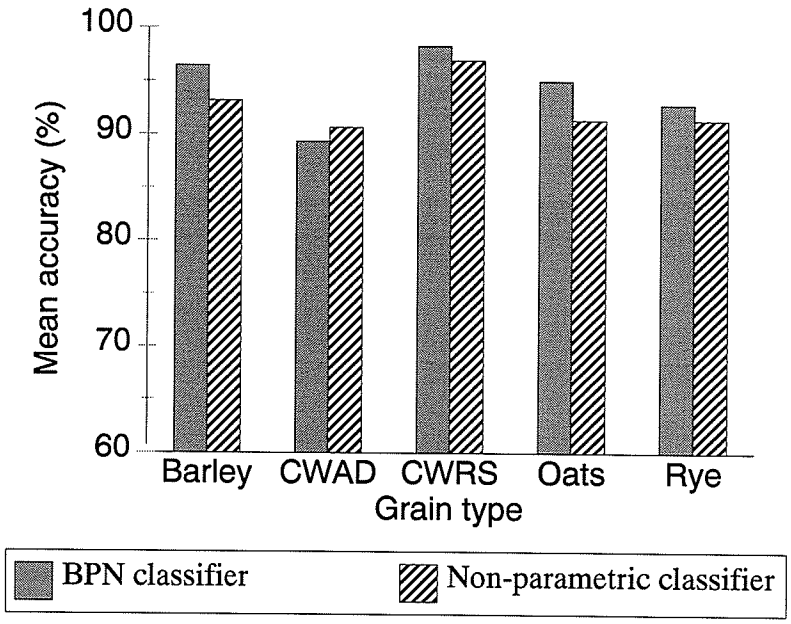

Fig. 5.1 Comparison of classification accuracies of the BPN and non-parametric classifier with morphological features as inputs

For both the neural network and statistical classifier, using morphology alone, the classification accuracies of CWAD wheat were very low. This can be attributed to the fact that the smaller and immature kernels of CWAD wheat are very close in shape and size to CWRS wheat kernels. Misclassification due to close morphological resemblance between CWAD and CWRS wheats was also reported by Majumdar et al. (2000a). It is also speculated that because of its distinct color and texture, the classification accuracy of rye would improve when color and texture are included in the feature model.

Table 5.5 The top 20 morphological, color, and textural features based on their respective contribution towards classification accuracy for cereal grains while using a non-parametric classifier

Rank	Feature set		
	Morphological	**Color**	**Textural**
1	Minor axis length	Red moment 2	Red GLRM entropy
2	Boundary FD 18	Saturation mean	Green GLRM long run
3	Radial FD 2	Green mean	Red GLRM color non-uniformity
4	Radial FD 7	Red moment 1	Green GLRM run length non-uniformity
5	Shape moment 2	Red mean	Green GLCM inertia
6	Major axis length	Green range	Blue GLCM mean
7	Shape moment 1	Blue range	Green GLCM variance
8	Area	Blue histogram range 1	Red GLRM runpercent
9	Boundary FD 6	Red variance	Blue GLRM color non-uniformity
10	Maximum radius	Red moment 3	Red GLCM variance
11	Radial FD 3	Red histogram range 22	Red GLCM homogeneity

...continued

Table 5.5 The top 20 morphological, color, and textural features based on their respective contribution towards classification accuracy for cereal grains while using a non-parametric classifier

Rank	Feature set		
	Morphological	**Color**	**Textural**
12	Perimeter	Blue histogram range 4	Blue GLRM entropy
13	Boundary FD 3	Green variance	Blue GLCM variance
14	Radial FD 4	Green moment 2	Red GLRM run length non-uniformity
15	Boundary FD 17	Green moment 1	Green GLRM runpercent
16	Shape moment 3	Blue variance	Green GLRM short run
17	Minimum radius	Red moment 4	Blue GLRM short run
18	Boundary FD 9	Blue histogram range 8	Green GLCM mean
19	Boundary FD 2	Red histogram range 6	Green GLRM entropy
20	Boundary FD 10	Blue histogram range 5	Red GLCM mean

5.2.2 Color feature model This model used all the 123 color features that were extracted for the grain kernels. Neural network and non-parametric classifiers were used to determine the classification accuracies.

5.2.2.1 Neural network classifier The BPN had 123 neurons in the input layer, 76 neurons in each of the hidden layers, and five neurons in the output layer. The network took approximately 64 h to train. The classification accuracies based on color features using a BPN classifier are shown in Table 5.6. Classification accuracy of CWRS wheat was very high using the color features. All the other grain types showed low to moderate classification results. The rankings of the contribution of color features to the classification process are given in Table 5.3. It is evident that the moments play a very significant role in the classification process. Four out of the top five color features were based on color moments. Although there were a lot of histogram features, their contribution to the classification was not very important with only five histogram features making it to the top 20 list of features. In an earlier study, Luo et al. (1999a) also found that the histogram features contributed very little to the classification process.

5.2.2.2 Statistical classifier Classification accuracies obtained using a non-parametric statistical classifier are shown in Table 5.7. It is evident that the classification accuracies with the statistical classifier were very low for all the grain types except for CWRS wheat. Figure 5.2 shows a comparison of the statistical classifier with its BPN counterpart.

Procedure STEPDISC of SAS was used to find out the relative importance of the input features in the classification process. Table 5.5 shows the rankings of color features in descending order of their contribution to the discriminatory power of the model. Out of

the three color bands, the red band contributed the most to the classification with eight red band features in the top 20 list followed by five features of green and six of the blue bands (the remaining one being mean saturation). Statistical parameters such as mean, variance, and range of the various color bands also contributed to the classification.

Table 5.6 Classification accuracies of cereal grains obtained using a BPN classifier with color features as inputs

Grain type	Classification accuracies for five validation sets, %					
	1	2	3	4	5	Mean
Barley	94.0	93.1	95.1	92.5	94.2	93.8
CWAD	90.5	92.2	93.4	95.2	93.3	92.9
CWRS	99.1	98.5	99.4	99.3	98.7	99.0
Oats	92.4	93.8	94.1	93.4	90.8	92.9
Rye	95.4	94.8	95.4	91.8	94.9	94.5

Table 5.7 Classification accuracies of cereal grains obtained using a non-parametric classifier with color features as inputs

Grain type	Classification accuracies for five validation sets, %					
	1	2	3	4	5	Mean
Barley	71.5	66.1	65.8	80.7	73.5	71.5
CWAD	81.1	80.6	81.7	73.4	78.5	79.1
CWRS	93.6	90.3	90.9	93.0	93.7	92.3
Oats	60.7	68.1	74.5	67.2	63.5	66.8
Rye	87.7	91.2	91.4	81.8	86.7	87.8

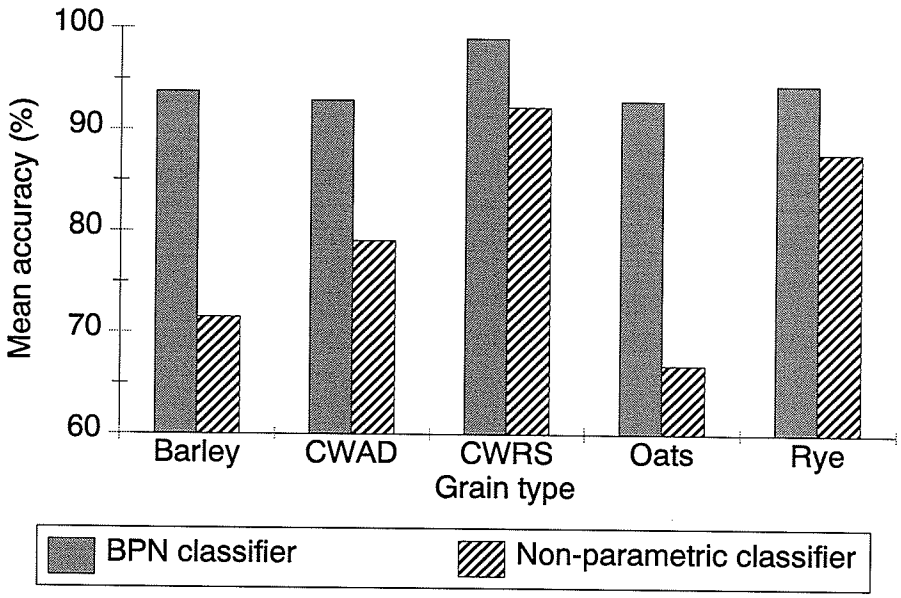

Fig. 5.2 Comparison of classification accuracies of the BPN and non-parametric classifier with color features as inputs

The non-parametric classifier's performance using color features was very inferior to its BPN counterpart. The reason behind this can be traced back to the basic fact that the non-parametric classifier retains all the training patterns and does the comparison when an unknown pattern is presented to it. In this case, because of a large number of features (multi-dimensional pattern space), it was very difficult for the classifier to process the information which resulted in a poor classification. The BPN classifier does not suffer from this shortcoming of a non-parametric classifier, and thus performed better. Luo et al. (1999b) also proved the superiority of neural network classifier over non-parametric classifier while using color features. As speculated in section 5.2.1, the classification accuracy of rye improved using the color features. The rankings of features for both the classifiers indicate that the HSI based features are not as important as the RGB model features for classification.

5.2.3 Texture feature model This model used all the 56 textural features that were extracted for the grain kernels. The images were reduced to 32 gray levels and classification accuracies were obtained using a neural network and a statistical classifier.

5.2.3.1 Neural network classifier The BPN had 56 neurons in the input layer, 58 neurons in each of the two hidden layers, and five neurons in the output layer. The network took approximately 15 h to train. The classification accuracies based on textural features using a BPN classifier are shown in Table 5.8. The textural feature model seemed to give less variation among the classification of different grain types in comparison to morphological and color feature models where there was a large fluctuation in classification accuracies for different grain types. Figure 5.3 shows a comparison of classification accuracies using morphological, color, and textural features with a BPN classifier. The bar charts clearly indicate that none of the feature models, in themselves, were capable of classifying all the grains with a high accuracy.

The rankings of the contribution of textural features to the classification process are shown in Table 5.3. For the textural features, the green band was very important with seven out of the top 10 features coming from the green band. Apart from that there was no clear pattern in the textural features. The top 20 features had equal number of run-length and co-occurrence matrix features.

5.2.3.2 Statistical classifier Classification accuracies obtained using the non-parametric statistical classifier are shown in Table 5.9. The classification accuracies with the non-parametric classifier also showed little variation among the grain types.

Table 5.8 Classification accuracies of cereal grains obtained using a BPN classifier with textural features as inputs

Grain type	Classification accuracies for five validation sets, %					
	1	2	3	4	5	Mean
Barley	93.1	96.3	95.9	93.0	92.8	94.2
CWAD	90.6	92.8	91.8	90.8	91.6	91.5
CWRS	94.1	90.4	96.8	96.8	96.1	94.9
Oats	93.9	91.0	89.0	89.7	90.4	90.8
Rye	96.1	96.0	96.2	93.1	94.4	95.2

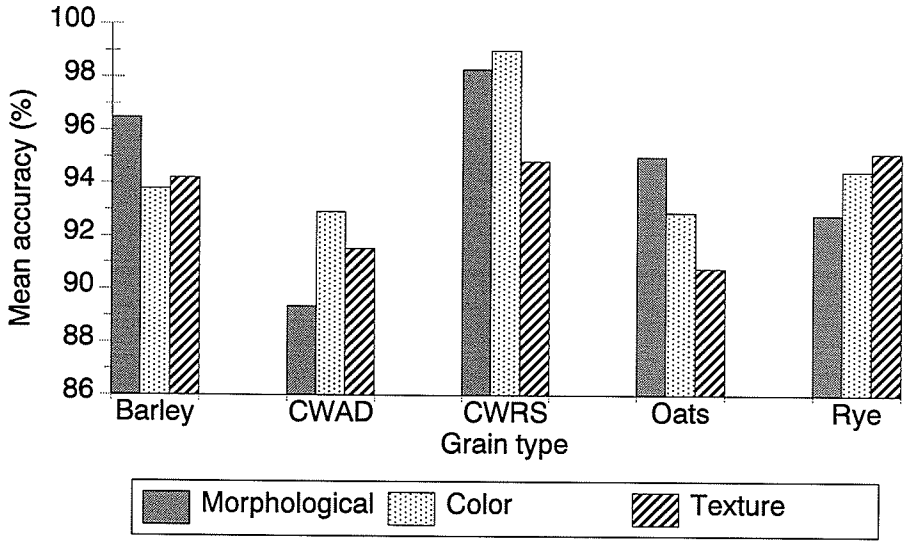

Fig. 5.3 Classification accuracies of a BPN classifier using morphological, color, and texture models

Table 5.9 Classification accuracies of cereal grains obtained using a non-parametric classifier with textural features as inputs

Grain type	Classification accuracies for five validation sets, %					
	1	2	3	4	5	Mean
Barley	91.7	91.3	90.9	90.8	92.4	91.4
CWAD	92.2	93.2	92.4	92.3	92.5	92.5
CWRS	95.2	96.3	97.0	94.7	94.6	95.6
Oats	89.8	92.2	92.7	90.7	90.0	91.1
Rye	96.9	96.9	96.2	94.4	96.5	96.2

Figure 5.4 shows a comparison of classification accuracies using morphological, color, and textural features with a non-parametric classifier. The classification accuracies obtained using the color feature model were much lower as compared to morphological or textural features. While using textural features, the non-parametric classifier gave better results than the BPN classifier for all the grain types except barley.

Procedure STEPDISC of SAS was used to find out the relative importance of the input features in the classification process. Table 5.5 shows the rankings of input features in descending order of their contribution to the discriminatory power of the model. The run-length matrices contribute more towards the classification as compared to the co-occurrence matrices. Similar to the case with the BPN classifier, the green band was more important than the red or blue bands.

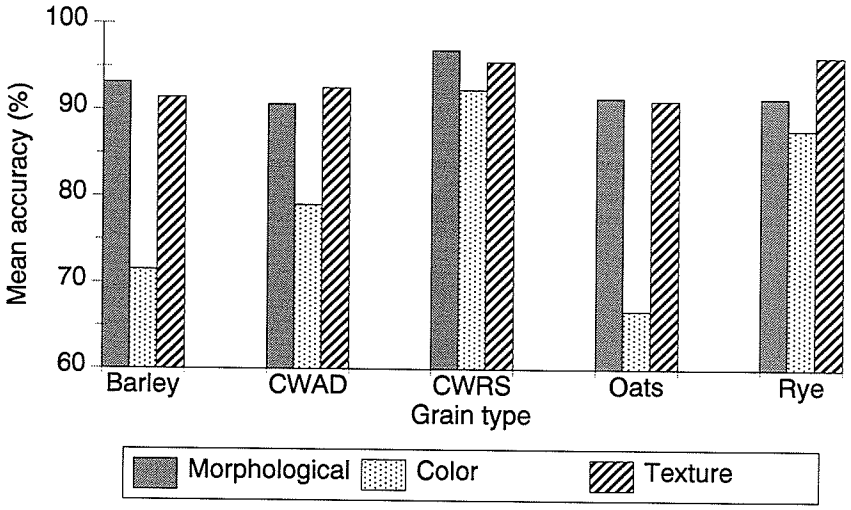

Fig. 5.4 Classification accuracies of a non-parametric classifier using morphological, color, and texture models

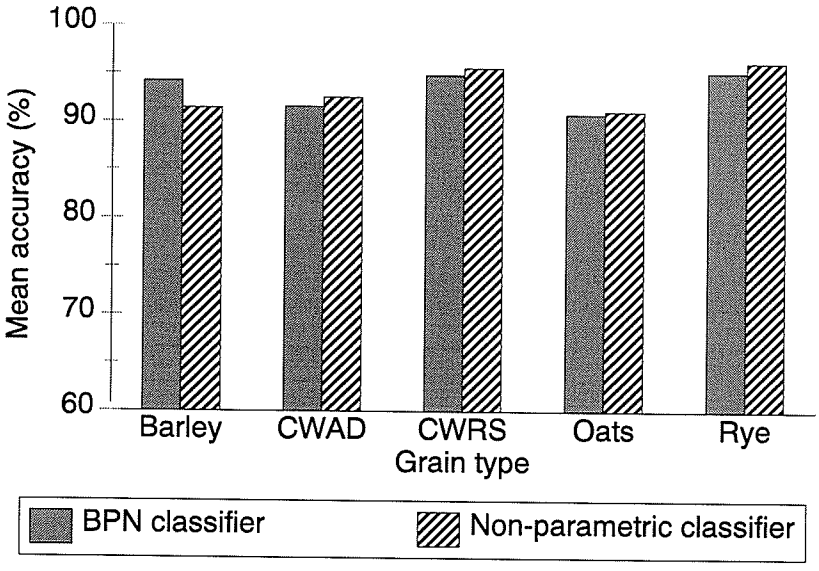

Fig. 5.5 Comparison of classification accuracies of the BPN and non-parametric classifier with texture features as inputs

5.2.4 All features model A complete set of 230 features (51 morphological, 123 color, and 56 textural) was used for classification of the five grain types using a neural network and a non-parametric statistical classifier.

5.2.4.1 Neural network classifier The BPN had 230 neurons in the input layer, 102 neurons in each of the two hidden layers and five neurons in the output layer and took approximately 75 h to train. Table 5.10 shows the summary of the classification accuracies obtained for the five cereal grain classes. Except for CWAD wheat, the classification accuracies improved considerably for all the other grain types using all features as compared to classification accuracies obtained using any one class of features. The improvement in classification accuracies is because all the three parameters, namely, morphology, color, and texture, together characterize a kernel much better than any one parameter alone. This can be seen from the rankings of the classification features for this model (Table 5.11) where all the parameters are contributing towards the classification process.

Table 5.10 Classification accuracies of cereal grains obtained using a BPN classifier with all features as inputs

Grain type	Classification accuracies for five validation sets, %					
	1	2	3	4	5	Mean
Barley	97.7	99.0	98.7	98.1	97.6	98.2
CWAD	90.5	91.7	91.9	90.2	90.4	90.9
CWRS	98.3	98.2	98.9	99.2	98.3	98.6
Oats	97.9	98.1	98.8	98.7	98.3	98.4
Rye	99.0	99.6	98.7	98.5	99.2	99.0

Table 5.11 The top 20 features based on their respective contribution towards classification accuracy for cereal grains while using BPN and non-parametric classifiers with all features as inputs

Rank	Classifier		
	Back propagation network	**Non-parametric**	**Non-parametric***
1	Hue mean	Radial FD 2	Length
2	Minor axis length	Boundary FD 18	Haralick ratio
3	Boundary FD 2	Radial FD 7	First Fourier descriptor
4	Saturation mean	Green GLCM inertia	Standard deviation of radii
5	Radial FD 2	Shape moment 2	Entropy
6	Boundary FD 20	Minor axis length	Area ratio
7	Perimeter	Saturation mean	Saturation
8	Blue GLRM short run	Green GLCM mean	Red
9	Boundary FD 18	Green range	Mean gray level
10	Green GLRM short run	Shape moment 1	Mean

* *Source:* Majumdar and Jayas (2000d)

...continued

Table 5.11 The top 20 features based on their respective contribution towards classification accuracy for cereal grains while using BPN and non-parametric classifiers with all features as inputs

Rank	Classifier		
	Back propagation network	**Non-parametric**	**Non-parametric***
11	Gray GLRM short run	Blue GLRM color non-uniformity	Radius ratio
12	Boundary FD 3	Green GLRM short run	Inertia
13	Blue histogram range 1	Blue GLRM entropy	Run-length non-uniformity
14	Radial FD 5	Radial FD 5	Run percent
15	Green GLRM runpercent	Green GLCM entropy	GLRM entropy
16	Green GLRM long run	Shape moment 3	Cluster prominence
17	Minimum radius	Red GLCM mean	Short run
18	Gray GLCM inertia	Red GLRM entropy	Blue
19	Boundary FD 16	Green GLRM runpercent	Minimum radius
20	Red GLRM short run	Boundary FD 17	Third invariant moment

* *Source:* Majumdar and Jayas (2000d)

5.2.4.2 Statistical classifier Classification accuracies obtained using the non-parametric statistical classifier are shown in Table 5.12. Once again, even for the non-parametric classifier, classification accuracies for all the grain types were better than using any one feature model by itself. The accuracies for each grain type were, however, lower than the neural network classifier (Fig. 5.6). This is because of the inherent shortcoming of a non-parametric classifier in handling a large number of input patterns. Thus, it can be safely concluded that when dealing with such a large number of input patterns, the use of a BPN network is advisable.

Procedure STEPDISC of SAS was used to find out the relative importance of the input features in the classification process. Table 5.11 shows the rankings of these features in descending order of their contribution to the discriminatory power of the model. For both the classifiers, the contribution of color features seemed to be very less as compared to the morphological or textural features. Among the top 20 features, there were only three and two color features for the BPN and non-parametric classifier, respectively. This result should be interpreted with reservation. As the contribution of textural features was substantial, it means that the spatial distribution of color played a more important part in classification rather than the color components themselves. The difference in rankings of features with the BPN and non-parametric classifiers can be attributed to their entirely different approach to the classification process.

The feature rankings for the non-parametric classifier were also compared to the previous work done by Majumdar and Jayas (2000d). In the present study, the shape features played a more important role in classification than the size features as there was not even one

size feature among the top five features. In their work, there were three features among the top five features. This can be explained by the difference in image resolution of the two studies. In the given thesis, because the resolution of the images was higher than those used by Majumdar and Jayas (2000d), the kernels were characterized by their fine boundary details. Among the textural features, the features obtained using the green band contributed more towards classification than the other two bands. This result was in accordance with the hypothesis of Majumdar and Jayas (2000d) that green band based textural features are the most important. Nevertheless, the presence of red and blue band based textural features indicates that they were important to a certain extent, both of which were not used in the earlier study.

It is also evident from Table 5.11 that, in the present thesis, textural features contributed more towards classification than color features. This, however, did not hold good in the study conducted by Majumdar and Jayas (2000d). Their study suffered from a hardware limitation where the images were captured in rectangular pixels which were then converted to square pixels using interpolation. This may have distorted the actual spatial distribution of colors in the objects which resulted in poor contribution of texture as a classification feature.

Table 5.12 Classification accuracies of cereal grains obtained using a non-parametric classifier with all features as inputs

Grain type	Classification accuracies for five validation sets, %					
	1	2	3	4	5	Mean
Barley	79.8	93.9	94.8	77.6	79.3	85.1
CWAD	85.0	92.3	92.5	87.7	86.8	88.9
CWRS	99.6	90.1	96.7	99.2	99.1	96.9
Oats	91.8	93.3	98.7	96.0	94.9	95.0
Rye	94.8	97.6	98.8	96.2	94.7	96.4

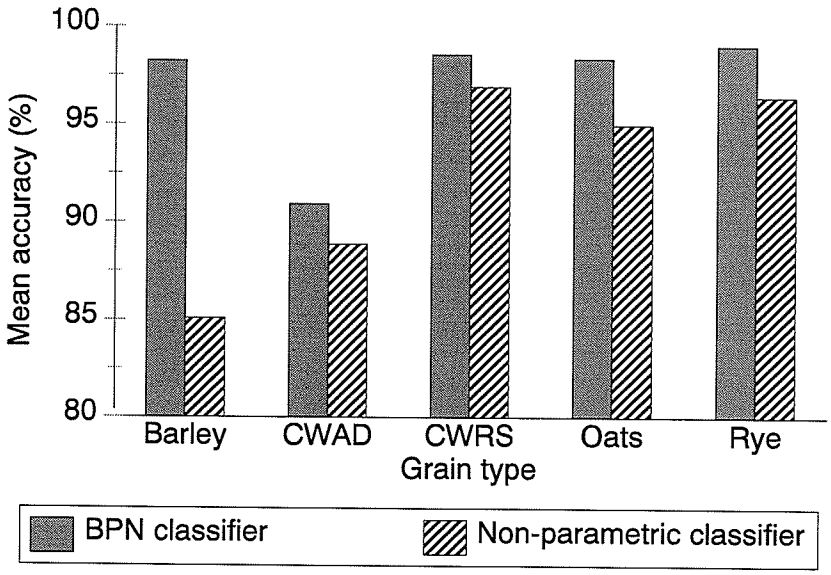

Fig. 5.6 Comparison of classification accuracies of the BPN and non-parametric classifier with all features as inputs

5.2.5 Combined 60 and top 60 features models

5.2.5.1 Neural network classifier The top 20 morphological, color, and textural features were obtained from Table 5.3 to create the combined 60 features model. This model was compared with the top 60 feature set obtained from the rankings of features obtained from the all features model. The combined 60 features model was based on the assumption that morphology, color, and texture contributed equally towards the classification process. These two reduced feature models were used to investigate if the reduction in number of features affects the classification accuracies. The networks had 60 neurons in the input layer, 60 in each of the two hidden layers and 5 neurons in the output layer and took approximately 28 h to train. Tables 5.13a and 5.13b show the classification accuracies obtained using the combined 60 and top 60 features models, respectively.

Table 5.13a indicates that a reduced set of combined features improved the classification accuracy. This can be attributed to the elimination of a lot of redundant features which did not contribute much to the classification process but induced errors in the weights on the nodes of the network instead. The top 60 features model, however, did not perform as well (Table 5.13b). The classification accuracies were lower than those obtained using the combined 60 features model. The feature rankings of the combined 60 features model (Table C7, Appendix C) show that all three classes of features (morphological, color, and texture) contributed to the classification process. Hence an optimized feature set should have all kinds of features in it.

Table 5.13a Classification accuracies of cereal grains obtained using a BPN classifier with combined 60 features as inputs

Grain type	Classification accuracies for five validation sets, %					
	1	2	3	4	5	Mean
Barley	97.6	98.8	98.0	98.5	97.7	98.1
CWAD	90.2	90.6	91.7	90.5	89.7	90.5
CWRS	98.6	98.9	98.1	98.7	99.0	98.7
Oats	97.6	98.6	99.1	98.6	97.9	98.4
Rye	98.8	99.1	99.0	98.8	98.9	98.9

Table 5.13b Classification accuracies of cereal grains obtained using a BPN classifier with top 60 features as inputs

Grain type	Classification accuracies for five validation sets, %					
	1	2	3	4	5	Mean
Barley	95.2	95.9	97.8	95.6	94.9	95.9
CWAD	83.4	84.5	88.8	85.8	85.4	85.6
CWRS	95.4	95.0	95.8	98.4	96.1	96.2
Oats	96.7	96.8	98.4	97.5	93.4	96.6
Rye	91.5	96.5	96.4	94.8	94.1	94.7

5.2.5.2 Statistical classifier The rankings of features obtained by using the morphological, color, and textural feature models were used to create the set of combined 60 features (Table 5.5). These 60 features (top 20 of each of the morphological, color, and textural classes) were used for classification using a non-parametric classifier. This combined 60 features model was compared against the top 60 feature set created using the best ranked 60 features from the all features model. Tables 5.14a and 5.14b show the results of classification using the combined 60 features and top 60 features models, respectively. Figure 5.7 shows a comparison of results obtained using the combined 60 and top 60 features models for BPN and non-parametric classifiers. Between the combined 60 and top 60 features models, the combined 60 features model gave better classification accuracies than the top 60 features model. The performance of the BPN classifier was superior to the non-parametric classifier for both combined 60 and top 60 features models.

The classification accuracy of CWAD wheat was lower than the other grain types irrespective of the classifier being used. But the classification accuracy (for CWAD wheat) did seem to improve with these 60 features in comparison to using all the features. This led us to believe that further reduction of the feature set might improve the results. This was done in the next section. The improvement in classification accuracy with a reduction in number of input features was consistent with the results obtained by Majumdar et al. (2000a, 2000b, 2000c) and Luo et al. (1999a).

Table 5.14a Classification accuracies of cereal grains obtained using a non-parametric classifier with combined 60 features as inputs

Grain type	Classification accuracies for five validation sets, %					
	1	2	3	4	5	Mean
Barley	89.2	96.3	93.8	86.5	85.9	90.4
CWAD	90.2	91.7	88.1	91.0	90.4	90.3
CWRS	99.0	98.4	89.9	99.0	98.9	97.1
Oats	94.5	97.3	96.4	95.2	95.3	95.8
Rye	98.0	98.7	98.0	97.9	97.5	98.0

Table 5.14b Classification accuracies of cereal grains obtained using a non-parametric classifier with top 60 features as inputs

Grain type	Classification accuracies for five validation sets, %					
	1	2	3	4	5	Mean
Barley	88.0	91.9	91.1	84.0	83.8	87.7
CWAD	85.4	85.6	83.0	84.4	86.7	85.0
CWRS	98.0	98.5	86.0	98.1	96.8	95.5
Oats	93.9	95.9	91.7	92.4	91.7	93.1
Rye	93.3	92.2	95.2	90.2	93.2	92.8

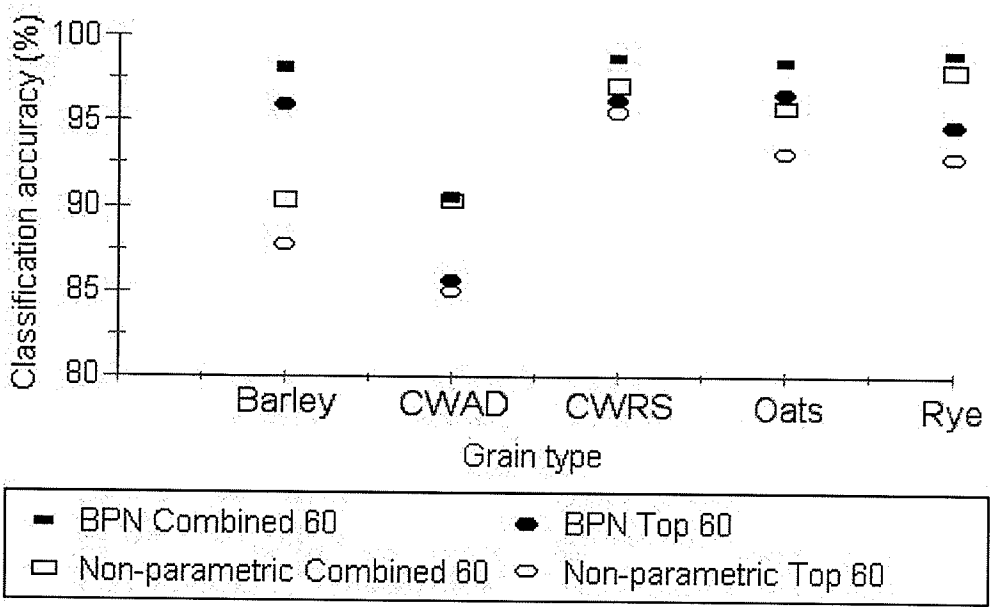

Fig. 5.7 Comparison of classification accuracies of the BPN and non-parametric classifier with combined 60 and top 60 features as inputs

5.2.6 Combined 30 and top 30 features models

5.2.6.1 Neural network classifier The top 10 morphological, color, and textural features were obtained from Table 5.3. The combined model of 30 features (10 each of the morphological, color, and textural class) was used to investigate if further reduction in number of features improves the classification accuracies. This model was also compared to the top 30 feature set consisting of the best 30 features obtained using the rankings of features from the all features model. The BPNs contained 30 neurons in the input layer, 52 neurons in each of the two hidden layers, and 5 neurons in the output layer. The training time for the network was approximately 10 h. Tables 5.15a and 5.15b show the classification accuracies obtained using the combined 30 and top 30 features models.

Table 5.15a Classification accuracies of cereal grains obtained using a BPN classifier with combined 30 features as inputs

Grain type	Classification accuracies for five validation sets, %					
	1	2	3	4	5	Mean
Barley	97.8	98.3	97.3	98.4	97.8	98.0
CWAD	89.3	90.4	91.5	90.0	89.3	90.1
CWRS	98.5	98.8	98.2	98.4	98.5	98.5
Oats	97.2	98.4	98.7	97.3	97.3	97.8
Rye	97.8	98.4	98.2	98.1	97.8	98.0

Table 5.15b Classification accuracies of cereal grains obtained using a BPN classifier with top 30 features as inputs

Grain type	Classification accuracies for five validation sets, %					
	1	2	3	4	5	Mean
Barley	95.7	91.2	93.0	89.3	89.3	91.7
CWAD	82.6	78.8	77.9	80.7	80.1	80.0
CWRS	93.7	90.2	91.8	95.3	91.7	92.5
Oats	94.9	94.7	92.5	91.9	93.9	93.6
Rye	87.2	89.3	89.7	88.0	87.9	88.4

Classification accuracies of the combined 30 features model were consistently higher than those of the top 30 features model. Therefore, it was concluded that the top 60 and top 30 features models did not perform as well when compared to the corresponding combined

features models.

Figure 5.8 shows a comparison of the classification accuracies obtained using all features, combined 60, and combined 30 features models, using a BPN classifier (for sake of clarity, the poorly performing top 60 and top 30 models not included in comparison). Analysis of variance showed that the classification accuracies shown in Fig. 5.8 were not significantly different ($P<0.05$) from each other for the respective grain types. Considering the amount of time saved in training of the network, it is advisable to use a less complicated network. In comparison to the combined 30 features model, the combined 60 features model gave slightly better classification accuracies for oats and rye. The only disadvantage of using the combined 60 features model over the combined 30 features model is that the former took about 1.5 times longer to train. So depending on whether training time is important or a higher classification accuracy is desired, the feature model can be chosen accordingly.

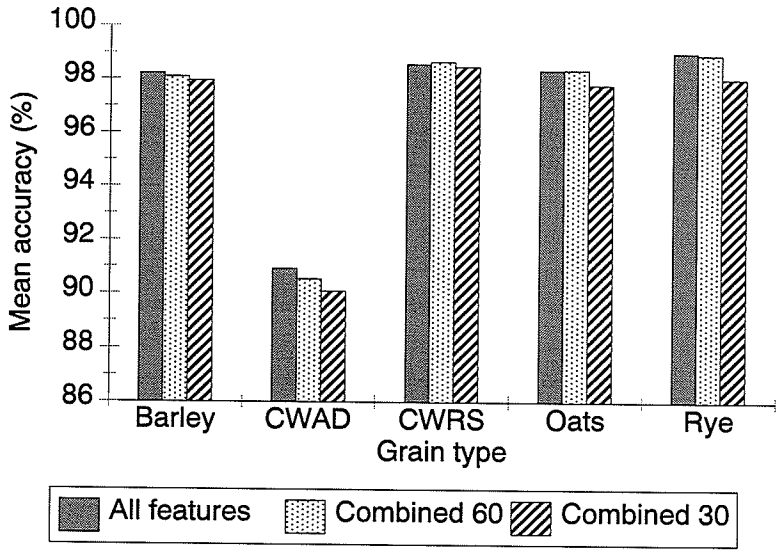

Fig. 5.8 Comparison of classification accuracies of the all features, combined 60, and combined 30 features models using a BPN classifier

5.2.6.2 Statistical classifier The combined 30 features model was created using the rankings obtained from Table 5.5. The 30 features (top 10 of each of the morphological, color, and textural classes) were used for classification using a non-parametric classifier. These were compared to the corresponding top 30 features model obtained from the feature rankings of the all features model using a non-parametric classifier. Tables 5.16a and 5.16b show the results of classification using the combined 30 and top 30 features models, respectively.

The combined 30 features model performed significantly better ($P<0.05$) than the top 30 features model (Fig. 5.9). For barley, CWRS wheat, and oats the classification accuracies of the BPN classifier were higher than the non-parametric classifier, whereas for CWAD wheat and rye the classification accuracies were very close. Thus the overall performance of BPN classifier with combined 30 features was better.

Figure 5.10 shows a comparison of the classification accuracies obtained using all features, combined 60, and combined 30 features models, with a non-parametric classifier (for sake of clarity, the poorly performing top 60 and top 30 models not included in comparison). The all features model fared badly in classifying barley and the combined 30 features model could not classify CWRS wheat as good as the other two models. For optimum performance while classifying these five grain types, the combined 60 features model is recommended.

The number of features in the classifiers were further reduced to investigate the affect on classification accuracies. When a set of 20 features was used for classification, the performance of the classifiers deteriorated drastically for both BPN and non-parametric classifiers (Tables C8 and C9 of Appendix C). This indicated that to obtain high

classification accuracies a minimum of about 30 features was necessary. Any further reduction in the number of features will have considerable adverse effect on the performance of the classifier.

Table 5.16a Classification accuracies of cereal grains obtained using a non-parametric classifier with combined 30 features as inputs

Grain type	Classification accuracies for the five validation sets, %					
	1	2	3	4	5	Mean
Barley	95.5	96.4	94.7	94.9	93.9	95.1
CWAD	89.7	91.8	90.0	90.8	90.7	90.6
CWRS	98.3	98.2	98.2	75.0	98.3	93.6
Oats	93.5	96.0	93.9	96.3	93.7	94.7
Rye	98.0	98.0	97.6	98.7	98.4	98.2

Table 5.16b Classification accuracies of cereal grains obtained using a non-parametric classifier with top 30 features as inputs

Grain type	Classification accuracies for the five validation sets, %					
	1	2	3	4	5	Mean
Barley	89.2	86.8	91.2	90.5	88.3	89.2
CWAD	77.7	80.1	80.5	81.1	85.0	80.9
CWRS	95.8	92.5	93.1	69.5	92.0	88.6
Oats	90.6	88.1	85.0	87.4	85.9	87.4
Rye	87.2	87.5	88.2	89.9	87.2	88.0

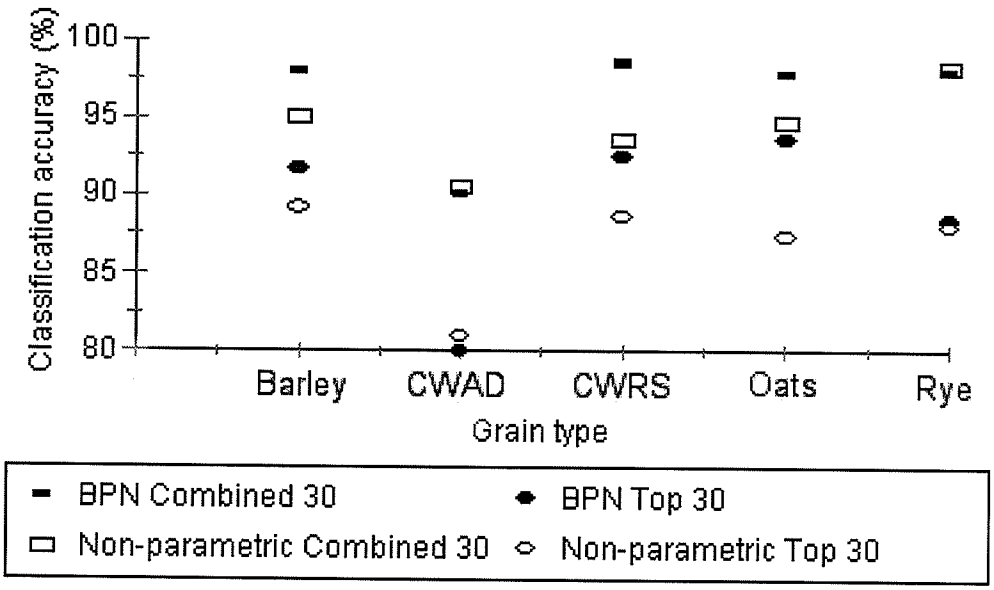

Fig. 5.9 Comparison of classification accuracies of the BPN and non-parametric classifier with combined 30 and top 30 features as inputs

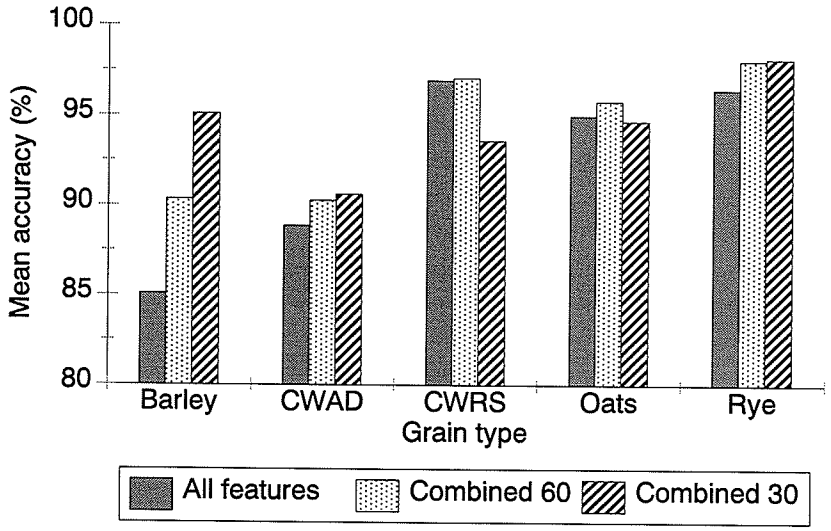

Fig. 5.10 Comparison of classification accuracies of the all features, combined 60, and combined 30 features models using a non-parametric classifier

5.3 Identification of Cereal Grains and Dockage

5.3.1 Morphological feature model A complete set of 51 morphological features was used for classification of the ten output classes (five grain types, namely, barley, CWAD wheat, CWRS wheat, oats, and rye, and five dockage fractions, namely, broken wheat kernels, chaff, wild buckwheat, wheat-heads, and canola) using neural network and statistical classifiers.

5.3.1.1 Neural network classifier The BPN had 51 neurons in the input layer, 32 neurons in each of the two hidden layers, and ten neurons in the output layer. The network took approximately 10 h to train.

The classification accuracies of the morphological model are given in Table C10 of Appendix C. The rankings of the features based on the morphological feature model using a BPN classifier are given in Tables 5.17. Among the 20 most important morphological features, although 13 were shape features, the six most important features were the size features. This is because there was a significant difference in sizes of the grain kernels and some of the dockage fractions. Hence size features were very important. In a previous study by Nair and Jayas (1998), the size features contributed more to classification than shape features.

Table 5.17 The top 20 morphological, color, and textural features based on their respective contribution towards classification accuracy for cereal grains and dockage fractions while using a BPN classifier

Rank	Feature set		
	Morphological	**Color**	**Textural**
1	Mean radius	Hue mean	Red GLRM entropy
2	Minor axis length	Red moment 1	Green GLRM entropy
3	Area	Saturation mean	Gray GLRM entropy
4	Minimum radius	Blue histogram range 1	Green GLCM cluster shade
5	Perimeter	Red mean	Blue GLCM mean
6	Major axis length	Red histogram range 7	Red GLCM correlation
7	Shape moment 4	Red moment 2	Red GLRM color non-uniformity
8	Maximum radius	Red histogram range 6	Green GLRM runpercent
9	Shape moment 3	Red histogram range 8	Blue GLRM entropy
10	Boundary FD 20	Red histogram range 9	Gray GLRM color non-uniformity
11	Boundary FD 2	Red variance	Red GLCM cluster shade

...continued

Table 5.17 The top 20 morphological, color, and textural features based on their respective contribution towards classification accuracy for cereal grains and dockage fractions while using a BPN classifier

Rank	Feature set		
	Morphological	**Color**	**Textural**
12	Radial FD 2	Green moment 1	Blue GLRM color non-uniformity
13	Boundary FD 19	Red histogram range 10	Green GLRM long run
14	Boundary FD 3	Blue histogram range 2	Green GLRM run length non-uniformity
15	Radial FD 4	Red range	Green GLRM color non-uniformity
16	Boundary FD 18	Green histogram range 1	Gray GLRM run length non-uniformity
17	Boundary FD 16	Blue moment 2	Blue GLCM entropy
18	Radial FD 19	Hue range	Red GLCM entropy
19	Radial FD 5	Red moment 3	Red GLRM run length non-uniformity
20	Radial FD 3	Green moment 2	Green GLRM short run

5.3.1.2 Statistical classifier The classification accuracies obtained using a non-parametric classifier are shown in Table C11 of Appendix C. Figure 5.11 shows the comparison of the results of the BPN and non-parametric classifier. Both the classifiers showed very similar classification accuracies. The classification of chaff was very low as compared to rest of the classes. This is because it is very difficult to classify chaff only on the basis of shape and size alone. In a two dimensional image chaff can be confused with any of the other grain types or dockage fractions. It is speculated that the classification accuracy of chaff would improve when color and textural features are also used in the classification process. Because of the uniqueness of their shape and sizes, dockage fractions like buckwheat and canola were classified with almost 100% accuracy.

The rankings of the features obtained using the procedure STEPDISC are presented in Table 5.18. Similar to the case of BPN classifier, the size features played an important role in the classification process. Size features become all the more important when the output classes vary largely in size, e.g., in this case there was a tremendous size difference in classes like wheat-heads and canola or buckwheat.

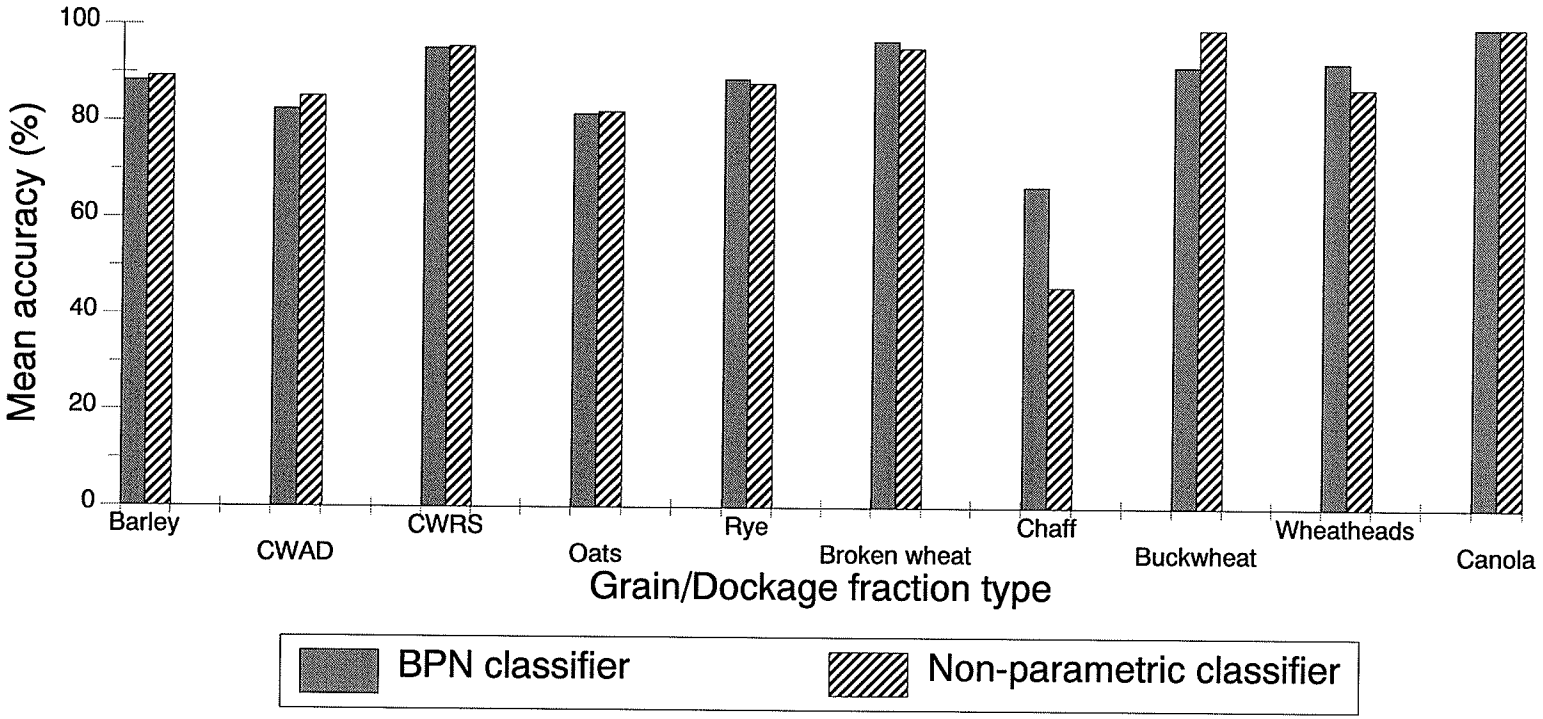

Fig. 5.11 Comparison of classification accuracies of the BPN and non-parametric classifier with morphological features as inputs

Table 5.18 The top 20 morphological, color, and textural features based on their respective contribution towards classification accuracy for cereal grains and dockage fractions while using a non-parametric classifier

Rank	Feature set		
	Morphological	**Color**	**Textural**
1	Mean radius	Hue mean	Gray GLRM long run
2	Area	Red mean	Blue GLCM mean
3	Minor axis length	Green mean	Green GLCM variance
4	Radial FD 2	Red moment 1	Red GLCM variance
5	Maximum radius	Red variance	Red GLCM cluster shade
6	Shape moment 2	Green variance	Blue GLCM variance
7	Shape moment 1	Saturation range	Red GLCM mean
8	Boundary FD 8	Saturation mean	Red GLRM run length non-uniformity
9	Perimeter	Red moment 2	Blue GLCM entropy
10	Boundary FD 2	Green range	Green GLCM entropy
11	Shape moment 4	Green moment 1	Gray GLRM entropy

...continued

Table 5.18 The top 20 morphological, color, and textural features based on their respective contribution towards classification accuracy for cereal grains and dockage fractions while using a non-parametric classifier

Rank	Feature set		
	Morphological	**Color**	**Textural**
12	Radial FD 10	Red histogram range 22	Green GLCM mean
13	Boundary FD 19	Blue histogram range 1	Blue GLCM inertia
14	Shape moment 3	Green histogram range 13	Blue GLRM run length non-uniformity
15	Radial FD 3	Blue histogram range 2	Gray GLCM entropy
16	Radial FD 15	Green moment 2	Green GLCM cluster shade
17	Radial FD 16	Blue range	Green GLRM run length non-uniformity
18	Boundary FD 1	Red histogram range 21	Red GLCM entropy
19	Boundary FD 3	Red range	Green GLCM homogeneity
20	Radial FD 6	Blue histogram range 6	Blue GLRM entropy

5.3.2 Color feature model For the color feature model, all the 123 color features were used as inputs to classify the 10 output classes using neural network and statistical classifiers.

5.3.2.1 Neural network classifier The neural network had 123 neurons in the input layer, 78 neurons in each of the two hidden layers, and 10 neurons in the output layer. The network took approximately 62.5 h for training. Table C12 (Appendix C) shows the classification accuracies of the color feature model. On the basis of color features only, the classification accuracy of oats was very low as compared to any of the other grains or dockage fractions. This is also in accordance with the poor classification accuracy of oats obtained in section 5.2.2. Buckwheat and canola showed the best classification accuracies. This can be attributed to their distinct colors. As speculated earlier, the classification accuracy of chaff improved considerably with the use of color features. The rankings of the color features are given in Table 5.17. The contribution of the red band seems to be very important for classification as seven of the top 10 features were based on the red band.

5.3.2.2 Statistical classifier The classification accuracies obtained using a non-parametric classifier are shown in Table C13 of Appendix C. The comparison of the results of the BPN and non-parametric classifier are shown in Fig. 5.12. The BPN classifier outperformed the non-parametric classifier for all the ten output classes. As stated in section 5.2.2, this can be attributed to the poor capability of non-parametric classifiers when dealing with a large number of input patterns. The classification of oats was very low as compared to rest of the classes. The rankings of the features obtained using the procedure STEPDISC are presented in Table 5.18.

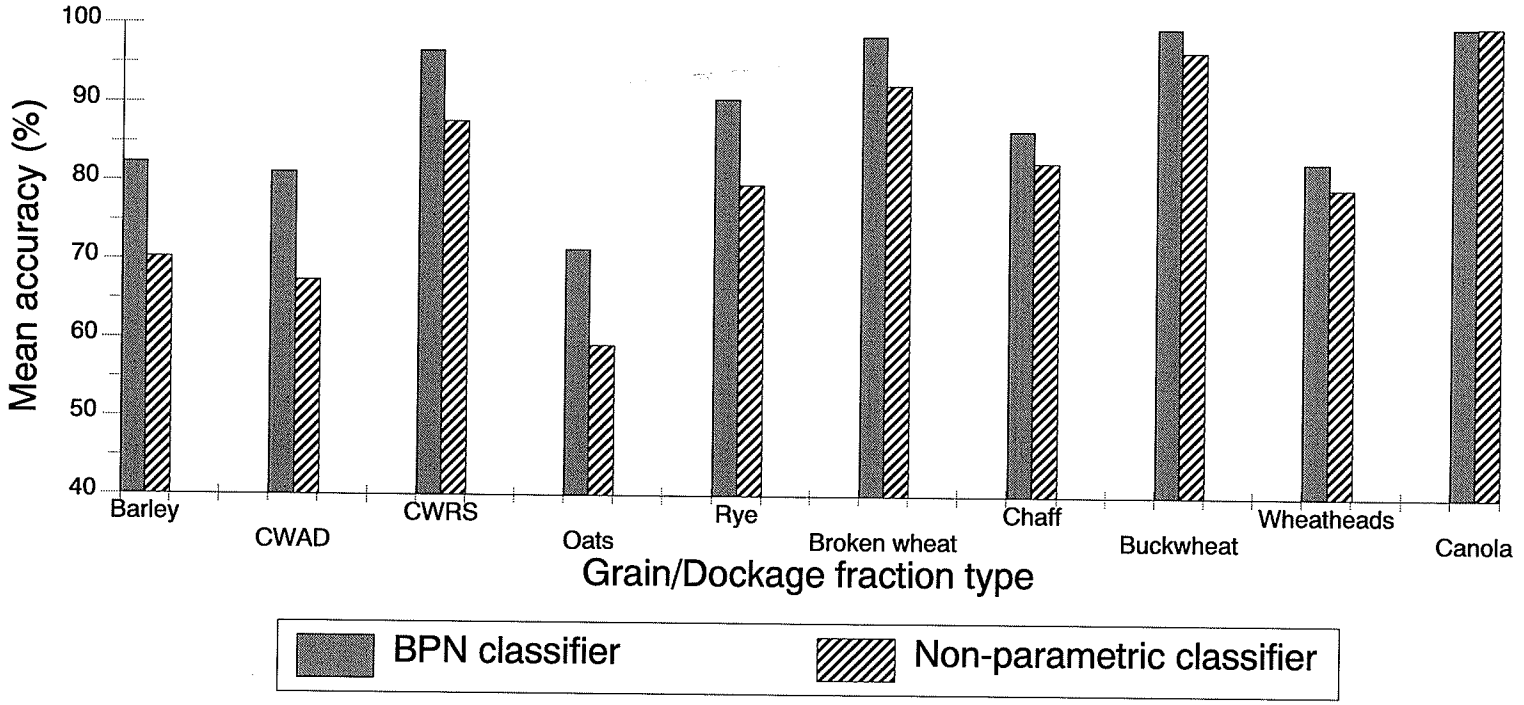

Fig. 5.12 Comparison of classification accuracies of the BPN and non-parametric classifier with color features as inputs

5.3.3 Texture feature model All the 56 textural features were used as inputs to classify the 10 output classes for this model using a BPN and a non-parametric classifier.

5.3.3.1 Neural network classifier The neural network had 56 neurons in the input layer, 38 neurons in each of the two hidden layers, and 10 neurons in the output layer. The network took approximately 10 h for training. Table C14 of Appendix C shows the classification accuracies of the texture feature model. The classification accuracy of oats was very low as compared to any of the other grains or dockage fractions which conforms with the poor results obtained for oats in section 5.2.3. The rankings of the textural features are given in Table 5.17. The contribution of the run-length matrix features seems to more important than the co-occurrence matrix features as seven of the top 10 features were run-length features.

5.3.2.2 Statistical classifier Table C15 of Appendix C shows the classification accuracies obtained using a non-parametric classifier. The comparison of the results of the BPN and non-parametric classifier are shown in Fig. 5.13. The non-parametric classifier outperformed the BPN classifier for almost all the output classes. The rankings of the features obtained using the procedure STEPDISC are presented in Table 5.18. The co-occurrence matrix features contributed more towards classification than run-length matrix features as 14 out of the top 20 features belonged to the former.

Figures 5.14 and 5.15 show the comparison of classification accuracies obtained using morphological, color, and textural feature models when using a BPN and non-parametric classifier, respectively. It is evident that none of the feature models, by itself, is good enough to classify all the cereal grains and dockage fractions. So a combination of the three models is desirable to achieve better results.

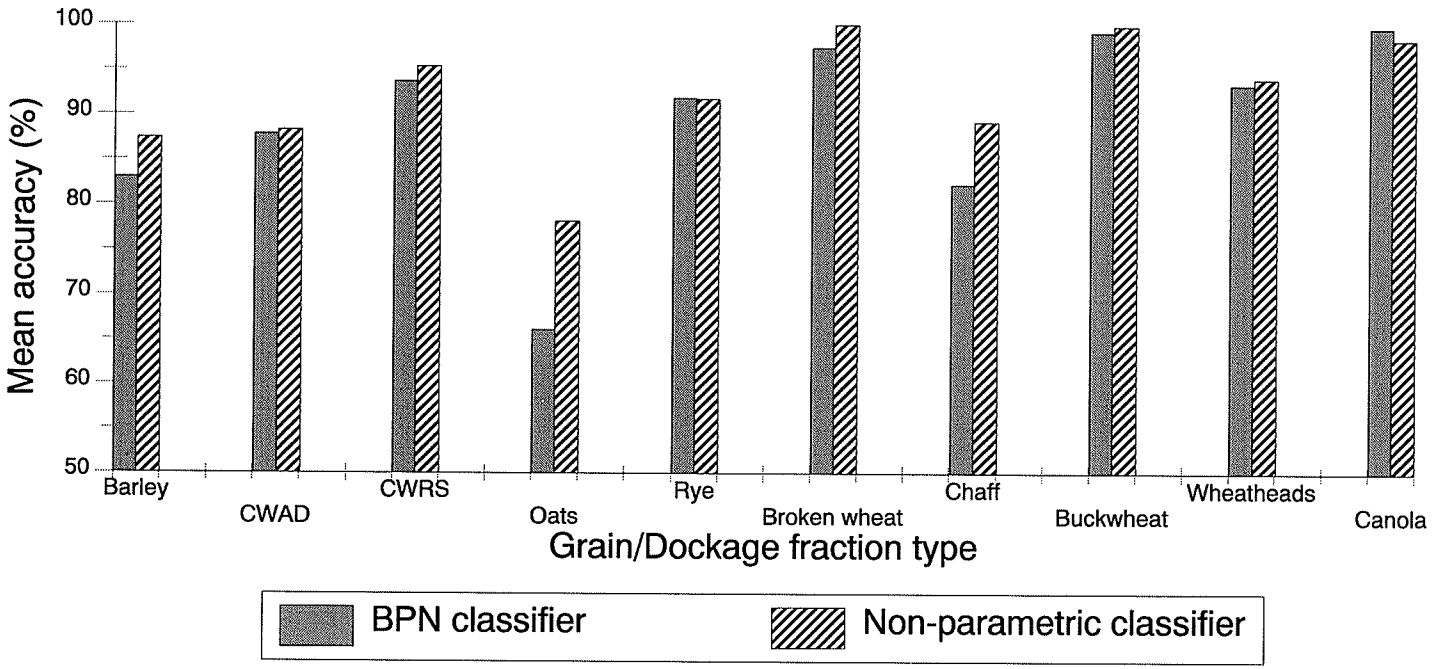

Fig. 5.13 Comparison of classification accuracies of the BPN and non-parametric classifier with textural features as inputs

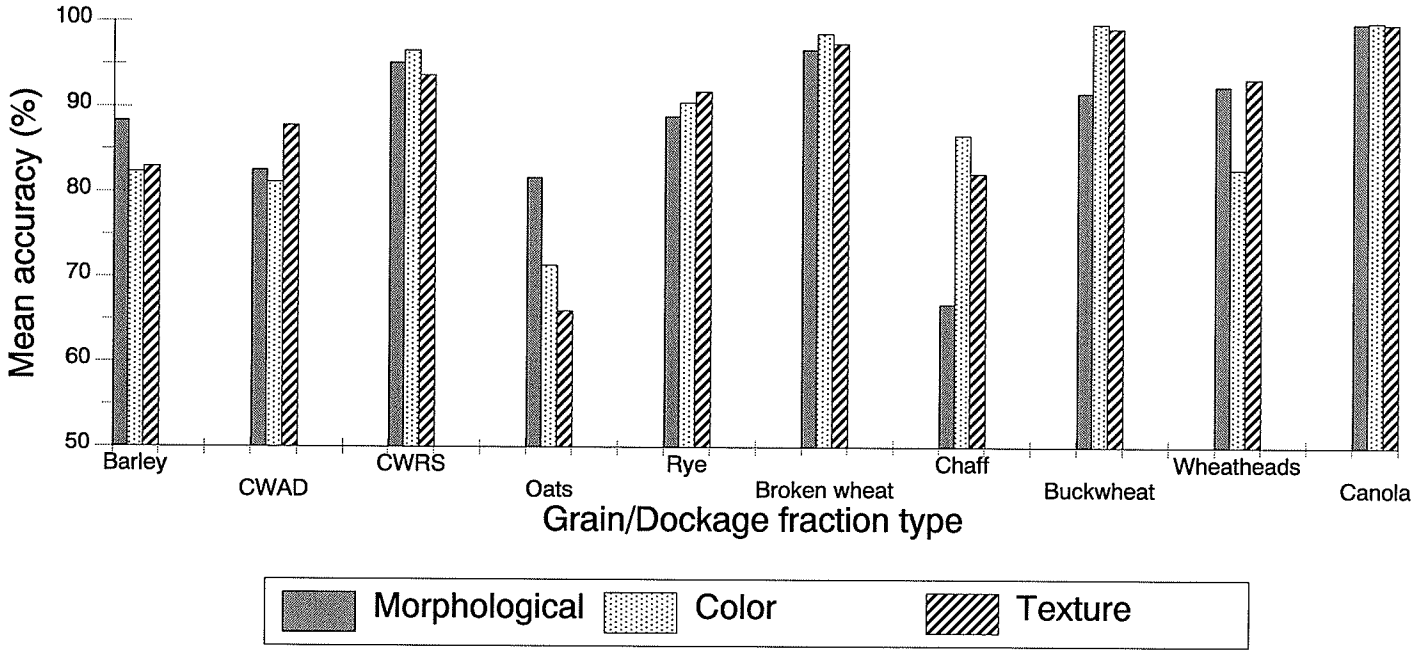

Fig. 5.14 Comparison of classification accuracies of the morphological, color, and texture feature models using a BPN classifier

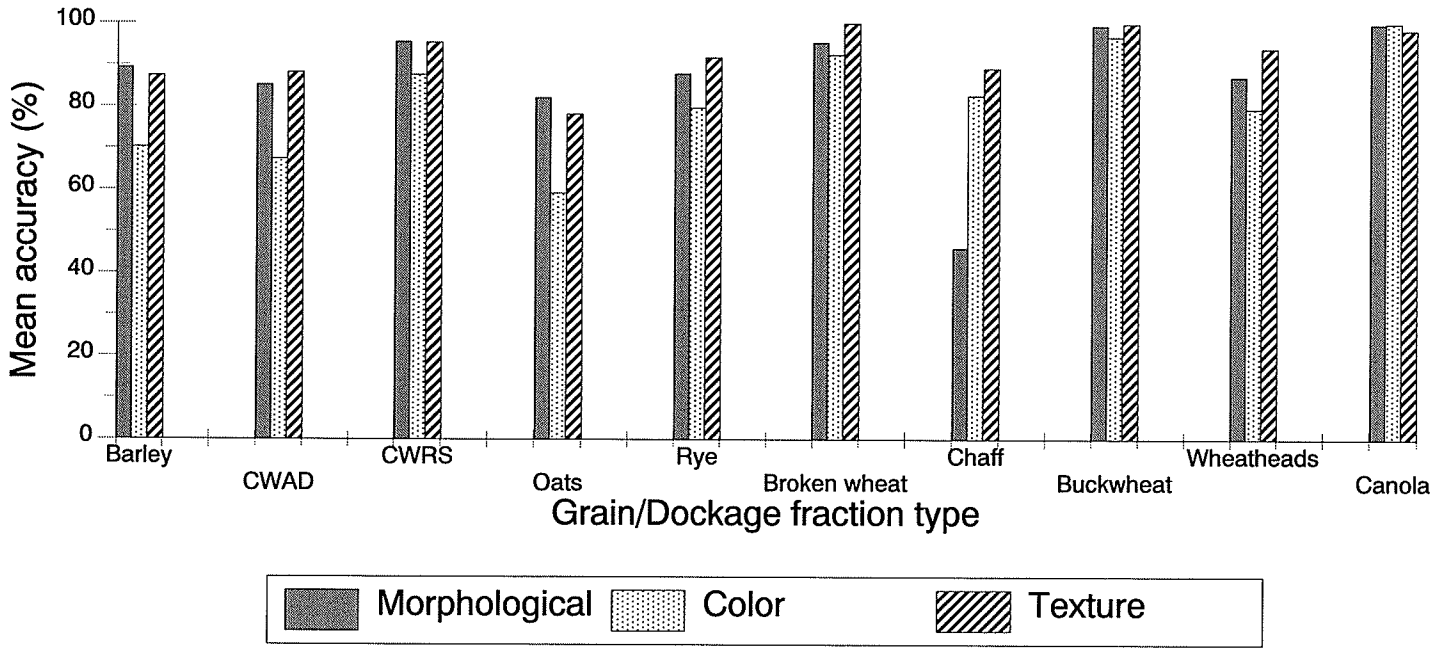

Fig. 5.15 Comparison of classification accuracies of the morphological, color, and texture feature models using a non-parametric classifier

5.3.4 All features model A complete set of 230 features (51 morphological, 123 color, and 56 textural) was used for classification of the 10 output classes using a BPN and a non-parametric classifier.

5.3.4.1 Neural network classifier The BPN had 230 neurons in the input layer, 77 neurons in each of the two hidden layers, and ten neurons in the output layer and took approximately 103 h to train. Table C16 (Appendix C) shows the summary of the classification accuracies obtained using the all features model. The accuracies of oats, chaff, and wheat-heads were still lower than the other grain types and dockage fractions, but had improved when compared to the classifications obtained using only one feature set. Broken wheat kernels, buckwheat, and canola were classified with almost 100% accuracy. The rankings of the features are given in Table 5.19. The top 20 most important features contain features from all the sets, i.e., morphological, color, and texture. Among the morphological features, however, there is only one size feature which indicates that shape is a better parameter than size when it comes to classify dockage fractions which may have a large size range.

5.3.4.2 Statistical classifier The classification accuracies obtained using a non-parametric classifier are shown in Table C17 of Appendix C. The comparison of the results of the BPN and non-parametric classifier are shown in Fig. 5.16. As expected for such a large number of input features, the BPN classifier outperformed the non-parametric classifier for almost all the output classes. The classification of oats, chaff, and wheat-heads were very low as compared to rest of the classes. The rankings of the features obtained using the procedure STEPDISC are presented in Table 5.19. The contribution of color and textural features is more than the morphological features.

Table 5.19 The top 20 features based on their respective contribution towards classification accuracy for cereal grains and dockage fractions while using BPN and non-parametric classifiers with all features as inputs

Rank	Classifier	
	Back propagation network	**Non-parametric**
1	Hue mean	Hue mean
2	Saturation mean	Red GLCM mean
3	Boundary FD 20	Green mean
4	Red GLCM correlation	Saturation mean
5	Radial FD 2	Red mean
6	Boundary FD 3	Gray GLRM long run
7	Blue histogram range 1	Blue range
8	Boundary FD 2	Minor axis length
9	Green GLRM runpercent	Red GLCM entropy
10	Blue GLRM runpercent	Intensity mean
11	Radial FD 4	Green GLCM mean
12	Minimum radius	Red moment 1
13	Red variance	Red GLCM variance
14	Gray GLRM entropy	Gray GLRM color non-uniformity
15	Gray GLRM short run	Green moment 1
16	Red GLCM cluster shade	Blue GLCM variance
17	Boundary FD 19	Red GLRM run length non-uniformity
18	Red GLRM entropy	Boundary FD 2
19	Green GLRM color non-uniformity	Radial FD 2
20	Red GLRM short run	Green GLCM homogeneity

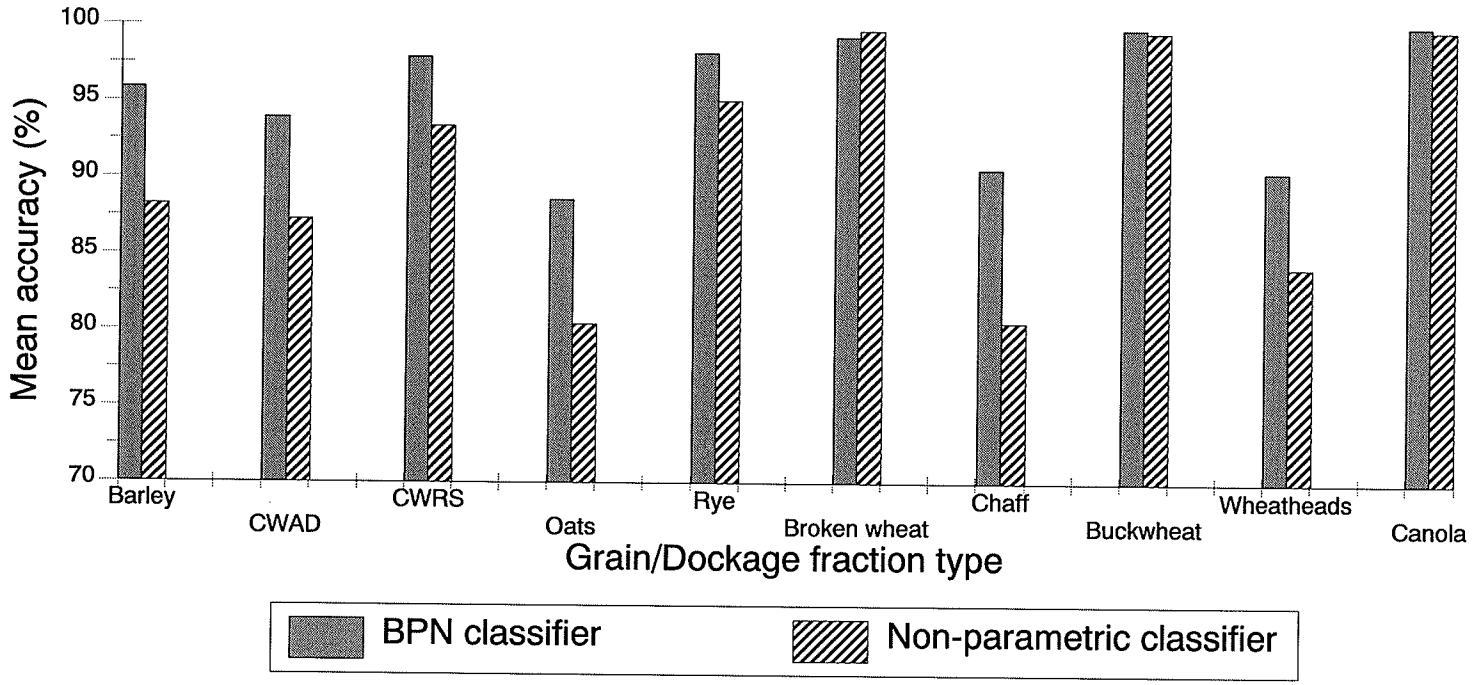

Fig. 5.16 Comparison of classification accuracies of the BPN and non-parametric classifier with all features as inputs

5.3.5 Combined 60 features model

5.3.5.1 Neural network classifier The top 20 morphological, color, and textural features were obtained from Table 5.17. This combined model of 60 features was used to investigate if a reduction in the number of features affects the classification accuracies. The network had 60 neurons in the input layer, 35 in each of the hidden layers, and 10 neurons in the output layer and took approximately 37.5 h to train. Table C18 (Appendix C) shows the classification accuracies obtained using the combined 60 features model. The classification accuracies of oats, chaff, and wheat-heads improved considerably by reducing the number of input features.

5.3.5.2 Statistical classifier The rankings of features obtained by using the morphological, color, and textural feature models were used to create this combined 60 features set (top 20 of each of the morphological, color, and textural classes, Table 5.18). Table C19 (Appendix C) shows the results of the classification accuracies using a non-parametric classifier. The comparison of the results of the BPN and non-parametric classifier are shown in Fig. 5.17. Except for the case of barley, the performance of the non-parametric classifier was inferior to that of the BPN classifier. Canola, buckwheat, CWRS wheat, and broken wheat kernels gave classification accuracies in the excess of 98%.

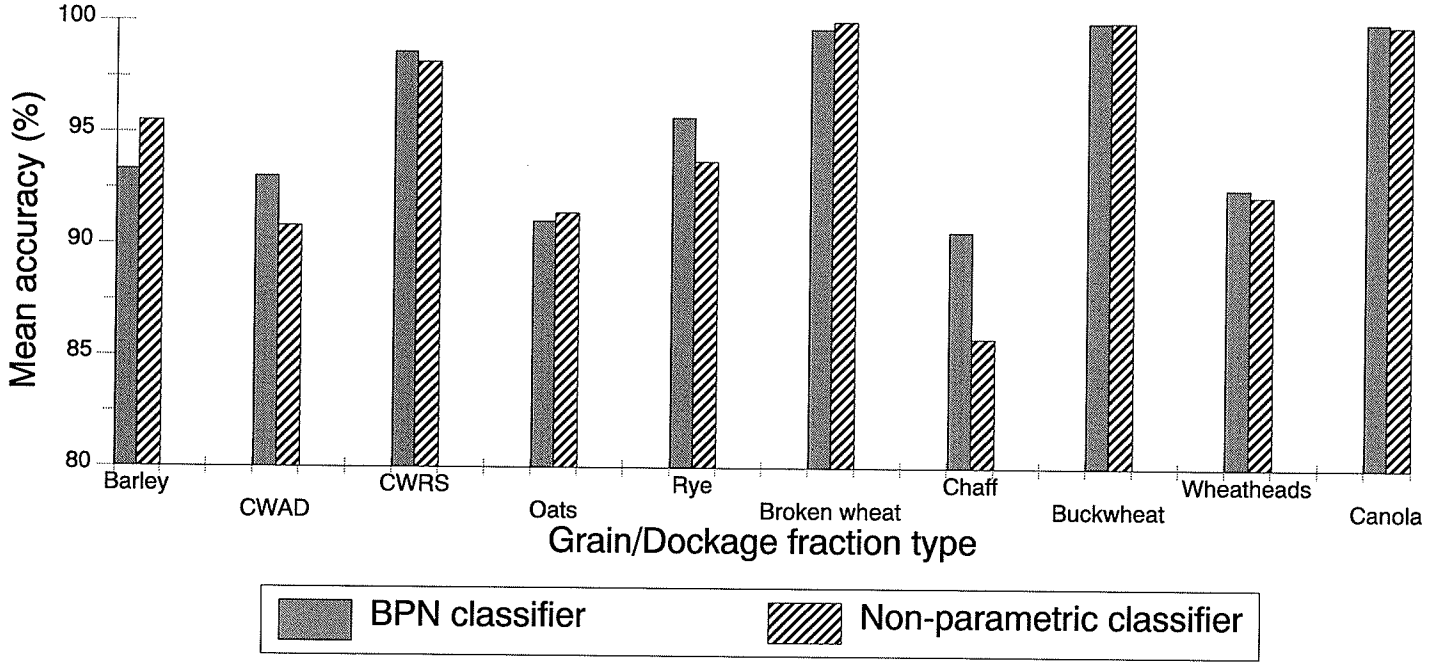

Fig. 5.17 Comparison of classification accuracies of the BPN and non-parametric classifier with combined 60 features as inputs

5.3.6 Combined 30 features model

5.3.6.1 Neural network classifier The top 10 morphological, color, and textural features were obtained from Table 5.17. This combined model of 30 features was used to investigate if a further reduction in the number of features affects the classification accuracies. The network had 30 neurons in the input layer, 27 in each of the two hidden layers, and 10 neurons in the output layer and took approximately 18.5 h to train. Table C20 (Appendix C) shows the classification accuracies obtained using the combined 30 features model.

5.3.6.2 Statistical classifier The rankings of features obtained by using the morphological, color, and textural feature models were used to create this set of combined 30 features (top 10 of each of the morphological, color, and textural classes, Table 5.18). A non-parametric classifier was used for classification, the results of which are shown in Table C21 (Appendix C).

Figure 5.18 shows the comparison of the classification accuracies of BPN and non-parametric classifier. Except for the case of broken wheat kernels, the performance of the BPN classifier was better than the non-parametric classifier.

Figures 5.19 and 5.20 show a comparison of the classification accuracies using a BPN and non-parametric classifier, respectively, as the number of input features were reduced. For both the classifiers, the combined 60 features model performed the best giving higher classification accuracies than the other models for eight out of ten output classes.

The results of section 5.3 indicate that it is very difficult to get higher classification accuracies for components like chaff and wheat-heads because of their vague shape and sizes. Their inclusion in the model also adversely affected classification of other grains.

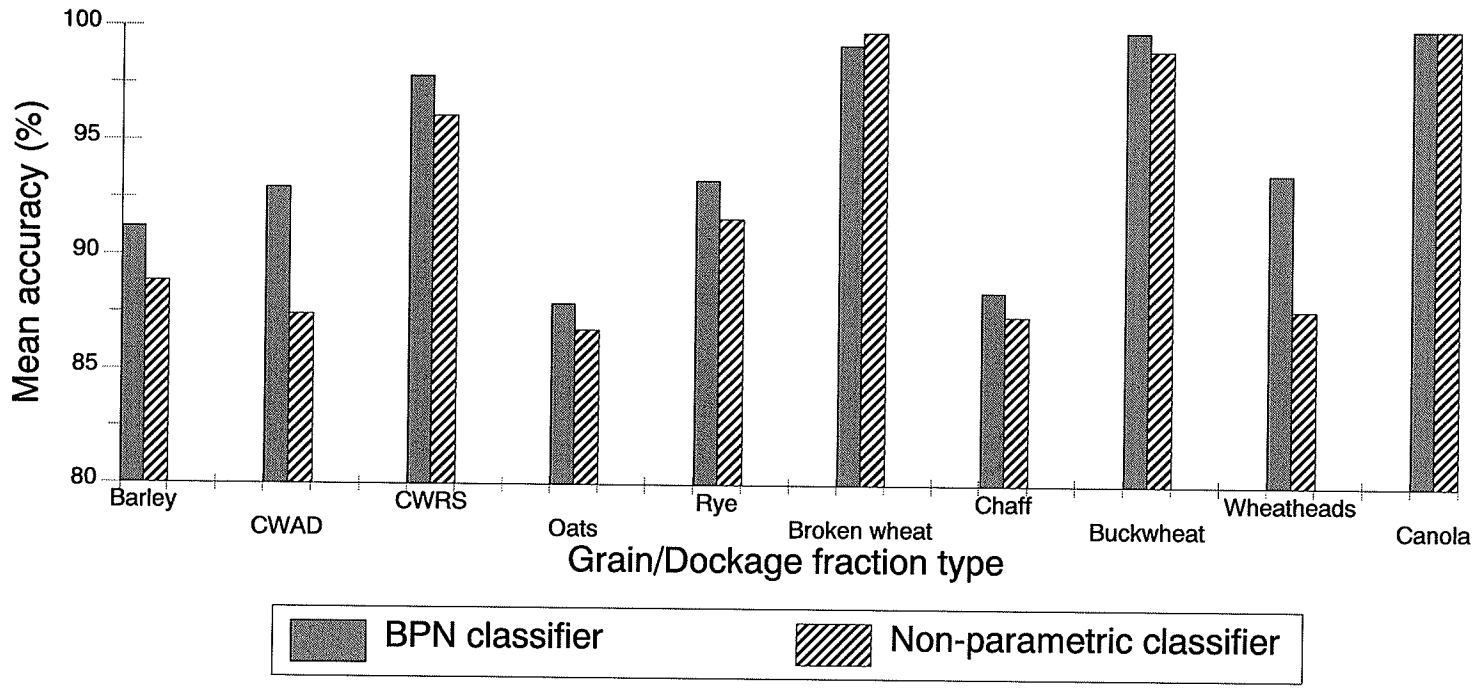

Fig. 5.18 Comparison of classification accuracies of the BPN and non-parametric classifier with combined 30 features as inputs

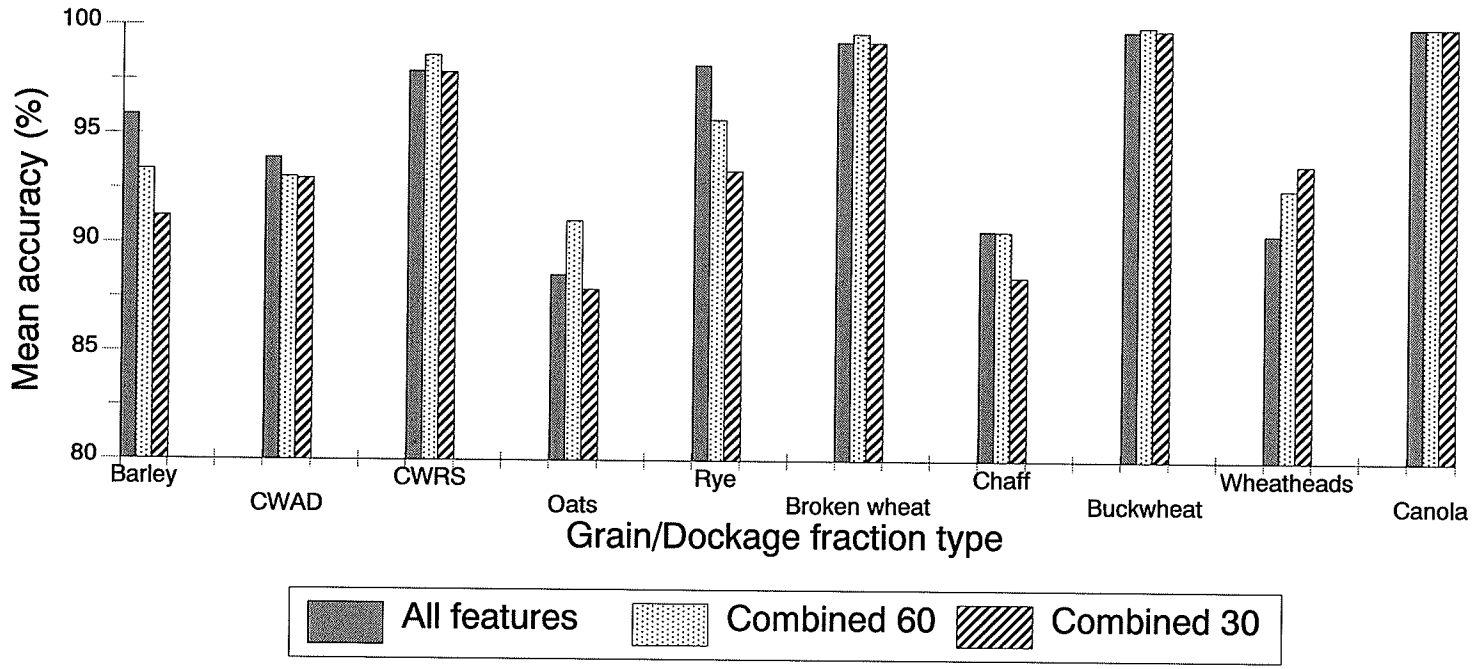

Fig. 5.19 Comparison of classification accuracies of the all features, combined 60, and combined 30 features models using a BPN classifier to classify cereal grains and dockage fractions

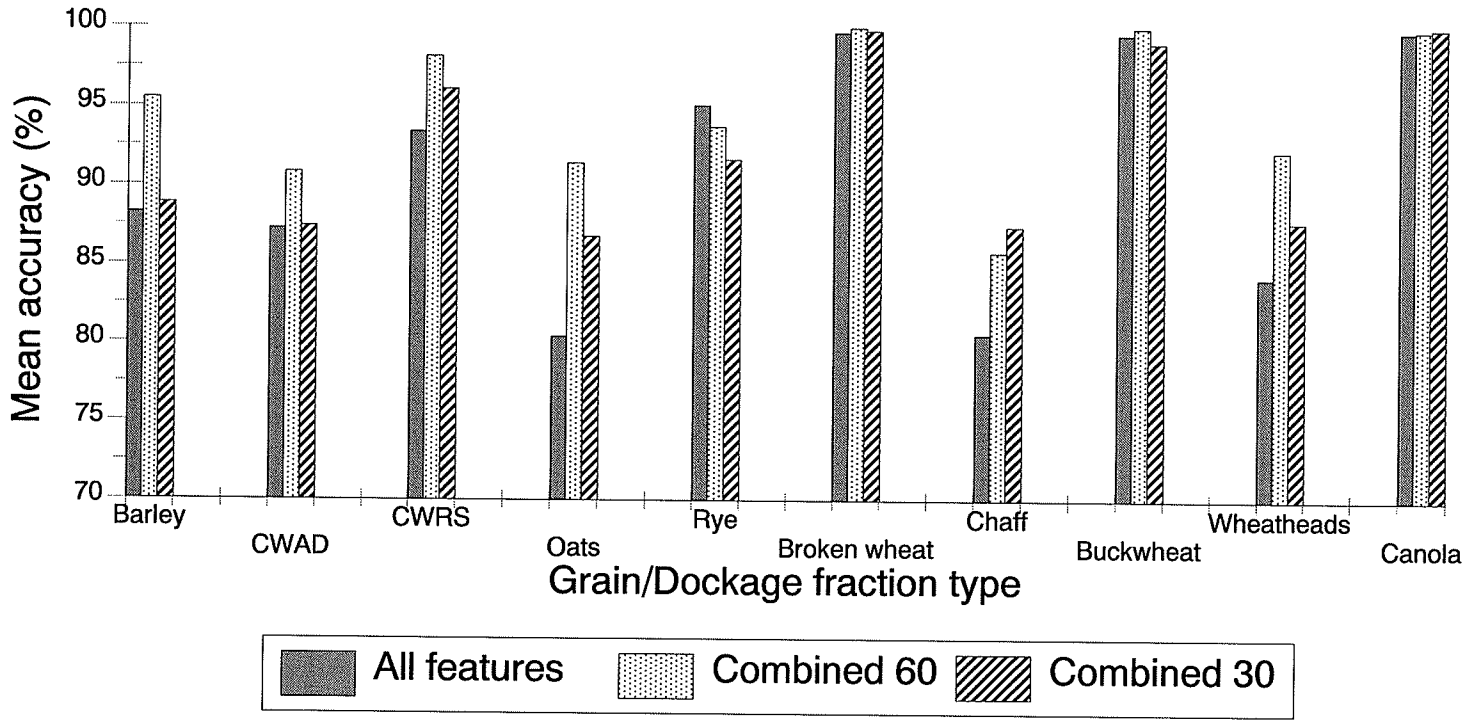

Fig. 5.20 Comparison of classification accuracies of the all features, combined 60, and combined 30 features models using a non-parametric classifier to classify cereal grains and dockage fractions

5.4 Quantification of Grain and Dockage Mass Using Morphological Features

To find a relationship between the mass of the particles and their morphology, seven morphological features, namely, area, perimeter, maximum radius, minimum radius, mean radius, major axis length, and minor axis length were tested. A linear regression was performed to find which morphological feature best described the mass of that particular class. The details of the regression analysis are shown in Appendices DA and DB.

It is clearly evident from the regression output and graphical plots that the area of the grain kernels and dockage particles gave the best estimate of their mass. The following regression equations were derived for the different classes:

Barley

$$m = -13.054 + 0.733\,A \tag{5.1}$$

CWAD wheat

$$m = -13.737 + 0.011\,A \tag{5.2}$$

CWRS wheat

$$m = 1.319 + 0.008\,A \tag{5.3}$$

Oats

$$m = 0.664 + 0.005\,A \tag{5.4}$$

Rye

$$m = 0.958 + 0.008\,A \tag{5.5}$$

Broken wheat kernels

$$m = 2.599 + 0.041\,A \tag{5.6}$$

Chaff

$$m = 0.087 + 3.66 \times 10^{-4} A \tag{5.7}$$

Buckwheat

$$m = -0.046 + 0.002 A \tag{5.8}$$

Wheat-heads

$$m = 4819.630 + 3.443 A \tag{5.9}$$

Canola

$$m = -0.019 + 1.47 \times 10^{-3} A \tag{5.10}$$

where A is the area in pixels and m is the mass in mg.

5.5 Testing of the Grain Cleaner

5.5.1 Cleaning efficiency The summarized results of the cleaning performance of the cleaner are shown in Table 5.20. The detailed results for all the replicates of different grain types are presented in Tables E1 through E5 of Appendix E. The cleaning efficiency (η) was calculated using the formula

$$\eta = \frac{(D_{bc} - F_{ac})}{D_{bc}} \times 100 \tag{5.11}$$

where D_{bc} is the mass of dockage in the sample before cleaning and F_{ac} is the mass of foreign material left in the sample after cleaning).

Table 5.20 Average cleaning efficiencies of the grain cleaner for different grain types at various flow rates

Grain type	Cleaning efficiency (%)					
	4 kg/h		8 kg/h		12 kg/h	
	Actual mass basis	Image basis	Actual mass basis	Image basis	Actual mass basis	Image basis
Barley	50.0	46.6	50.0	46.3	50.6	50.5
CWAD wheat	58.3	58.4	61.7	62.7	60.0	59.2
CWRS wheat	62.2	62.6	61.5	61.7	59.8	61.0
Oats	48.3	51.5	48.9	47.8	52.0	51.8
Rye	41.3	46.1	39.7	39.3	39.1	39.1

The cleaning efficiencies calculated based on the imaging technique were very close to the actual efficiencies (Table 5.20). There seemed to be no observable affect of the flow rates on the cleaning efficiencies. It is important to note that the purpose of this study was not to obtain very high cleaning efficiencies but to prove that the imaging technique was robust enough to give very similar results to the actual weighing method used commercially.

5.5.2 Ranges of morphological features before and after cleaning For grain samples containing 5% dockage, the ranges of seven size-based morphological features were calculated. These unclean samples were passed through the grain cleaner at 8 kg/h and the ranges of the same morphological features were calculated for the cleaned grain. Table 5.21 shows the results of this experiment.

Table 5.21 The ranges of morphological features for different grain types with 5% dockage, before and after being passed through the grain cleaner (3 replicates)

Grain type	Range of Morphological Features													
	Area		Perimeter		Maximum radius		Minimum radius		Mean radius		Major axis length		Minor axis length	
	Dirty	Clean	Dirty	Clean	Dirty	Clean	Dirty	Clean	Dirty	Clean	Dirty	Clean	Dirty	Clean
Barley	30782	27620	1640	1432	253	205	57	38	127	88	466	367	192	166
	29825	26548	1671	1397	231	198	61	33	134	88	459	363	187	160
	30249	27167	1653	1406	261	200	64	41	126	86	462	358	192	159
CWAD	29846	26893	1673	1577	234	214	54	45	132	100	453	402	184	181
	30689	25730	1638	1467	250	212	58	42	130	97	457	405	180	175
	29137	25394	1649	1508	243	187	52	45	131	101	451	409	190	182
CWRS	30284	28834	1657	1507	246	225	58	40	126	101	450	409	189	171
	30246	27943	1628	1438	275	241	58	39	138	105	462	405	192	170
	30014	27086	1630	1485	267	233	60	38	132	99	458	411	192	176

...continued

Table 5.21 The ranges of morphological features for different grain types before and after being passed through the grain cleaner

Grain type	Range of Morphological Features													
	Area		Perimeter		Maximum radius		Minimum radius		Mean radius		Major axis length		Minor axis length	
	Dirty	Clean	Dirty	Clean	Dirty	Clean	Dirty	Clean	Dirty	Clean	Dirty	Clean	Dirty	Clean
Oats	30049	28719	1667	1467	249	209	52	42	127	93	452	387	185	174
	31039	28144	1658	1435	249	201	51	42	129	90	460	390	188	179
	30080	27841	1633	1404	273	222	59	40	129	91	453	381	193	182
Rye	29954	28643	1662	1472	249	216	53	43	125	95	461	392	186	173
	30145	28435	1657	1439	244	208	60	44	127	94	458	395	180	172
	30672	27901	1625	1457	232	201	52	43	129	94	451	390	191	175

Analysis of variance (ANOVA) was done on individual morphological features (Appendix F). The results indicate that there was a significant difference ($P < 0.05$) in the ranges of all the morphological features before and after the grain was passed through the cleaner. This is a very important result as this change in the range of any of these morphological features, can be used as a feedback to evaluate if the grain is being cleaned properly or not.

6. CONCLUSIONS AND RECOMMENDATIONS

This thesis research has brought the technology of machine vision one step closer to its application in the grain industry. An optimum set of morphological, color, and textural features now exists that can classify barley, CWAD wheat, CWRS wheat, oats, and rye, with accuracies of over 96%. It has been proven that all the morphological, color, and textural characteristics are important in defining the appearance of these biological entities and thus should be included in the classification process. It was also seen that the presence of too many features in the classifier hinders its performance as the redundant features increase the complexity of the classifier unnecessarily. Therefore, an optimized feature set is desirable.

In a practical situation, it is not only necessary for the machine-vision-based system to identify cereal grains, but it should also be able to recognize the various impurities that are generally present in the grain. We now have a system that is capable of recognizing these impurities.

To compare the performance of statistical and neural network classifier, the classification was done using a non-parametric classifier and a 4-layer back propagation network. The back propagation network outperformed the non-parametric classifier in almost all the instances of classification. A back propagation network is thus recommended for classification of cereal grains.

The identification of impurities in a grain sample will be essential to design a machine-vision-based grain cleaning system. It has been shown that the machine vision technique is capable of quantifying the amount of impurity in a grain sample. This quantification can be used as a measure of the cleaner's performance. Apart from that, the

change in ranges of several morphological features can serve as a feedback to control parameters like vibration and feed rates of the cleaner. This study has paved a way for the implementation of machine vision techniques in designing an automatic imaging-based grain cleaner. We now know that the cleanliness levels of cereal grains can be estimated without actually weighing them physically. A few bottlenecks, however, still need to be overcome to implement this concept in practice. The following recommendations will help in taking this research to the next level from where it can be applied on a commercial scale:

- a commercial scale grain cleaner needs to be tested using a machine vision system;
- the system needs to be trained to recognize a wider variety of impurities, e.g., stones, mildewed and bin-burnt grain kernels, wild oats, etc.;
- the dockage removed from the grain can be analyzed for the amount of salvageable grain;
- the image acquisition and data analysis (classification) needs to be done in real-time by integrating the hardware and software of the system; and
- hardware implementation of the software will be needed to make it more efficient for data processing.

7. REFERENCES

Al-Janobi, A.A. and G. Kranzler. 1994. Machine vision inspection of date fruits. ASAE Paper No. 94-3575. St. Joseph, MI: ASAE.

Barker, D.A., T.A. Vouri, M.R. Hegedus, and D.G. Myers. 1992a. The use of ray parameters for the discrimination of Australian wheat varieties. *Plant Varieties and Seeds* 5(1):35-45.

Barker, D.A., T.A. Vouri, and D.G. Myers. 1992b. The use of slice and aspect ratio parameters for the discrimination of Australian wheat varieties. *Plant Varieties and Seeds* 5(1):47-52.

Barker, D.A., T.A. Vouri, and D.G. Myers. 1992c. The use of Fourier descriptors for the discrimination of Australian wheat varieties. *Plant Varieties and Seeds* 5(2):93-102.

Barker, D.A., T.A. Vouri, M.R. Hegedus, and D.G. Myers. 1992d. The use of Chebychev coefficients for the discrimination of Australian wheat varieties. *Plant Varieties and Seeds* 5(2):103-111.

Batchelor, B.C., D.A. Hill, and D.C. Hodgson. 1985. *Automated Visual Inspection.* London, UK: IFS (Publications) Ltd.

Bochereau, L., P. Bourgine, and B. Palagos. 1992. A method for prediction by combining data analysis and neural networks: application to prediction of apple quality using near infra-red spectra. *Journal of Agricultural Engineering Research* 51(3):207-216.

Casady, W.W., M.R. Paulsen, J.F. Reid, and J.B. Sinclair. 1992. A trainable algorithm for inspection of soybean seed quality. *Transactions of the ASAE* 35(6):2027-2034.

Chen, C., Y.P. Chiang, and Y. Pomeranz. 1989. Image analysis and characterization of cereal grains with a laser range finder and camera contour extractor. *Cereal Chemistry* 66:466-470

Chen, Y.R., S.R. Delwiche, and W.R. Hruschka. 1995. Classification of hard red wheat by feedforward backpropagation neural networks. *Cereal Chemistry* 72(3):317-319.

Chester, D.L. 1990. Why two hidden layers are better than one. In *Proceedings of the International Joint Conference on Neural Networks*, 1:265-268. IEEE, San Diago, CA.

Devijver, P.A. and J. Kittler. 1982. *Pattern Recognition: A Statistical Approach*. London, UK: Prentice Hall International Inc.

Dowell, F.E. 1993. Neural network classification of undamaged and damaged peanut kernels using spectral data. ASAE Paper No. 93-3050. St. Joseph, MI: ASAE.

Duda, R.O. and P.E. Hart. 1973. *Pattern Classification and Scene Analysis*. New York, NY: John Wiley and Sons, Inc.

El-Faki, M.S., N.Q. Zhang, D.E. Peterson, and N.Q. Zhang. 1997. Field factors affecting weed detection. ASAE Paper No. 97-3098. St. Joseph, MI: ASAE.

Emmerson, M.D. and R.I. Damper. 1993. Determining and improving the fault tolerance of multi-layer perceptrons in a pattern recognition application. *IEEE Transactions on Neural Networks* 4(5):788-793.

Fukunaga, K. 1990. *Statistical Pattern Recognition.* San Diego, CA: Academic Press, Inc.

Galloway, M.M. 1975. Textural analysis using gray level run lengths. *Computer Vision Graphics and Image Processing* 4(1975):172-179.

Ghazanfari, A., D. Wulfsohn, and J. Irudayaraj. 1998. Machine vision grading of pistachio nuts using gray-level histogram. *Canadian Agricultural Engineering* 40(1):61-66.

Ghazanfari, A., J. Irudayaraj, A. Kusalik, and M. Romaniuk. 1997. Machine vision grading of pistachio nuts using Fourier descriptors. *Journal of Agricultural Engineering Research* 68(3):247-252.

Gonzalez, R.C. and R.E. Woods. 1992. *Digital Image Processing*. Reading, MA: Addison-Wesley Publishing Co.

Gupta, L. and A.M. Upadhye. 1991. Non-linear alignment of neural net outputs for partial shape classification. *Pattern Recognition* 24(10):943-948.

Hand, D.J. 1981. *Discrimination and Classification*. New York, NY: John Wiley and Sons, Inc.

Haralick, R.M., K. Shanmugam, and I. Dinstein. 1973. Texture features for image classification. *IEEE Transactions on Systems, Man and Cybernetics* 3(6):610-621.

Haralick, R.M. 1979. Statistical and structural approach to texture. *Proceedings of the IEEE* 67(5):786-804.

Hayes, J.C. and Y.J. Han. 1993. Comparison of crop-cover measuring systems. *Transactions of the ASAE* 36(6):1727-1732.

Hush, D.R. and B.G. Horne. 1993. Progress in supervised neural networks, What's new since Lippmann? *IEEE Signal Processing Magazine* 10(1):8-39.

Jayas, D.S., J. Paliwal, and N.S. Visen. 2000. Multi-layer neural networks for image analysis of agricultural products. *Journal of Agricultural Engineering Research* 77(2):119-128.

Jou, I.C., S.S. You, and L.W. Chang. 1994. Analysis of hidden nodes for multi-layer perceptron neural networks. *Pattern Recognition* 27(6):859-864.

Keefe, P.D. 1992. A dedicated wheat grain image analyser. *Plant Varieties and Seeds* 5(1):27-33.

Keefe, P.D. and S.R. Draper. 1988. An automated machine vision system for the morphometry of new cultivars and plant genebank accessions. *Plant Varieties and Seeds* 1(1):1-11.

Keefe, P.D. and S.R. Draper. 1986. The measurement of new characters for cultivar identification in wheat using machine vision. *Seed Science and Technology* 14(3):715-724.

Keppler, K.M., W.D. Batchelor, and X.B. Yang. 1996. Evaluation of neural network architectures: A case study. ASAE Paper No. 96-3044. St. Joseph, MI: ASAE.

Kranzler, G.A. 1985. Applying digital image processing in agriculture. *Agricultural Engineering* 66(3):11-13.

Khotanzad, A. and J.H. Lu. 1991. Shape and texture recognition by a neural network. In *Machine Intelligence and Pattern Recognition,* Vol. 11*: Artificial Neural Networks and Statistical Pattern Recognition*, ed. Sethi, I.K. and A.K. Jain, 109-131. Amsterdam, The Netherlands: Elsevier Science Publishers.

Lippmann, R.P. 1987. An introduction to computing with neural nets. *IEEE, Acoustics, Speech and Signal Recognition Magazine* 4(2):4-22.

Lu, R., D.E. Guyer, and R.M. Beaudry. 2000. Determination of firmness and sugar content of apples using near-infrared diffuse reflectance. *Journal of Texture Studies* 31(6):615-630.

Luo, X., D.S. Jayas, T.G. Crowe, and N.R. Bulley. 1997. Evaluation of light sources for machine vision. *Canadian Agricultural Engineering* 39(4):309-315.

Luo, X.Y., D.S. Jayas, and S.J. Symons. 1999a. Identification of damaged kernels in wheat using a color machine vision system. *Journal of Cereal Science* 30(1):49-59.

Luo, X.Y., D.S. Jayas, and S.J. Symons. 1999b. Comparison of statistical and neural network methods for classifying cereal grains using machine vision. *Transactions of the ASAE* 42(2): 413-419.

Majumdar, S., D.S. Jayas, J.L. Hehn, and N.R. Bulley. 1996. Classification of various grains using optical properties. *Canadian Agricultural Engineering* 38(2):139-144.

Majumdar, S., D.S. Jayas, and S.J. Symons. 1999. Textural features for grain identification. *Agricultural Engineering Journal* 8(4):213-222.

Majumdar, S. and D.S. Jayas. 2000a. Classification of cereal grains using machine vision. I. Morphology models. *Transactions of the ASAE* 43(6):1669-1675.

Majumdar, S. and D.S. Jayas. 2000b. Classification of cereal grains using machine vision. II. Color models. *Transactions of the ASAE* 43(6):1677-1680.

Majumdar, S. and D.S. Jayas. 2000c. Classification of cereal grains using machine vision. III. Texture models. *Transactions of the ASAE* 43(6):1681-1687.

Majumdar, S. and D.S. Jayas. 2000d. Classification of cereal grains using machine vision. IV. Combined morphology, color, and texture models. *Transactions of the ASAE* 43(6):1689-1694.

Makhoul, J., A. El-Jaroudi, and R. Schwartz. 1989. Formation of disconnected decision regions with a single hidden layer. In *Proceedings of the International Joint Conference on Neural Networks*, 1:455-460. IEEE, San Diago, CA.

Mehrotra, K., C.K. Mohan, and S. Ranka. 1996. *Elements of Artificial Neural Networks.* Cambridge, MA: MIT Press.

Miller, B.K. and M.J. Delwiche. 1989. A color vision system for peach grading. *Transactions of the ASAE* 32(4):1484-1490.

Minsky, M. and S. Papert. 1969. *Perceptrons*. Cambridge, MA: MIT Press.

Morrow, C.T., P.H. Heinemann, H.J. Sommer, Y. Tao, and Z. Varghese. 1990. Automated inspection of potatoes, apples, and mushrooms. In *Proceeding of International Advanced Robotics Programme*, 179-188. Avignon, France.

Murase, H., Y. Nishiura, N. Honami, and N. Kondo. 1992. Neural network model for tomato fruit cracking. ASAE Paper No. 92-3593. St. Joseph, MI: ASAE.

Nair, M. and D.S. Jayas. 1998. Dockage identification in wheat using machine vision. *Canadian Agricultural Engineering* 40(4):293-298.

Neuman, M., H.D. Sapirstein, E. Shwedyk, and W. Bushuk. 1987. Discrimination of wheat class and variety by digital image analysis of whole grain samples. *Journal of Cereal Science* 6:125-132.

Neuman, M., H.D. Sapirstein, E. Shwedyk, and W. Bushuk. 1989a. Wheat grain color analysis by digital image processing: I. Methodology. *Journal of Cereal Science* 10(3):175-182.

Neuman, M., H.D. Sapirstein, E. Shwedyk, and W. Bushuk. 1989b. Wheat grain color analysis by digital image processing: II. Wheat class determination. *Journal of Cereal Science* 10(3):183-182.

Ng, H.F., W.F. Wilcke, R.V. Morey, and J.P. Lang. 1998. Machine vision evaluation of corn kernel mechanical and mold damage. *Transactions of the ASAE* 41(2):415-420.

Paliwal, J., N.S. Shashidhar, and D.S. Jayas. 1999. Grain kernel identification using kernel signature. *Transactions of the ASAE* 42(6): 1921-1924.

Paliwal, J., N.S. Visen, and D.S. Jayas. 2001. Evaluation of neural network architectures for cereal grain classification using morphological features. *Journal of Agricultural Engineering Research* 79(4):361-370.

Park, B. and Y. R. Chen. 1994. Intensified multi-spectral imaging system for poultry carcass inspection. In *Food Processing Automation III, Proceedings of the FAAC III Conference*, 97-106. ASAE, Orlando, FL.

Parker, J.R. 1994. *Practical Computer Vision Using C*. New York, NY: John Wiley and Sons, Inc.

Patel, V.C., R.W. McClendon, and J.W. Goodrum. 1995. Detection of cracks in eggs using computer vision and artificial neural networks. ASAE Paper No. 95-3258. St. Joseph, MI: ASAE.

Pao, Y.H. 1989. *Adaptive Pattern Recognition and Neural Networks*. Reading, MA: Addison-Wesley Pub. Co.

Putnam, D.F. and R.G. Putnam. 1970. *Canada: A Regional Analysis*. Toronto, ON: J.M. Dent and Sons, Inc.

Romaniuk, M.D., S. Sokhansanj, and H.C. Wood. 1993. Barley seed recognition using a multi-layer neural network. ASAE Paper No. 93-6569. St. Joseph, MI: ASAE.

Rosenblatt, F. 1958. The perceptron: A probabilistic model for information storage and organization in the brain. *Psychology Review* 65:386-408.

Sarkar, N.R. 1986. Machine vision in the food industry. In *ASAE Food Engineering News,* October, 3-5. St. Joseph, MI: ASAE.

Sapirstein, H.D., R. Rowler, and W. Bushuk. 1989. Instrumental measurement of bread crumb grain by digital image analysis. *Cereal Chemistry* 71(4):383-391.

Sapirstein, H.D. and J.M. Kohler. 1995. Physical uniformity of graded railcar and vessel shipments of Canada Western Red Spring wheat determined by digital image analysis. *Canadian Journal of Plant Science* 75(2):363-369.

SAS. 1990. *SAS User's Guide: Statistics*. Raleigh, NC: Statistical Analysis System, Inc.

Sayeed, M.S., A.D. Whittaker, and N.D. Ksehtarnavaz. 1995. Snack quality evaluation method based on image feature extraction and neural network prediction. *Transactions of the ASAE* 38(4):1239-1245.

Segerlind, L. and B. Weinberg. 1972. Grain kernel identification by profile analysis. ASAE Paper No. 72-314. St. Joseph, MI: ASAE.

Sethi, I.K. 1991. Decision tree performance enhancement using artificial neural network implementation. In *Machine Intelligence and Pattern Recognition,* Vol. 11*: Artificial Neural Networks and Statistical Pattern Recognition*, ed. Sethi, I.K. and A.K. Jain, 71-88 Amsterdam, The Netherlands: Elsevier Science Publishers.

Shatadal, P., D.S. Jayas, J.L. Hehn, and N.R. Bulley. 1995. Seed classification using machine vision. *Canadian Agricultural Engineering* 37(3):163-167.

Shibata, T., K. Iwao, and T. Takano. 1996. Evaluating tomato ripeness using a neural network. *Journal of the Society of High Technology in Agriculture* 8(3):160-167.

Silva, F.M. and L.B. Almedia. 1990. Acceleration technique for back propagation algorithm. In *Proceedings of the Neural Networks EURASIP Workshop*, ed. Goos, G. and J. Hartmanis, 110-119. Sesimbra, Portugal.

Spirkovska, L. and M.B. Reid. 1993. Coarse-coded higher-order neural networks for PSRI object recognition. *IEEE Transactions on Neural Networks* 4(2):276-283.

Symons, S.J. and R.G. Fulcher. 1988a. Relationship between oat kernel weight and milling yield. *Journal of Cereal Science* 7(3):215-217.

Symons, S.J. and R.G. Fulcher. 1988b. Determination of variation in oat kernel morphology by digital image analysis. *Journal of Cereal Science* 7(3):219-228.

Tao, Y., C.T. Morrow, P.H. Heinemann, and H.J. Sommer III. 1995. Fourier-based separation technique for shape grading potatoes using machine vision. *Transactions of the ASAE* 38(3):949-957.

Thai, C.N. and R.L. Shewfelt. 1991. Modeling sensory color quality of tomato and peach: neural networks and statistical regression. *Transactions of the ASAE* 34(3):950-955.

Tillet, R.D. 1990. Image analysis for agricultural processes. *Div. Note DN 1585, AFRC Institute of Engineering Research*, Silsoe, UK. 15p.

Villiers, J. and E. Barnard. 1992. Back propagation neural nets with one and two hidden layers. *IEEE Transaction on Neural Networks* 4(1):136-141.

Wang, D., F.E. Dowell, and R.E. Lacey. 1999. Single wheat kernel color classification using neural networks. *Transactions of the ASAE* 42(1):233-240.

Ward Systems Group. 1998. NeuroShell 2, Version 4. Frederick, MD.

Widrow, B. and M.E. Hoff. 1960. Adaptive switching circuits. *IRE WECON Convention* 4:96-104.

Wigger, W.D., M.R. Paulsen, J.B. Litchfield, and J.B. Sinclair. 1988. Classification of fungal-damaged soybeans using color-image processing. ASAE Paper No. 88-3053. St. Joseph, MI: ASAE. 33p.

Ying, J.P., M.D. Evans, S.R. Ghate, and P.Y. Jia. 1996. Catfish feature identification via computer vision. *Transactions of the ASAE* 39(5):1923-1931.

Zahn, C.T. and Z.R. Roskies. 1972. Fourier Descriptors for plane closed curves. *IEEE Transactions on Computers* 21(3):269-281.

Zayas, I., F.S. Lai, and Y. Pomeranz. 1986. Discrimination between wheat classes and varieties by image analysis. *Cereal Chemistry* 63(1):52-56.

Zayas, I., Y. Pomeranz, and F.S. Lai. 1989. Discrimination of wheat and non-wheat components in grain samples by digital image analysis. *Cereal Chemistry* 66(3):233-237.

Zayas, I. 1993. Digital image texture analysis for bread crumb grain evaluation. *Cereal Foods World* 38(10):760-766.

Zurada, J.M. 1992. *Introduction to Artificial Neural Systems.* St. Paul, MN: West Publishing Co.

Appendix A

C++ code for feature extraction

The C++ code was developed in Microsoft Visual C++ (Version 6.0) environment. The code reads an image file in tiff format. It then thresholds the image to extract the objects from the background. Once the objects are segmented, it extracts a total of 230 (51 morphological, 123 color, and 56 textural) features from every object. The information about the files and how to run the program is as follows:

C++ code filename: *features.cpp*

Header filename: *positionlist.h*

Executable file obtained by compiling the code: *features.exe*

Command line syntax (in dos prompt): *features.exe imagelist.txt results.txt*

where *imagelist.txt* is the list of image files to be processed (filenames with complete path) and *results.txt* is the text file to which all the output will be written. The program was capable of ignoring corrupt and non-existent files in the *imagelist.txt*. In the *results.txt*, the features of every kernel were written in one row and were delimited by a tab.

[Electronic copy of the program is available on request from Dr. D.S. Jayas]

Appendix B

Complete list of morphological, color and textural features

Table B1. Complete list of morphological features that were extracted from the grain kernels and dockage particles

Feature Number	Measurement
1	Area
2	Perimeter
3	Maximum radius
4	Minimum radius
5	Mean radius
6	Major axis length
7	Minor axis length
8 - 11	Shape moments 1 through 4
12 - 31	Radial Fourier descriptors 1 through 20
32 - 51	Boundary Fourier descriptors 1 through 20

Table B2. Complete list of color features that were extracted from the grain kernels and dockage particles

Feature Number	Measurement
1	Red mean
2	Green mean
3	Blue mean
4	Red range
5	Green range
6	Blue range
7	Red variance
8	Green variance
9	Blue variance
10	Hue mean
11	Saturation mean
12	Intensity mean
13	Hue range
14	Saturation range
15	Intensity range
16 - 19	Red moments 1 through 4
20 - 23	Green moments 1 through 4
24 - 27	Blue moments 1 through 4
28 - 59	Red histogram ranges 1 through 32
60 - 91	Green histogram ranges 1 through 32
92 - 123	Blue histogram ranges 1 through 32

Table B3. Complete list of textural features that were extracted from the grain kernels and dockage particles

Feature Number	Measurement	Code
1	Gray level co-occurrence matrix mean for gray band	Gray GLCM mean
2	Gray level co-occurrence matrix variance for gray band	Gray GLCM variance
3	Gray level co-occurrence matrix uniformity for gray band	Gray GLCM uniformity
4	Gray level co-occurrence matrix correlation for gray band	Gray GLCM correlation
5	Gray level co-occurrence matrix cluster shade for gray band	Gray GLCM cluster shade
6	Gray level co-occurrence matrix entropy for gray band	Gray GLCM entropy
7	Gray level co-occurrence matrix homogeneity for gray band	Gray GLCM homogeneity
8	Gray level co-occurrence matrix inertia for gray band	Gray GLCM inertia
9	Gray level co-occurrence matrix mean for red band	Red GLCM mean
10	Gray level co-occurrence matrix variance for red band	Red GLCM variance
11	Gray level co-occurrence matrix uniformity for red band	Red GLCM uniformity
12	Gray level co-occurrence matrix correlation for red band	Red GLCM correlation
13	Gray level co-occurrence matrix cluster shade for red band	Red GLCM cluster shade
14	Gray level co-occurrence matrix entropy for red band	Red GLCM entropy
15	Gray level co-occurrence matrix homogeneity for red band	Red GLCM homogeneity

...continued

Table B3. Complete list of textural features that were extracted from the grain kernels and dockage particles

Feature Number	Measurement	Code
16	Gray level co-occurrence matrix inertia for red band	Red GLCM inertia
17	Gray level co-occurrence matrix mean for green band	Green GLCM mean
18	Gray level co-occurrence matrix variance for green band	Green GLCM variance
19	Gray level co-occurrence matrix uniformity for green band	Green GLCM uniformity
20	Gray level co-occurrence matrix correlation for green band	Green GLCM correlation
21	Gray level co-occurrence matrix cluster shade for green band	Green GLCM cluster shade
22	Gray level co-occurrence matrix entropy for green band	Green GLCM entropy
23	Gray level co-occurrence matrix homogeneity for green band	Green GLCM homogeneity
24	Gray level co-occurrence matrix inertia for green band	Green GLCM inertia
25	Gray level co-occurrence matrix mean for blue band	Blue GLCM mean
26	Gray level co-occurrence matrix variance for blue band	Blue GLCM variance
27	Gray level co-occurrence matrix uniformity for blue band	Blue GLCM uniformity
28	Gray level co-occurrence matrix correlation for blue band	Blue GLCM correlation
29	Gray level co-occurrence matrix cluster shade for blue band	Blue GLCM cluster shade

...continued

Table B3. Complete list of textural features that were extracted from the grain kernels and dockage particles

Feature Number	Measurement	Code
30	Gray level co-occurrence matrix entropy for blue band	Blue GLCM entropy
31	Gray level co-occurrence matrix homogeneity for blue band	Blue GLCM homogeneity
32	Gray level co-occurrence matrix inertia for blue band	Blue GLCM inertia
33	Gray level run length matrix short run for gray band	Gray GLRM short run
34	Gray level run length matrix long run for gray band	Gray GLRM long run
35	Gray level run length matrix color non-uniformity for gray band	Gray GLRM color non-uniformity
36	Gray level run length matrix run length non-uniformity for gray band	Gray GLRM run length non-uniformity
37	Gray level run length matrix entropy for gray band	Gray GLRM entropy
38	Gray level run length matrix runpercent for gray band	Gray GLRM runpercent
39	Gray level run length matrix short run for red band	Red GLRM short run
40	Gray level run length matrix long run for red band	Red GLRM long run
41	Gray level run length matrix color non-uniformity for red band	Red GLRM color non-uniformity
42	Gray level run length matrix run length non-uniformity for red band	Red GLRM run length non-uniformity
43	Gray level run length matrix entropy for red band	Red GLRM entropy
44	Gray level run length matrix runpercent for red band	Red GLRM runpercent

...continued

Table B3. Complete list of textural features that were extracted from the grain kernels and dockage particles

Feature Number	Measurement	Code
45	Gray level run length matrix short run for green band	Green GLRM short run
46	Gray level run length matrix long run for green band	Green GLRM long run
47	Gray level run length matrix color non-uniformity for green band	Green GLRM color non-uniformity
48	Gray level run length matrix run length non-uniformity for green band	Green GLRM run length non-uniformity
49	Gray level run length matrix entropy for green band	Green GLRM entropy
50	Gray level run length matrix runpercent for green band	Green GLRM runpercent
51	Gray level run length matrix short run for blue band	Blue GLRM short run
52	Gray level run length matrix long run for blue band	Blue GLRM long run
53	Gray level run length matrix color non-uniformity for blue band	Blue GLRM color non-uniformity
54	Gray level run length matrix run length non-uniformity for blue band	Blue GLRM run length non-uniformity
55	Gray level run length matrix entropy for blue band	Blue GLRM entropy
56	Gray level run length matrix runpercent for blue band	Blue GLRM runpercent

Appendix C

Classification accuracies and feature rankings obtained using different feature models and classifiers

Table C1. Classification accuracies of various grain types using 8 gray levels

Grain type	Classification accuracies for three validation sets, %			
	1	2	3	Mean
Barley	85.9	89.3	90.3	88.5
CWAD	91.3	93.6	94.6	93.2
CWRS	87.5	87.2	86.8	87.2
Oats	93.5	95.7	94.7	94.6
Rye	93.3	93.5	92.5	93.1

Table C2. Classification accuracies of various grain types using 16 gray levels

Grain type	Classification accuracies for three validation sets, %			
	1	2	3	Mean
Barley	89.0	89.8	89.5	89.4
CWAD	90.1	93.1	89.7	91.0
CWRS	89.0	88.8	90.3	89.4
Oats	95.2	96.5	94.7	95.4
Rye	95.7	94.5	95.7	95.3

Table C3. Classification accuracies of various grain types using 32 gray levels

Grain type	Classification accuracies for three validation sets, %			
	1	2	3	Mean
Barley	87.9	89.1	91.0	89.3
CWAD	87.5	95.5	92.1	91.7
CWRS	86.8	88.3	90.5	88.6
Oats	96.7	97.7	96.0	96.8
Rye	95.8	91.5	96.2	94.5

Table C4. Classification accuracies of various grain types using 64 gray levels

Grain type	Classification accuracies for three validation sets, %			
	1	2	3	Mean
Barley	90.0	89.0	92.5	90.5
CWAD	89.1	94.4	92.9	92.1
CWRS	88.7	88.2	88.5	88.4
Oats	96.8	98.2	95.7	96.9
Rye	96.5	94.3	96.8	95.9

Table C5. Classification accuracies of various grain types using 128 gray levels

Grain type	Classification accuracies for three validation sets, %			
	1	2	3	Mean
Barley	89.8	87.8	90.1	89.2
CWAD	90.7	93.4	90.1	91.4
CWRS	87.0	87.5	89.2	87.9
Oats	96.8	97.8	95.2	96.6
Rye	95.8	91.2	94.7	93.9

Table C6. Classification accuracies of various grain types using 256 gray levels

Grain type	Classification accuracies for three validation sets, %			
	1	2	3	Mean
Barley	90.1	89.5	90.8	90.1
CWAD	92.4	93.9	91.3	92.5
CWRS	84.2	82.7	87.0	84.6
Oats	98.2	96.7	95.3	96.7
Rye	94.2	95.0	95.5	94.9

Table C7. Rankings of features in the combined 60 feature model using a BPN classifier

Rank	Feature	Rank	Feature	Rank	Feature
1	Boundary FD 18	21	Boundary FD 12	41	Boundary FD 17
2	Hue mean	22	Green GLCM cluster shade	42	Blue variance
3	Green GLRM long run	23	Green moment 2	43	Green GLCM variance
4	Red GLCM homogeneity	24	Green GLCM entropy	44	Red GLRM run length non-uniformity
5	Green GLRM short run	25	Red variance	45	Green GLCM mean
6	Minor axis length	26	Minimum radius	46	Blue GLCM correlation
7	Radial FD 2	27	Blue GLRM runpercent	47	Blue GLCM mean
8	Green GLRM runpercent	28	Shape moment 3	48	Mean radius
9	Perimeter	29	Blue GLRM run length non-uniformity	49	Green range
10	Saturation mean	30	Major axis length	50	Red histogram range 11
11	Boundary FD 2	31	Green moment 1	51	Blue GLRM color non-uniformity
12	Green GLCM correlation	32	Boundary FD 3	52	Green histogram range 1
13	Boundary FD 20	33	Blue moment 1	53	Green GLRM run length non-uniformity
14	Red GLCM variance	34	Blue GLCM variance	54	Red range
15	Area	35	Radial FD 3	55	Boundary FD 1
16	Maximum radius	36	Blue histogram range 1	56	Red histogram range 9
17	Blue range	37	Red moment 2	57	Shape moment 4
18	Radial FD 5	38	Blue mean	58	Boundary FD 5
19	Blue GLRM short run	39	Gray GLRM run length non-uniformity	59	Red moment 3
20	Green variance	40	Red moment 1	60	Red histogram range 10

Table C8. Classification accuracies of cereal grains obtained using a BPN classifier with top 20 features as inputs.

Output class	Classification accuracies for five validation sets, %					
	1	2	3	4	5	Mean
Barley	85.9	85.4	86.2	88.5	83.2	85.8
CWAD	78.3	77.5	78.0	78.8	77.9	78.1
CWRS	85.8	85.3	83.6	86.8	86.4	85.6
Oats	83.3	87.9	84.5	86.9	83.0	85.1
Rye	86.2	84.4	84.8	84.3	84.8	84.9

Table C9. Classification accuracies of cereal grains obtained using a non-parametric classifier with top 20 features as inputs.

Output class	Classification accuracies for five validation sets, %					
	1	2	3	4	5	Mean
Barley	81.3	84.8	85.2	82.3	82.4	83.2
CWAD	76.9	78.4	77.0	81.4	79.6	78.6
CWRS	86.3	86.0	87.7	65.1	87.9	82.6
Oats	82.6	86.3	82.1	83.9	81.3	83.2
Rye	84.8	85.7	86.9	86.3	87.1	86.1

Table C10. Classification accuracies of cereal grains and dockage fractions obtained using a BPN classifier with morphological features as inputs

Output class	Classification accuracies for five validation sets, %					
	1	2	3	4	5	Mean
Barley	90.6	80.8	90.3	89.6	90.4	88.3
CWAD	86.3	74.0	81.3	81.8	89.5	82.6
CWRS	93.3	94.6	95.5	96.4	95.9	95.2
Oats	77.7	85.2	79.2	83.3	83.2	81.7
Rye	89.1	92.9	88.1	87.7	86.6	88.9
Broken wheat	96.8	96.0	97.3	97.5	96.1	96.7
Chaff	57.9	68.8	67.4	74.7	65.2	66.8
Wild buckwheat	91.3	90.7	89.7	92.3	94.2	91.6
Wheat-heads	92.3	94.7	90.7	93.2	91.2	92.4
Canola	99.6	99.7	99.9	99.9	99.8	99.8

Table C11. Classification accuracies of cereal grains and dockage fractions obtained using a non-parametric classifier with morphological features as inputs

Output class	Classification accuracies for five validation sets, %					
	1	2	3	4	5	Mean
Barley	93.9	86.9	89.1	90.8	85.7	89.3
CWAD	83.8	82.9	83.6	86.8	89.1	85.2
CWRS	91.4	94.8	95.8	96.7	98.7	95.5
Oats	82.4	83.5	76.9	81.5	86.4	82.2
Rye	81.7	88.9	89.8	89.1	90.3	87.9
Broken wheat	93.8	95.1	94.6	96.6	96.4	95.3
Chaff	40.2	49.8	50.1	49.3	40.3	45.9
Wild buckwheat	99.1	98.2	99.2	100.0	99.9	99.3
Wheat-heads	83.7	90.4	88.2	89.4	84.0	87.2
Canola	99.6	99.9	99.8	99.7	99.9	99.8

Table C12. Classification accuracies of cereal grains and dockage fractions obtained using a BPN classifier with color features as inputs

Output class	Classification accuracies for five validation sets, %					
	1	2	3	4	5	Mean
Barley	86.2	72.0	84.1	85.2	84.5	82.4
CWAD	88.0	78.7	77.1	80.2	82.0	81.2
CWRS	96.3	94.6	96.9	97.2	97.9	96.6
Oats	62.6	76.4	71.9	78.4	67.6	71.4
Rye	85.5	91.7	89.7	94.5	91.3	90.5
Broken wheat	97.8	98.4	97.3	100.0	99.1	98.5
Chaff	81.7	88.8	88.2	88.5	86.2	86.7
Wild buckwheat	99.0	99.9	100.0	99.8	99.6	99.7
Wheat-heads	78.4	85.8	80.2	85.2	84.0	82.7
Canola	99.7	99.9	100.0	99.9	100.0	99.9

Table C13. Classification accuracies of cereal grains and dockage fractions obtained using a non-parametric classifier with color features as inputs

Output class	Classification accuracies for five validation sets, %					
	1	2	3	4	5	Mean
Barley	75.2	69.4	65.7	67.8	73.3	70.3
CWAD	66.3	61.4	62.9	71.3	75.1	67.4
CWRS	86.8	91.0	88.8	85.2	86.7	87.7
Oats	50.7	60.9	62.3	60.5	61.6	59.2
Rye	71.4	80.6	82.7	84.1	79.6	79.7
Broken wheat	92.7	86.9	94.3	94.6	93.7	92.4
Chaff	71.5	85.1	87.9	85.7	82.8	82.6
Wild buckwheat	95.8	98.9	97.6	97.7	93.8	96.8
Wheat-heads	79.7	84.7	77.6	75.9	79.3	79.4
Canola	100.0	100.0	100.0	100.0	100.0	100.0

Table C14. Classification accuracies of cereal grains and dockage fractions obtained using a BPN classifier with textural features as inputs

Output class	Classification accuracies for five validation sets, %					
	1	2	3	4	5	Mean
Barley	81.1	81.9	88.4	85.2	78.5	83.0
CWAD	89.6	87.0	87.9	85.8	88.8	87.8
CWRS	93.8	94.0	93.4	94.3	92.9	93.7
Oats	69.8	59.5	61.1	69.5	70.3	66.0
Rye	89.2	90.0	92.9	93.6	93.3	91.8
Broken wheat	97.5	96.3	98.0	97.2	98.1	97.4
Chaff	77.1	84.0	82.8	85.6	81.6	82.2
Wild buckwheat	98.4	99.4	99.6	99.4	98.9	99.2
Wheat-heads	93.2	95.2	92.7	94.4	90.9	93.3
Canola	99.6	99.7	99.4	99.9	99.8	99.7

Table C15. Classification accuracies of cereal grains and dockage fractions obtained using a non-parametric classifier with textural features as inputs

Output class	Classification accuracies for five validation sets, %					
	1	2	3	4	5	Mean
Barley	89.4	92.4	87.4	84.2	83.3	87.4
CWAD	92.1	88.8	86.2	88.0	86.2	88.2
CWRS	94.4	95.6	96.8	95.8	93.9	95.3
Oats	76.9	81.9	77.6	76.6	77.7	78.1
Rye	90.1	90.9	91.3	93.3	93.1	91.7
Broken wheat	100.0	100.0	100.0	100.0	100.0	100.0
Chaff	88.2	90.1	88.8	89.1	89.7	89.2
Wild buckwheat	99.3	99.9	100.0	100.0	100.0	99.9
Wheat-heads	94.0	95.1	93.4	93.4	93.9	94.0
Canola	97.4	95.8	99.9	99.2	99.4	98.4

Table C16. Classification accuracies of cereal grains and dockage fractions obtained using a BPN classifier with all features as inputs

Output class	Classification accuracies for five validation sets, %					
	1	2	3	4	5	Mean
Barley	96.9	97.9	95.8	94.4	94.3	95.9
CWAD	93.9	95.9	91.4	93.2	95.1	93.9
CWRS	95.8	100.0	98.4	98.2	97.0	97.9
Oats	83.4	92.6	85.9	89.0	91.9	88.6
Rye	97.1	99.9	98.7	97.9	97.3	98.2
Broken wheat	98.9	99.3	98.7	99.4	100.0	99.3
Chaff	86.6	93.4	90.9	93.9	88.2	90.6
Wild buckwheat	99.1	100.0	99.9	100.0	99.9	99.8
Wheat-heads	82.7	97.0	90.1	92.9	89.5	90.5
Canola	100.0	100.0	100.0	100.0	100.0	100.0

Table C17. Classification accuracies of cereal grains and dockage fractions obtained using a non-parametric classifier with all features as inputs

Output class	Classification accuracies for five validation sets, %					
	1	2	3	4	5	Mean
Barley	87.7	96.3	84.4	86.4	86.4	88.2
CWAD	85.8	86.3	88.7	87.8	87.7	87.3
CWRS	89.6	95.6	98.7	96.6	86.4	93.4
Oats	73.5	84.6	81.5	79.0	83.4	80.4
Rye	93.5	97.0	95.7	94.6	94.6	95.1
Broken wheat	100.0	100.0	99.2	99.2	100.0	99.7
Chaff	78.5	87.7	77.7	78.3	80.5	80.5
Wild buckwheat	98.9	99.6	99.9	100.0	99.4	99.6
Wheat-heads	85.7	91.2	71.6	88.3	84.1	84.2
Canola	99.8	100.0	99.6	100.0	99.3	99.8

Table C18. Classification accuracies of cereal grains and dockage fractions obtained using a BPN classifier with combined 60 features as inputs

Output class	Classification accuracies for five validation sets, %					
	1	2	3	4	5	Mean
Barley	95.5	92.9	91.5	93.5	93.3	93.3
CWAD	91.9	91.2	94.5	93.7	93.9	93.0
CWRS	98.4	99.0	98.4	98.8	98.5	98.6
Oats	91.9	93.2	88.7	90.7	90.8	91.0
Rye	96.6	93.7	96.8	95.9	95.4	95.7
Broken wheat	99.8	99.4	99.2	100.0	99.9	99.7
Chaff	92.5	88.8	89.8	89.4	92.4	90.6
Wild buckwheat	100.0	100.0	100.0	100.0	99.9	100.0
Wheat-heads	91.6	94.5	91.4	93.4	91.8	92.5
Canola	100.0	100.0	100.0	100.0	100.0	100.0

Table C19. Classification accuracies of cereal grains and dockage fractions obtained using a non-parametric classifier with combined 60 features as inputs

Output class	Classification accuracies for five validation sets, %					
	1	2	3	4	5	Mean
Barley	96.3	92.6	94.5	97.6	96.6	95.5
CWAD	86.9	96.6	88.3	91.6	90.8	90.8
CWRS	92.6	99.3	100.0	99.6	99.3	98.2
Oats	85.4	94.1	93.2	92.0	92.3	91.4
Rye	89.1	94.6	97.9	93.7	93.3	93.7
Broken wheat	100.0	100.0	100.0	100.0	100.0	100.0
Chaff	84.8	85.7	83.2	87.6	87.8	85.8
Wild buckwheat	100.0	100.0	100.0	100.0	100.0	100.0
Wheat-heads	89.9	93.4	90.1	93.0	94.7	92.2
Canola	99.3	100.0	100.0	100.0	100.0	99.9

Table C20. Classification accuracies of cereal grains and dockage fractions obtained using a BPN classifier with combined 30 features as inputs

Output class	Classification accuracies for five validation sets, %					
	1	2	3	4	5	Mean
Barley	92.6	89.8	94.1	88.2	91.4	91.2
CWAD	96.2	91.9	91.7	90.7	94.4	93.0
CWRS	97.9	96.9	98.1	97.8	98.5	97.8
Oats	84.8	91.2	85.3	89.6	88.6	87.9
Rye	91.9	93.2	95.3	92.4	93.8	93.3
Broken wheat	99.6	99.2	98.4	99.3	99.8	99.2
Chaff	85.1	89.2	91.3	87.2	89.6	88.5
Wild buckwheat	99.9	99.7	99.9	100.0	99.7	99.8
Wheat-heads	92.6	95.1	94.6	94.4	91.6	93.7
Canola	100.0	100.0	100.0	100.0	100.0	100.0

Table C21. Classification accuracies of cereal grains and dockage fractions obtained using a non parametric classifier with combined 30 features as inputs

Output class	Classification accuracies for five validation sets, %					
	1	2	3	4	5	Mean
Barley	86.1	92.6	90.2	87.2	88.3	88.9
CWAD	89.1	87.7	87.1	86.8	86.4	87.4
CWRS	92.9	97.4	99.3	95.8	95.1	96.1
Oats	89.0	88.4	83.7	87.8	84.9	86.8
Rye	90.9	91.7	93.8	91.7	90.1	91.7
Broken wheat	99.6	99.5	99.9	100.0	100.0	99.8
Chaff	83.2	89.8	86.8	89.4	87.8	87.4
Wild buckwheat	96.3	99.3	100.0	100.0	99.6	99.0
Wheat-heads	88.1	90.5	84.8	88.6	86.7	87.7
Canola	100.0	100.0	100.0	100.0	100.0	100.0

Appendix DA

Mass and morphology relationship charts for cereal grains

Table DA1. Relationship between mass and morphological features of barley

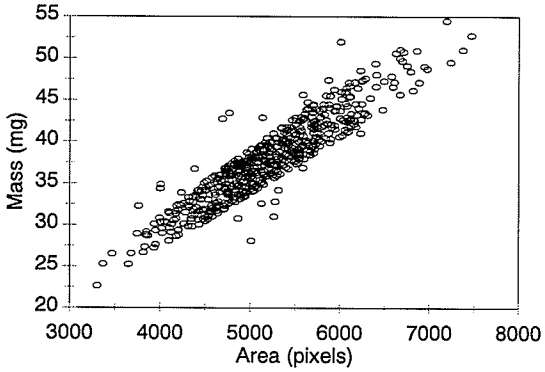

Regression Output

Constant	1.8899597126742
Std Err of Y Est	1.9357064903428
R Squared	0.8520045008483
X Coefficient(s)	0.0069076902966
Std Err of Coef.	0.0001177295747

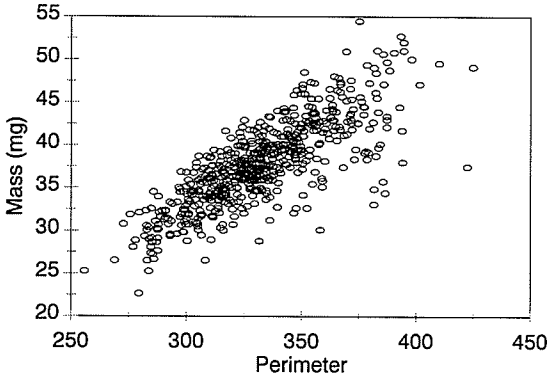

Regression Output

Constant	-10.8363865547
Std Err of Y Est	3.056365510587
R Squared	0.631039328632
X Coefficient(s)	0.146522268878
Std Err of Coef.	0.004581575709

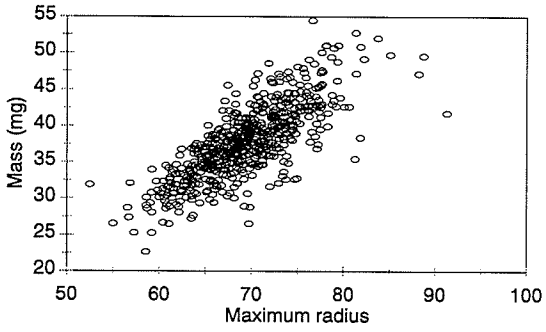

Regression Output

Constant	-13.05443083289
Std Err of Y Est	3.199284849042
R Squared	0.595726463172
X Coefficient(s)	0.732767658465
Std Err of Coef.	0.024684816985

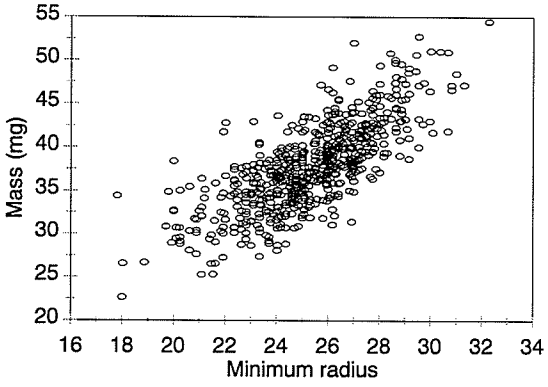

Regression Output

Constant	-3.924657441118
Std Err of Y Est	3.2806506666795
R Squared	0.5749015992430
X Coefficient(s)	1.6512436787219
Std Err of Coef.	0.0580642142370

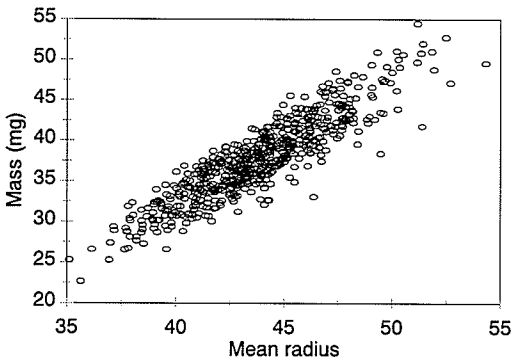

Regression Output:

Constant	-27.169804102170
Std Err of Y Est	2.18091355027127
R Squared	0.81213477499855
X Coefficient(s)	1.48228093379873
Std Err of Coef.	0.02915339086943

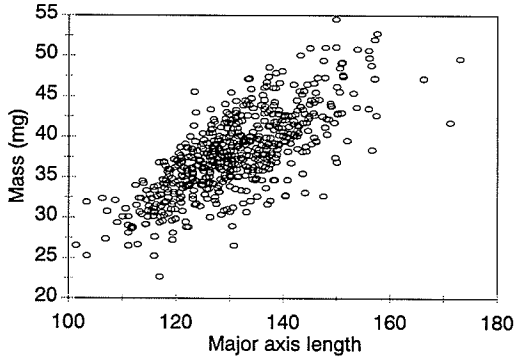

Regression Output:

Constant	-7.2104302673307
Std Err of Y Est	3.39599135497015
R Squared	0.54448503713136
X Coefficient(s)	0.34434833593871
Std Err of Coef.	0.01287969994600

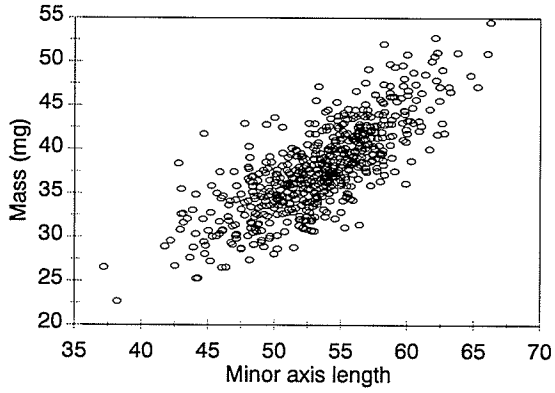

Regression Output

Constant	-8.97335835719
Std Err of Y Est	3.190010726677
R Squared	0.598066891233
X Coefficient(s)	0.876222433166
Std Err of Coef.	0.029374182351

Table DA2. Relationship between mass and morphological features of CWAD wheat

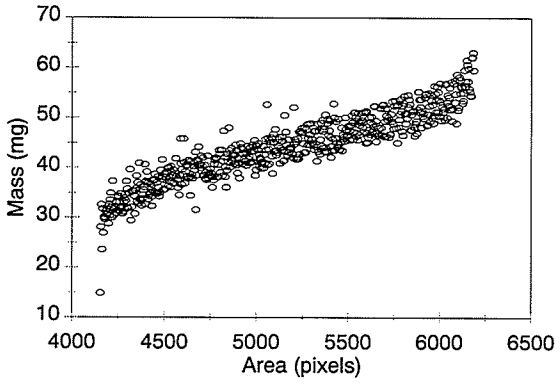

Regression Output

Constant	-13.73727788462
Std Err of Y Est	2.6585220309788
R Squared	0.8600143218374
X Coefficient(s)	0.0111970257396
Std Err of Coef.	0.0001862957616

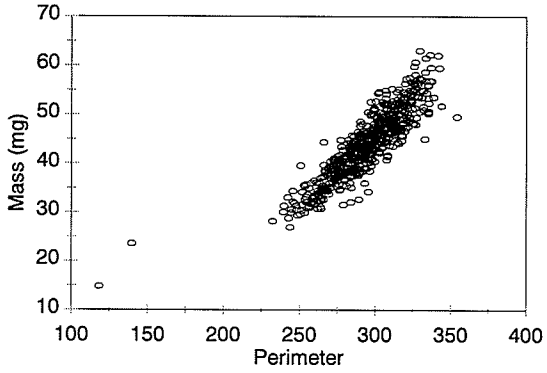

Regression Output

Constant	-33.08234508513
Std Err of Y Est	3.2622884663701
R Squared	0.7892110698022
X Coefficient(s)	0.2618384068923
Std Err of Coef.	0.0055804857390

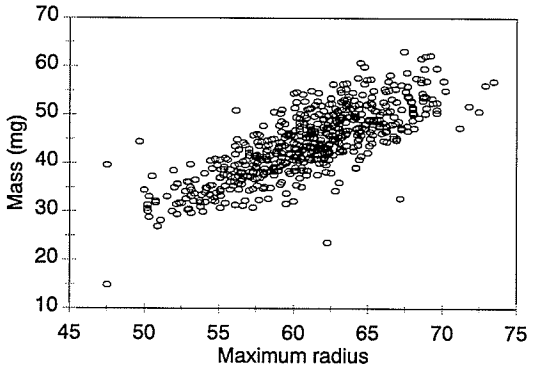

Regression Output

Constant	-30.30038989747
Std Err of Y Est	4.4041039551227
R Squared	0.6158346406266
X Coefficient(s)	1.2209704957096
Std Err of Coef.	0.0397688973827

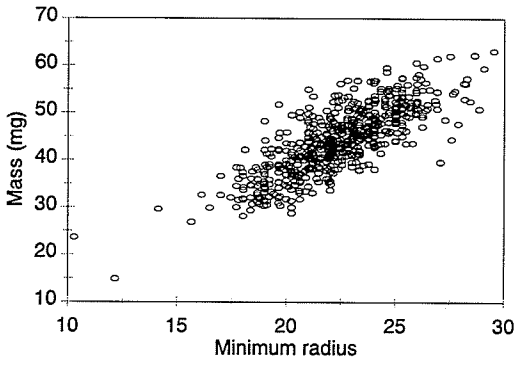

Regression Output

Constant	-6.2738379979723
Std Err of Y Est	4.33386601408978
R Squared	0.62799049246967
X Coefficient(s)	2.25144061192498
Std Err of Coef.	0.07146153127263

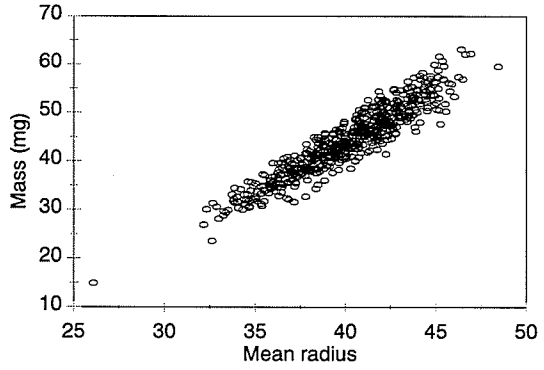

Regression Output

Constant	-41.928388326461
Std Err of Y Est	2.46389262355216
R Squared	0.87976064635069
X Coefficient(s)	2.14692184313611
Std Err of Coef.	0.03273170455883

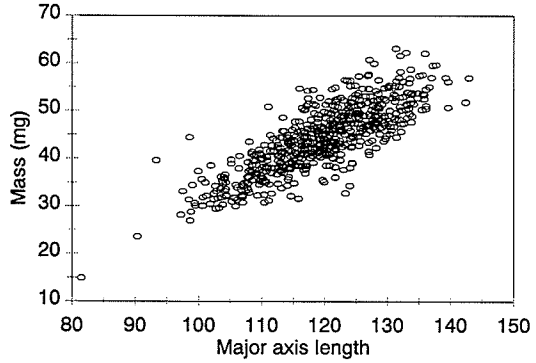

Regression Output

Constant	-31.265942909486
Std Err of Y Est	4.09934846248639
R Squared	0.66716211630811
X Coefficient(s)	0.63176324637536
Std Err of Coef.	0.01840205738980

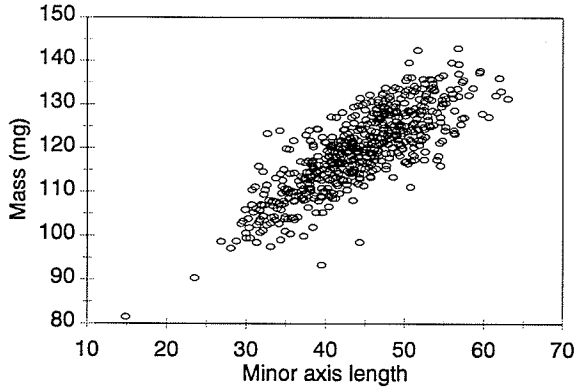

Regression Output

Constant	-12.95010332206
Std Err of Y Est	3.6914388920254
R Squared	0.7301052446375
X Coefficient(s)	1.1984279275299
Std Err of Coef.	0.0300488424469

Table DA3. Relationship between mass and morphological features of CWRS wheat

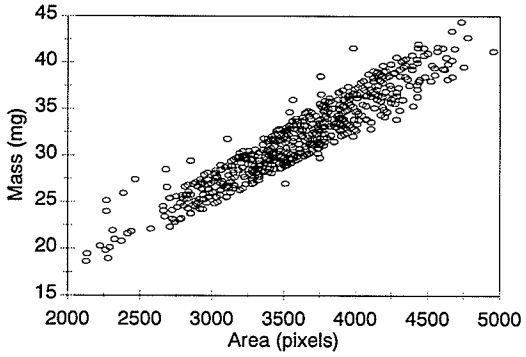

Regression Output

Constant	1.31913193804326
Std Err of Y Est	1.57108893801176
R Squared	0.88386923372106
X Coefficient(s)	0.00846975992873
Std Err of Coef.	0.00012554520957

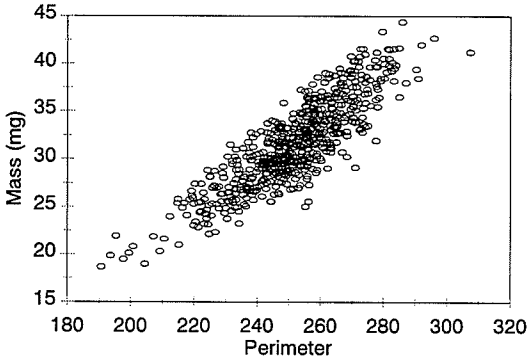

Regression Output

Constant	-27.245277504428
Std Err of Y Est	0.31475102944421
R Squared	0.74791075244024
X Coefficient(s)	0.23407321179262
Std Err of Coef.	0.00555716631788

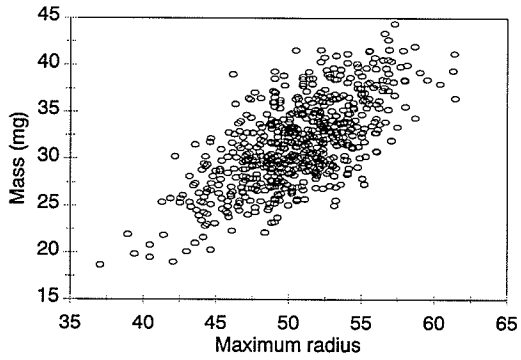

Regression Output

Constant	-9.4386734558032
Std Err of Y Est	3.45072358655103
R Squared	0.43977034369397
X Coefficient(s)	0.81319773831558
Std Err of Coef.	0.03753320475844

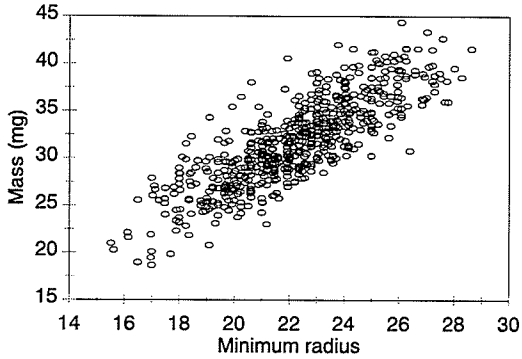

Regression Output

Constant	-2.3082667415092
Std Err of Y Est	2.5979722737613
R Squared	0.68244805738873
X Coefficient(s)	1.53102393610688
Std Err of Coef.	0.04270748278863

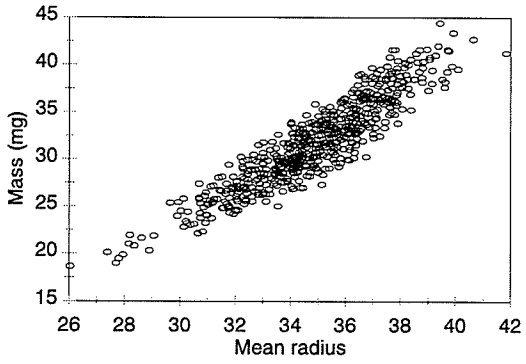

Regression Output

Constant	-30.921108817559
Std Err of Y Est	1.7977300678405
R Squared	0.84794709751542
X Coefficient(s)	1.79787742167816
Std Err of Coef.	0.03113310703857

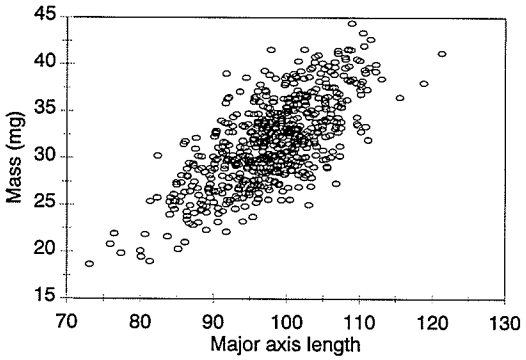

Regression Output

Constant	-14.137628921064
Std Err of Y Est	3.29145356732979
R Squared	0.49029227479472
X Coefficient(s)	0.46783926236306
Std Err of Coef.	0.01950649123525

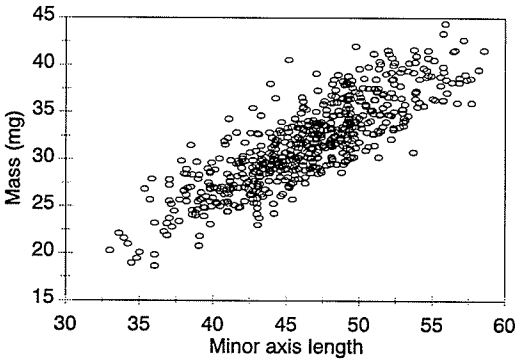

Regression Output

Constant	-4.8621946464506
Std Err of Y Est	2.51091173104116
R Squared	0.70337439186562
X Coefficient(s)	0.78839441795914
Std Err of Coef.	0.02093649574362

Table DA4. Relationship between mass and morphological features of oats

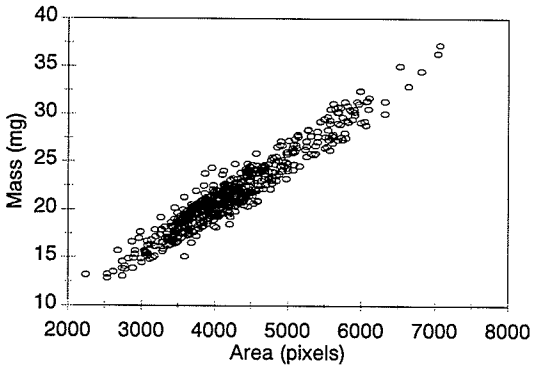

Regression Output

Constant	0.66384747473396
Std Err of Y Est	1.12580745325715
R Squared	0.92122795074341
X Coefficient(s)	0.00495128040016
Std Err of Coef.	5.9206508208E-05

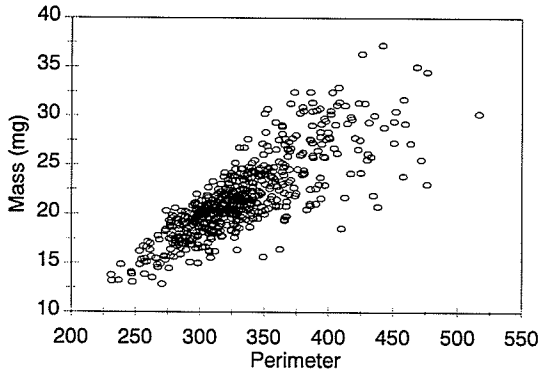

Regression Output

Constant	-2.9174167079882
Std Err of Y Est	2.3600221956765
R Squared	0.65384063964428
X Coefficient(s)	0.07395963358021
Std Err of Coef.	0.00220062601801

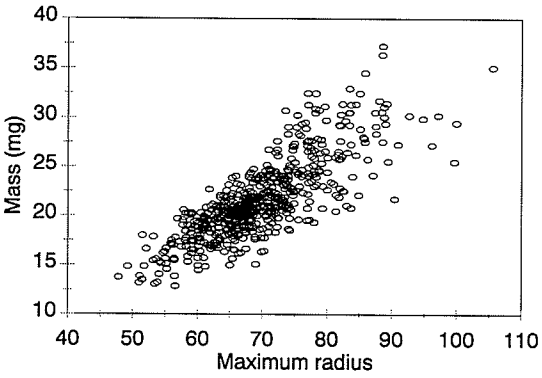

Regression Output

Constant	-4.8770405455355
Std Err of Y Est	2.36291579940188
R Squared	0.65299127299619
X Coefficient(s)	0.38067650949631
Std Err of Coef.	0.01134806975076

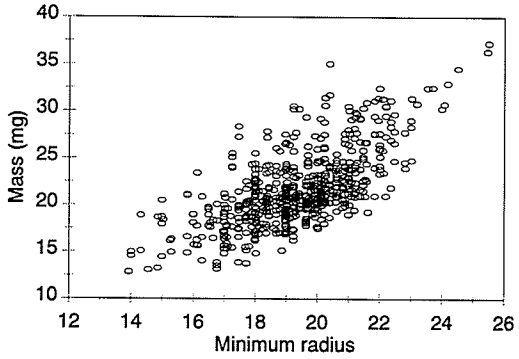

Regression Output

Constant	-7.6472632190688
Std Err of Y Est	0.91699065298546
R Squared	0.47117256261706
X Coefficient(s)	1.51442367502429
Std Err of Coef.	0.06560905643124

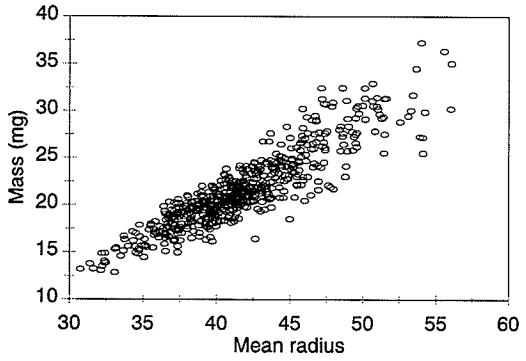

Regression Output

Constant	-12.328825523359
Std Err of Y Est	1.74549709788143
R Squared	0.81064265010033
X Coefficient(s)	0.81312010601604
Std Err of Coef.	0.01607053987563

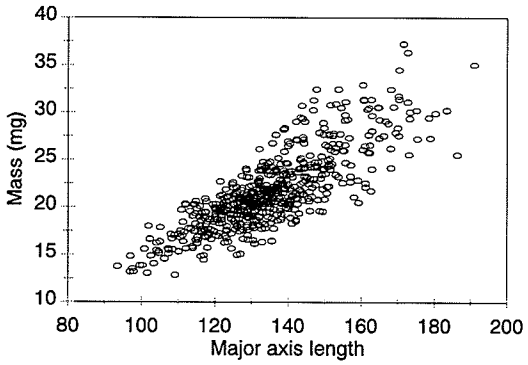

Regression Output

Constant	-6.1009683866827
Std Err of Y Est	2.30570795188004
R Squared	0.66959051999712
X Coefficient(s)	0.20565621003599
Std Err of Coef.	0.00590762388431

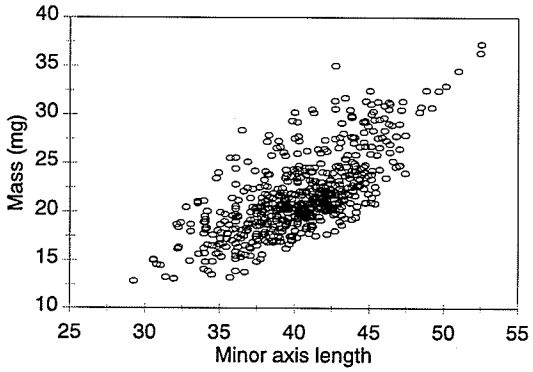

Regression Output

Constant	-9.7405954578056
Std Err of Y Est	2.85953700518299
R Squared	0.49179919695558
X Coefficient(s)	0.77663653224524
Std Err of Coef.	0.03228427138335

Table DA5. Relationship between mass and morphological features of rye

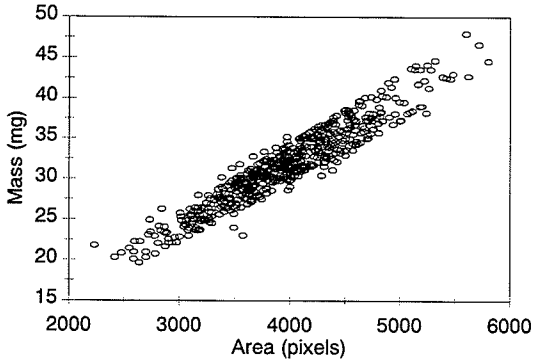

Regression Output

Constant	0.95774055402487
Std Err of Y Est	1.5512826575294
R Squared	0.90073379725106
X Coefficient(s)	0.00775833123314
Std Err of Coef.	0.00010532226751

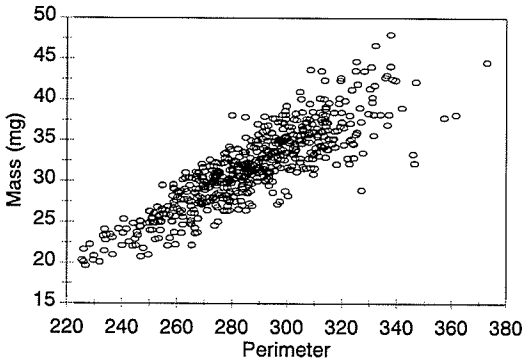

Regression Output

Constant	-18.562057247153
Std Err of Y Est	2.48208837764146
R Squared	0.74587112357108
X Coefficient(s)	0.17499265117379
Std Err of Coef.	0.00417699860425

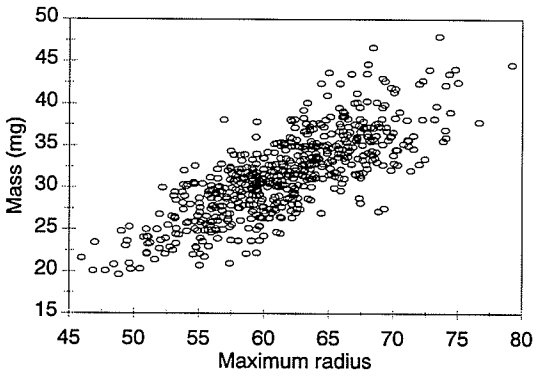

Regression Output

Constant	-11.322779733006
Std Err of Y Est	3.08665298550741
R Squared	0.60699764902439
X Coefficient(s)	0.69663743635032
Std Err of Coef.	0.02292241055927

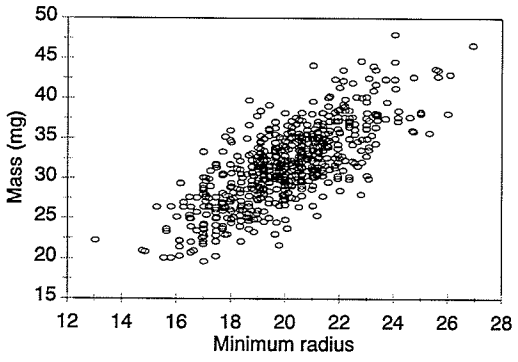

Regression Output

Constant	-4.9723915167990
Std Err of Y Est	3.24158165440728
R Squared	0.56655553050640
X Coefficient(s)	1.82806810237621
Std Err of Coef.	0.06538637639118

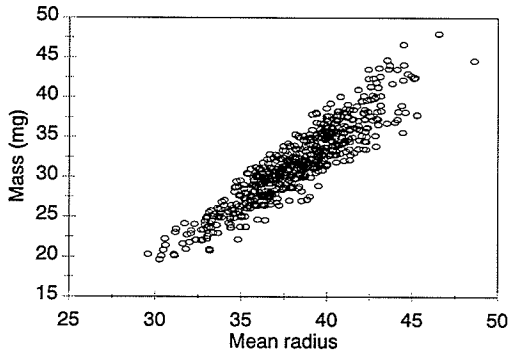

Regression Output

Constant	-25.436841300208
Std Err of Y Est	1.95744224988873
R Squared	0.84194892636462
X Coefficient(s)	1.49473394979831
Std Err of Coef.	0.02648312059575

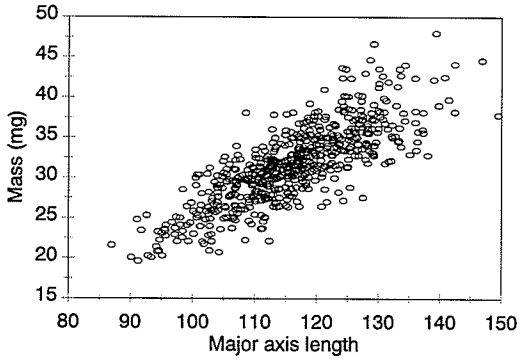

Regression Output

Constant	-12.886285426985
Std Err of Y Est	2.93065197325556
R Squared	0.64571886373414
X Coefficient(s)	0.38353047720533
Std Err of Coef.	0.01161720267936

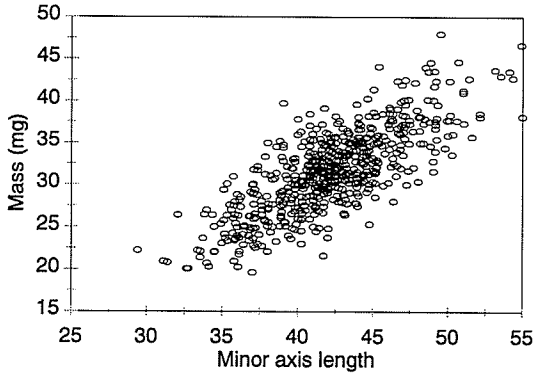

Regression Output

Constant	-7.7349172844127
Std Err of Y Est	3.11794116414326
R Squared	0.59898984942947
X Coefficient(s)	0.93252924273296
Std Err of Coef.	0.03120181223423

Appendix DB

Mass and morphology relationship charts for dockage fractions

Table DB1. Relationship between mass and morphological features of broken wheat kernels

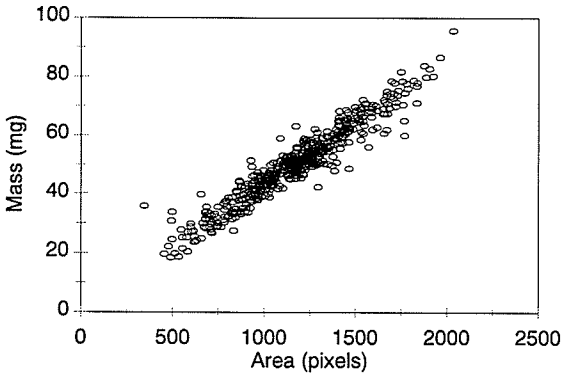

Regression Output

Constant	2.59940887229985
Std Err of Y Est	3.77405496241425
R Squared	0.91694831394251
X Coefficient(s)	0.04068827557832
Std Err of Coef.	0.00054872710294

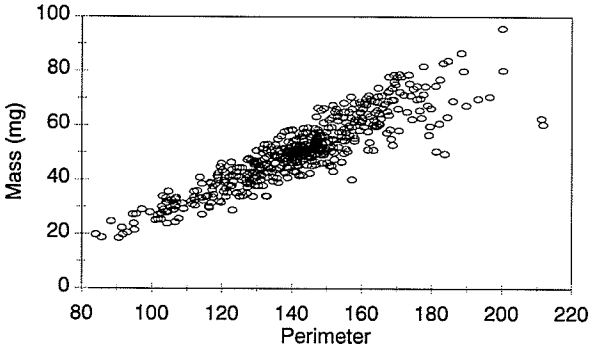

Regression Output

Constant	-27.814165593342
Std Err of Y Est	5.69011015002222
R Squared	0.81121244599218
X Coefficient(s)	0.55008666882926
Std Err of Coef.	0.01189147770451

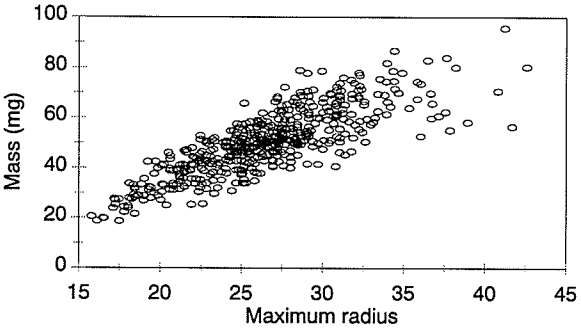

Regression Output

Constant	-11.510518083778
Std Err of Y Est	7.46239711435019
R Squared	0.67529518755065
X Coefficient(s)	2.33402238056063
Std Err of Coef.	0.07252502380518

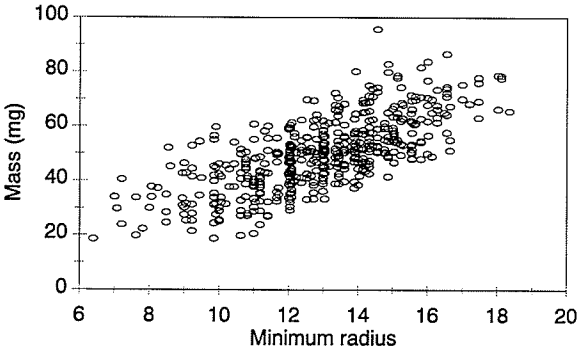

Regression Output

Constant	-4.9705933119749
Std Err of Y Est	9.17033640182898
R Squared	0.50965410105057
X Coefficient(s)	4.27394027682647
Std Err of Coef.	0.18785695989641

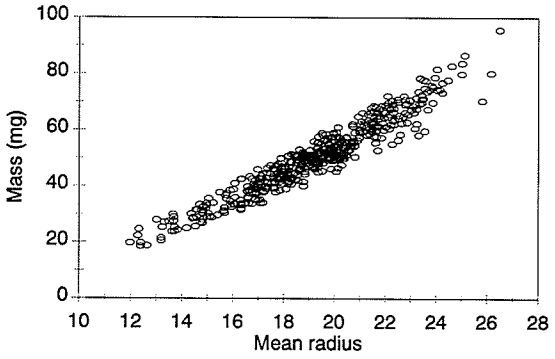

Regression Output

Constant	-39.828194831524
Std Err of Y Est	3.63170516413544
R Squared	0.92309524736869
X Coefficient(s)	4.69352732083228
Std Err of Coef.	0.06070689370417

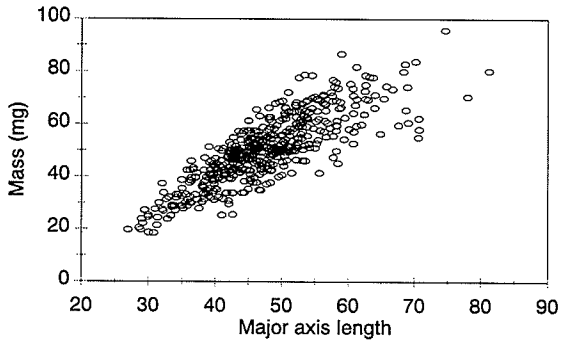

Regression Output

Constant	-9.8470207223970
Std Err of Y Est	7.23362306519399
R Squared	0.69489890846185
X Coefficient(s)	1.26690317606583
Std Err of Coef.	0.03761749045686

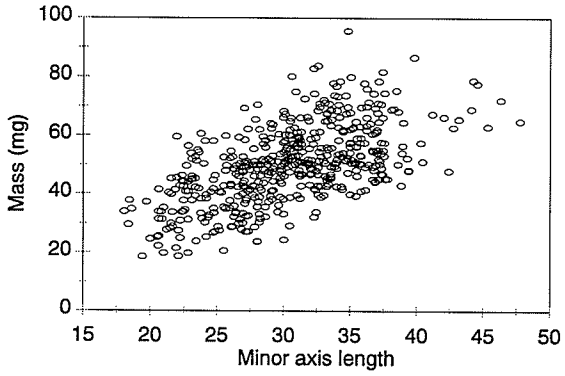

Regression Output

Constant	4.92049964313258
Std Err of Y Est	10.4678263677556
R Squared	0.36108213319588
X Coefficient(s)	1.48434715986705
Std Err of Coef.	0.08847902559883

Table DB2. Relationship between mass and morphological features of chaff

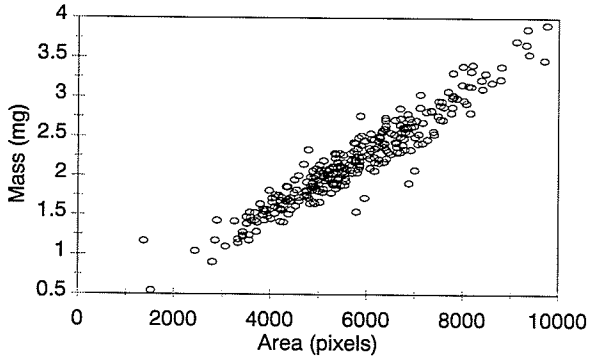

Regression Output

Constant	0.087054659680656
Std Err of Y Est	0.167731566758127
R Squared	0.908049184388513
X Coefficient(s)	0.000366368868068
Std Err of Coef.	6.75357204647E-06

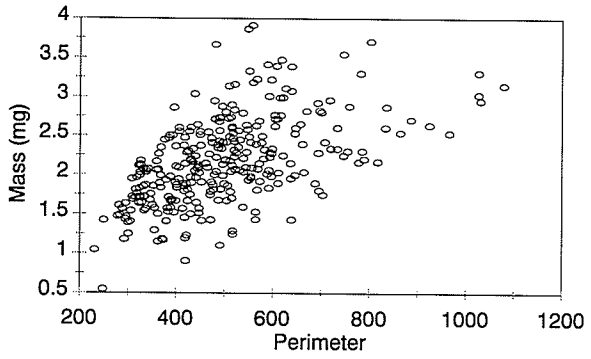

Regression Output

Constant	1.13369053274661
Std Err of Y Est	0.459843813157528
R Squared	0.308890800519712
X Coefficient(s)	0.002088648534950
Std Err of Coef.	0.000180978958061

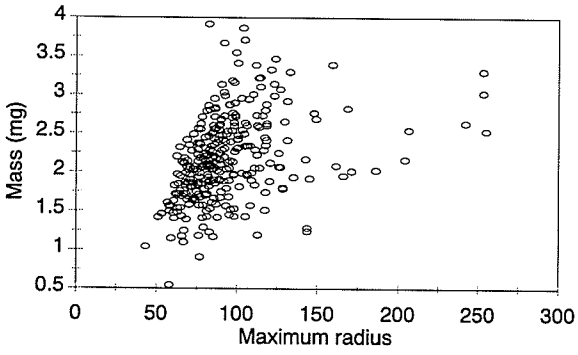

Regression Output

Constant	1.5273620717483
Std Err of Y Est	0.511704030587761
R Squared	0.144217001810817
X Coefficient(s)	0.006878448637818
Std Err of Coef.	0.000970635033524

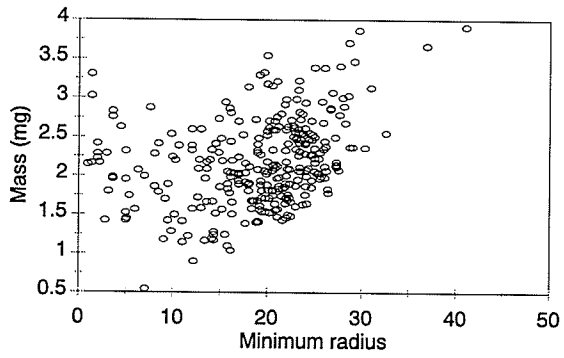

Regression Output

Constant	1.67593222673365
Std Err of Y Est	0.522452723263618
R Squared	0.107886784397431
X Coefficient(s)	0.026356581604568
Std Err of Coef.	0.004390427524786

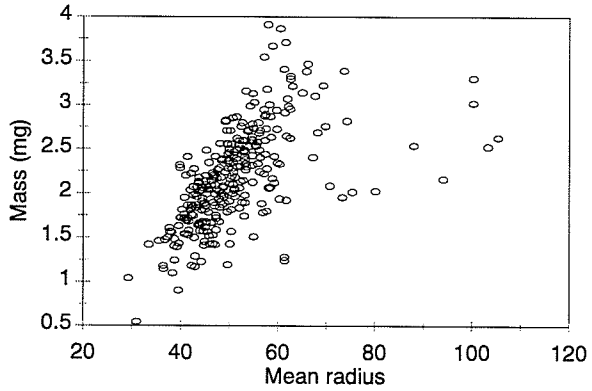

Regression Output

Constant	0.607466578318577
Std Err of Y Est	0.448689172296087
R Squared	0.342013236561029
X Coefficient(s)	0.030651288045418
Std Err of Coef.	0.002462791912281

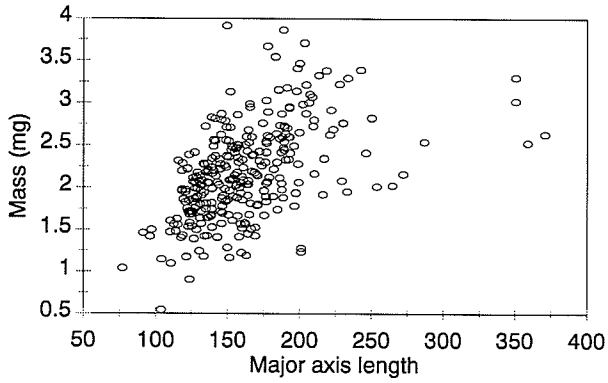

Regression Output

Constant	1.04041759079141
Std Err of Y Est	0.475769144761129
R Squared	0.260192849266673
X Coefficient(s)	0.006990832643385
Std Err of Coef.	0.000682861074913

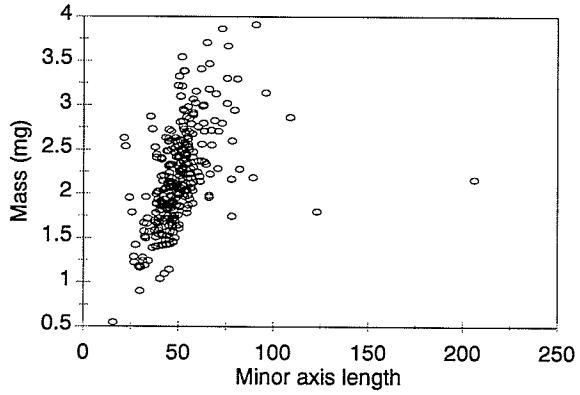

Regression Output

Constant	1.36344971537918
Std Err of Y Est	0.49324251166851
R Squared	0.20485381497390
X Coefficient(s)	0.01610183604749
Std Err of Coef.	0.00183767509628

Table DB3. Relationship between mass and morphological features of buckwheat

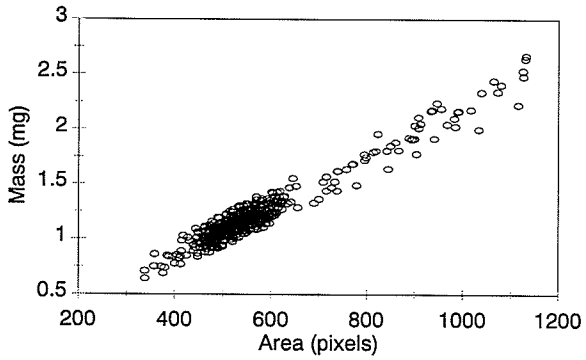

Regression Output

Constant	-0.04599655400595
Std Err of Y Est	0.077856786259407
R Squared	0.940736359787279
X Coefficient(s)	0.002221392542810
Std Err of Coef.	2.64602547806E-05

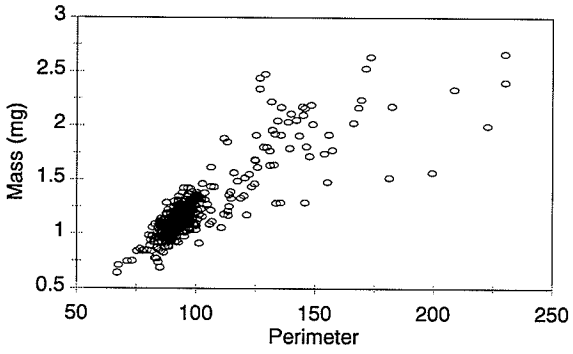

Regression Output

Constant	-0.03006401898803
Std Err of Y Est	0.169241663246662
R Squared	0.719966526488013
X Coefficient(s)	0.012563683475342
Std Err of Coef.	0.000371855596816

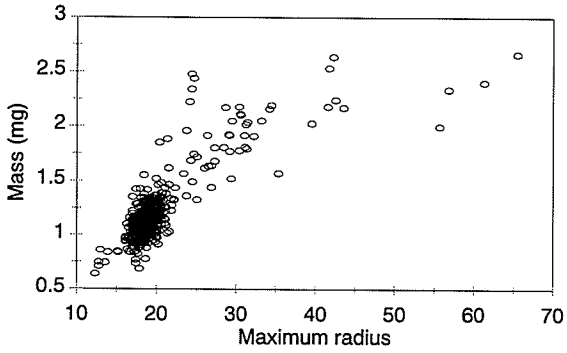

Regression Output

Constant	0.287011330017293
Std Err of Y Est	0.1885768319117
R Squared	0.652326132649103
X Coefficient(s)	0.046181480999855
Std Err of Coef.	0.001600036931207

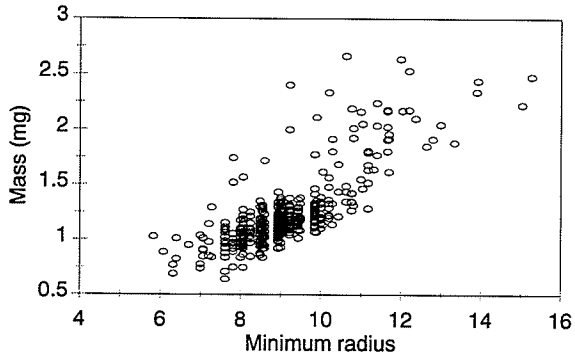

Regression Output

Constant	-0.59771247394033
Std Err of Y Est	0.20004161284154
R Squared	0.608766465970438
X Coefficient(s)	0.200433825853191
Std Err of Coef.	0.007625568153999

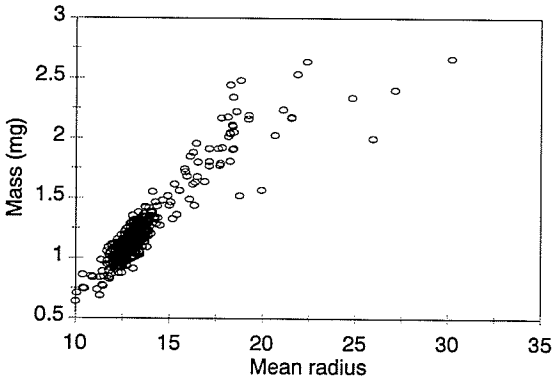

Regression Output

Constant	-0.56163770156266
Std Err of Y Est	0.129847481230357
R Squared	0.835160064040422
X Coefficient(s)	0.131289257363961
Std Err of Coef.	0.002768114599003

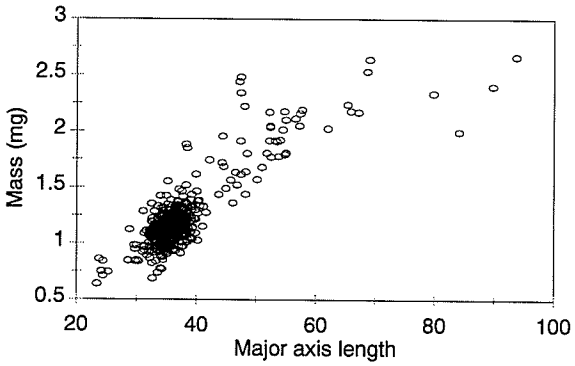

Regression Output

Constant	-0.09865554690416
Std Err of Y Est	0.169546859488973
R Squared	0.718955638003985
X Coefficient(s)	0.035064260650201
Std Err of Coef.	0.001040422157727

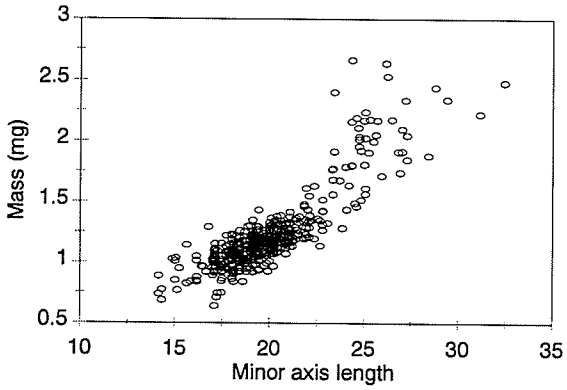

Regression Output

Constant	-0.865377690502
Std Err of Y Est	0.1607686380515
R Squared	0.7473041886548
X Coefficient(s)	0.1047708389748
Std Err of Coef.	0.0028913405688

Table DB4. Relationship between mass and morphological features of wheatheads

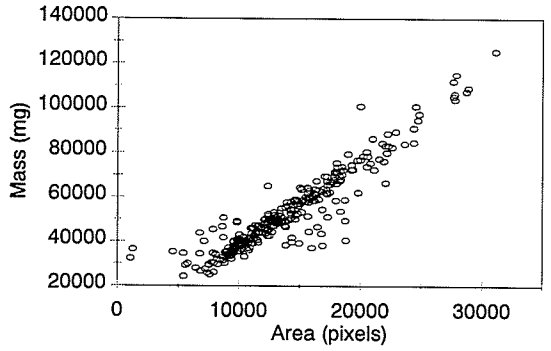

Regression Output

Constant	4819.63016406315
Std Err of Y Est	6429.85616734966
R Squared	0.87363620247299
X Coefficient(s)	3.44314268082667
Std Err of Coef.	0.07624125475466

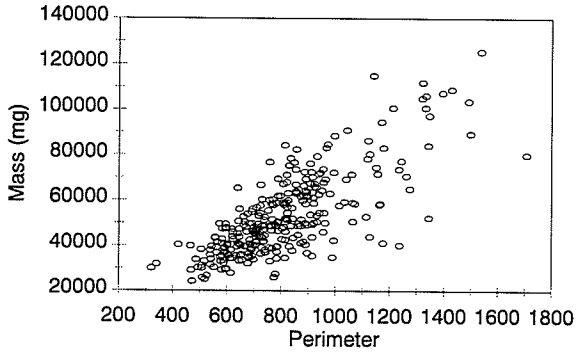

Regression Output

Constant	1240.46084072766
Std Err of Y Est	11647.5872657745
R Squared	0.58534004262338
X Coefficient(s)	63.8162354101096
Std Err of Coef.	3.12724642735992

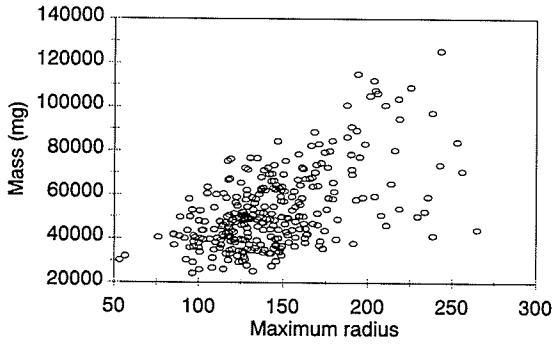

Regression Output

Constant	11125.599756134
Std Err of Y Est	14899.2322676552
R Squared	0.32150299667970
X Coefficient(s)	289.647447286972
Std Err of Coef.	24.4985370929426

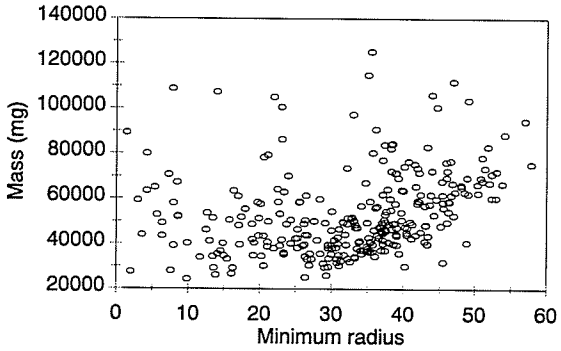

Regression Output

Constant	39894.1885849035
Std Err of Y Est	17426.3025053226
R Squared	0.07182332530602
X Coefficient(s)	402.148039826116
Std Err of Coef.	84.170037203736

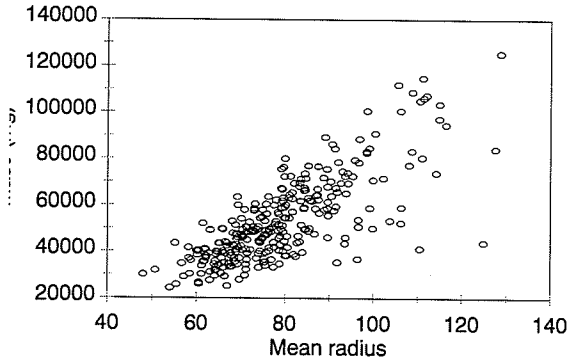

Regression Output

Constant	-25320.034287569
Std Err of Y Est	11512.2506187397
R Squared	0.59492016552347
X Coefficient(s)	990.931924564599
Std Err of Coef.	47.607324934089

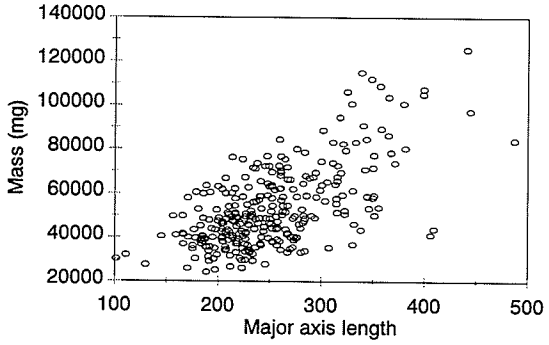

Regression Output

Constant	3728.58188682305
Std Err of Y Est	14002.7271888489
R Squared	0.40069844005251
X Coefficient(s)	195.738265662882
Std Err of Coef.	13.9372986473881

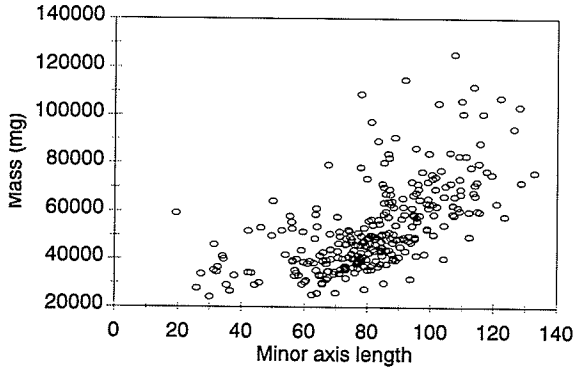

Regression Output

Constant	7550.47136464785
Std Err of Y Est	14149.8228802225
R Squared	0.38804123417557
X Coefficient(s)	553.235860797358
Std Err of Coef.	40.4502729802625

Table DB5. Relationship between mass and morphological features of canola

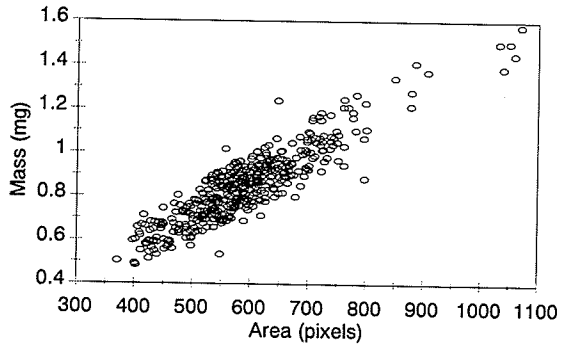

Regression Output

Constant	-0.01913061039824
Std Err of Y Est	0.074530622613672
R Squared	0.812678478343065
X Coefficient(s)	0.001467600894133
Std Err of Coef.	3.39000667541E-05

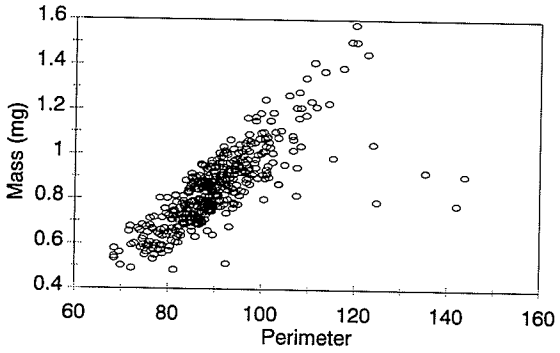

Regression Output

Constant	-0.33288886850805
Std Err of Y Est	0.109232979885118
R Squared	0.597629862615093
X Coefficient(s)	0.013061176916912
Std Err of Coef.	0.000515628797256

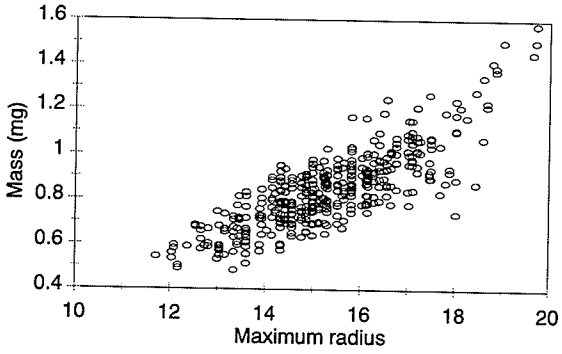

Regression Output

Constant	-0.62562808316145
Std Err of Y Est	0.098150714887727
R Squared	0.675133362885432
X Coefficient(s)	0.095962529829504
Std Err of Coef.	0.003202709784950

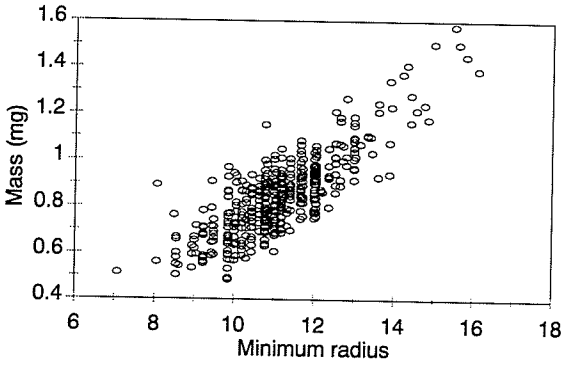

Regression Output

Constant	-0.36411364099789
Std Err of Y Est	0.098254027122045
R Squared	0.674449101705767
X Coefficient(s)	0.108745677689578
Std Err of Coef.	0.003635004806099

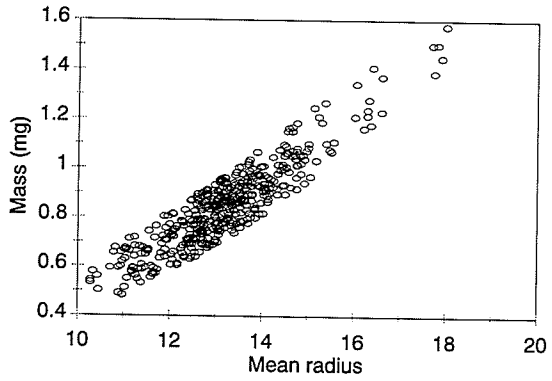

Regression Output

Constant	-0.7858732053941
Std Err of Y Est	0.071314871622888
R Squared	0.8284943673001
X Coefficient(s)	0.123794176360711
Std Err of Coef.	0.002709896819360

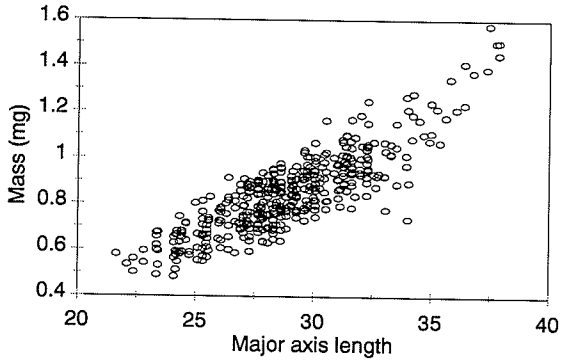

Regression Output

Constant	-0.58680842506155
Std Err of Y Est	0.089144944633083
R Squared	0.73201430159396
X Coefficient(s)	0.049552339758128
Std Err of Coef.	0.001442508291534

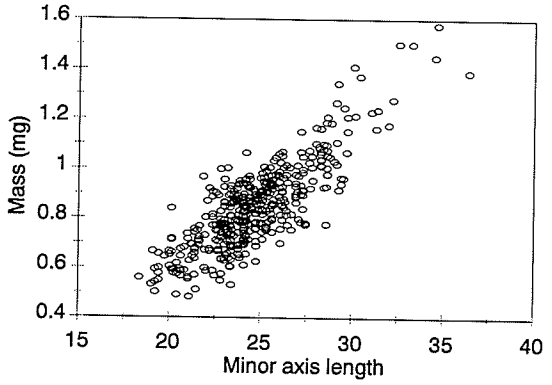

Regression Output

Constant	-0.45983581802134
Std Err of Y Est	0.096589095388509
R Squared	0.685388657569235
X Coefficient(s)	0.052963908224275
Std Err of Coef.	0.001726461437518

Appendix E

Performance evaluation of the grain cleaner

Table E1. Actual and imaging based cleaning efficiencies for barley at different flow rates

Flow rate (kg/h)	Before cleaning				After cleaning				Cleaning efficiency (%)	
	Grain sample		Dockage		Clean grain		Foreign material			
	Actual mass (g)	Image mass (g)	Actual mass (g)	Image mass (g)	Actual mass (g)	Image mass (g)	Actual mass (g)	Image mass (g)	Actual mass basis	Image basis
4.00	100.00	100.59	5.00	4.85	95.64	95.95	2.34	2.46	53.2	49.3
	100.00	101.22	5.00	5.21	96.42	96.73	2.49	2.54	50.2	51.3
	100.00	99.34	5.00	4.62	95.55	95.91	2.67	2.81	46.6	39.2
8.00	100.00	100.68	5.00	5.04	96.02	96.37	2.50	2.72	50.0	46.0
	100.00	101.73	5.00	5.17	95.86	96.03	2.36	2.49	52.8	51.8
	100.00	100.61	5.00	4.82	94.92	95.10	2.64	2.84	47.2	41.1
12.00	100.00	101.28	5.00	5.13	95.37	95.36	2.49	2.61	50.2	49.1
	100.00	101.36	5.00	5.20	95.81	95.99	2.37	2.33	52.6	55.2
	100.00	100.24	5.00	4.95	96.23	96.15	2.55	2.62	49.0	47.1

Table E2. Actual and imaging based cleaning efficiencies for CWAD wheat at different flow rates

Flow rate (kg/h)	Before cleaning				After cleaning				Cleaning efficiency (%)	
	Grain sample		Dockage		Clean grain		Foreign material			
	Actual mass (g)	Image mass (g)	Actual mass (g)	Image mass (g)	Actual mass (g)	Image mass (g)	Actual mass (g)	Image mass (g)	Actual mass basis	Image basis
4.00	100.00	101.28	5.00	5.19	98.90	99.32	1.86	1.93	62.8	62.8
	100.00	100.67	5.00	5.47	99.57	100.46	2.31	2.64	53.8	51.7
	100.00	102.11	5.00	5.61	98.61	99.01	2.08	2.20	58.4	60.8
8.00	100.00	101.09	5.00	5.24	97.94	97.68	1.93	2.02	61.4	61.5
	100.00	100.88	5.00	5.38	96.83	96.99	1.88	1.97	62.4	63.4
	100.00	101.49	5.00	4.97	96.81	97.00	1.94	1.83	61.2	63.2
12.00	100.00	102.37	5.00	5.09	97.62	97.57	1.93	2.05	61.4	59.7
	100.00	100.82	5.00	4.82	97.24	97.38	1.88	2.02	62.4	58.1
	100.00	100.56	5.00	4.94	96.53	96.78	2.19	1.99	56.2	59.7

Table E3. Actual and imaging based cleaning efficiencies for CWRS wheat at different flow rates

Flow rate (kg/h)	Before cleaning				After cleaning				Cleaning efficiency (%)	
	Grain sample		Dockage		Clean grain		Foreign material			
	Actual mass (g)	Image mass (g)	Actual mass (g)	Image mass (g)	Actual mass (g)	Image mass (g)	Actual mass (g)	Image mass (g)	Actual mass basis	Image basis
4.00	100.00	100.55	5.00	5.34	97.68	97.69	1.94	1.88	61.2	64.8
	100.00	100.43	5.00	5.42	98.24	98.54	1.67	1.75	66.6	67.7
	100.00	99.68	5.00	4.82	97.82	97.61	2.06	2.16	58.8	55.2
8.00	100.00	102.16	5.00	4.95	98.00	97.82	1.99	2.08	60.2	58.0
	100.00	101.29	5.00	5.61	98.21	98.52	1.74	1.68	65.2	70.1
	100.00	99.94	5.00	4.97	98.75	98.84	2.04	2.13	59.2	57.1
12.00	100.00	101.37	5.00	5.20	97.83	97.98	2.18	2.22	56.4	57.3
	100.00	100.67	5.00	5.34	98.03	98.16	1.92	1.84	61.6	65.5
	100.00	100.08	5.00	4.73	97.64	97.51	1.93	1.88	61.4	60.3

Table E4. Actual and imaging based cleaning efficiencies for oats at different flow rates

Flow rate (kg/h)	Before cleaning				After cleaning				Cleaning efficiency (%)	
	Grain sample		Dockage		Clean grain		Foreign material			
	Actual mass (g)	Image mass (g)	Actual mass (g)	Image mass (g)	Actual mass (g)	Image mass (g)	Actual mass (g)	Image mass (g)	Actual mass basis	Image basis
4.00	100.00	101.49	5.00	5.04	95.61	95.80	2.36	2.16	52.8	57.1
	100.00	102.57	5.00	5.43	95.37	95.16	2.71	2.74	45.8	49.5
	100.00	102.46	5.00	5.29	94.88	95.01	2.68	2.76	46.4	47.8
8.00	100.00	100.94	5.00	5.17	96.12	96.34	2.55	2.31	49.0	55.3
	100.00	101.26	5.00	4.83	95.34	95.27	2.61	2.70	47.8	44.1
	100.00	100.34	5.00	4.67	95.84	96.02	2.50	2.62	50.0	43.9
12.00	100.00	101.62	5.00	4.81	95.18	95.40	2.37	2.51	52.6	47.8
	100.00	101.71	5.00	5.26	95.73	95.91	2.19	2.27	56.2	56.8
	100.00	101.31	5.00	5.19	95.46	95.63	2.64	2.55	47.2	50.9

Table E5. Actual and imaging based cleaning efficiencies for rye at different flow rates

Flow rate (kg/h)	Before cleaning				After cleaning				Cleaning efficiency (%)	
	Grain sample		Dockage		Clean grain		Foreign material			
	Actual mass (g)	Image mass (g)	Actual mass (g)	Image mass (g)	Actual mass (g)	Image mass (g)	Actual mass (g)	Image mass (g)	Actual mass basis	Image basis
4.00	100.00	100.37	5.00	5.21	93.54	93.69	3.03	3.11	39.4	40.3
	100.00	101.68	5.00	5.27	93.67	93.82	2.97	2.62	40.6	50.3
	100.00	102.49	5.00	5.34	94.05	94.10	2.80	2.79	44.0	47.8
8.00	100.00	101.61	5.00	5.09	95.24	95.21	3.16	3.23	36.8	36.5
	100.00	101.55	5.00	5.19	94.68	94.85	3.08	3.14	38.4	39.5
	100.00	102.34	5.00	4.97	94.28	94.60	2.80	2.89	44.0	41.9
12.00	100.00	101.62	5.00	5.31	95.27	95.61	3.06	3.20	38.8	39.7
	100.00	100.94	5.00	5.19	94.67	94.63	3.14	3.13	37.2	39.7
	100.00	100.82	5.00	4.85	93.84	94.11	2.94	3.01	41.2	37.9

Appendix F

Results of analysis of variance done on ranges of morphological features before and after passing the samples through the cleaner

The GLM Procedure

Class Level Information

Class	Levels	Values
type	5	barley durum oats rye wheat
treat	2	1 2

Number of observations 30

The GLM Procedure

Dependent Variable: area

Source	DF	Sum of Squares	Mean Square	F Value	Pr > F
Model	9	65490210.97	7276690.11	21.87	<.0001
Error	20	6655516.00	332775.80		
Corrected Total	29	72145726.97			

R-Square	Coeff Var	Root MSE	area Mean
0.907749	1.998595	576.8672	28863.63

Source	DF	Type I SS	Mean Square	F Value	Pr > F
type	4	7747746.47	1936936.62	5.82	0.0028
treat	1	53635092.30	53635092.30	161.17	<.0001
type*treat	4	4107372.20	1026843.05	3.09	0.0394

Source	DF	Type III SS	Mean Square	F Value	Pr > F
type	4	7747746.47	1936936.62	5.82	0.0028
treat	1	53635092.30	53635092.30	161.17	<.0001
type*treat	4	4107372.20	1026843.05	3.09	0.0394

The GLM Procedure

Duncan's Multiple Range Test for area

NOTE: This test controls the Type I comparisonwise error rate, not the experimentwise error rate.

Alpha	0.05
Error Degrees of Freedom	20
Error Mean Square	332775.8

Number of Means	2	3	4	5
Critical Range	694.7	729.2	751.2	766.5

Means with the same letter are not significantly different.

Duncan Grouping	Mean	N	type
A	29312.0	6	oats
A			
A	29291.7	6	rye
A			
A	29067.8	6	wheat
A			
A	28698.5	6	barley
B	27948.2	6	durum

The GLM Procedure

Dependent Variable: perimeter

Source	DF	Sum of Squares	Mean Square	F Value	Pr > F
Model	9	290855.8667	32317.3185	43.28	<.0001
Error	20	14933.3333	746.6667		
Corrected Total	29	305789.2000			

R-Square	Coeff Var	Root MSE	perimeter Mean
0.951165	1.757926	27.32520	1554.400

Source	DF	Type I SS	Mean Square	F Value	Pr > F
type	4	9187.5333	2296.8833	3.08	0.0398
treat	1	270750.0000	270750.0000	362.61	<.0001
type*treat	4	10918.3333	2729.5833	3.66	0.0216

Source	DF	Type III SS	Mean Square	F Value	Pr > F
type	4	9187.5333	2296.8833	3.08	0.0398
treat	1	270750.0000	270750.0000	362.61	<.0001
type*treat	4	10918.3333	2729.5833	3.66	0.0216

Duncan's Multiple Range Test for perimeter

NOTE: This test controls the Type I comparisonwise error rate, not the experimentwise error rate.

Alpha	0.05
Error Degrees of Freedom	20
Error Mean Square	746.6667

Number of Means	2	3	4	5
Critical Range	32.91	34.54	35.58	36.31

Means with the same letter are not significantly different.

Duncan Grouping	Mean	N	type
A	1585.33	6	durum
A			
B A	1557.50	6	wheat
B A			
B A	1552.00	6	rye
B			
B	1544.00	6	oats
B			
B	1533.17	6	barley

The GLM Procedure

Dependent Variable: maxrad

Source	DF	Sum of Squares	Mean Square	F Value	Pr > F
Model	9	14291.20000	1587.91111	12.50	<.0001
Error	20	2540.66667	127.03333		
Corrected Total	29	16831.86667			

R-Square	Coeff Var	Root MSE	maxrad Mean
0.849056	4.880589	11.27091	230.9333

Source	DF	Type I SS	Mean Square	F Value	Pr > F
type	4	2557.53333	639.38333	5.03	0.0057
treat	1	11368.53333	11368.53333	89.49	<.0001
type*treat	4	365.13333	91.28333	0.72	0.5892

Source	DF	Type III SS	Mean Square	F Value	Pr > F
type	4	2557.53333	639.38333	5.03	0.0057
treat	1	11368.53333	11368.53333	89.49	<.0001
type*treat	4	365.13333	91.28333	0.72	0.5892

Duncan's Multiple Range Test for maxrad

NOTE: This test controls the Type I comparisonwise error rate, not the experimentwise error rate.

Alpha	0.05
Error Degrees of Freedom	20
Error Mean Square	127.0333

Number of Means	2	3	4	5
Critical Range	13.57	14.25	14.68	14.98

Means with the same letter are not significantly different.

Duncan Grouping	Mean	N	type
A	247.833	6	wheat
B	233.833	6	oats
B			
B	225.000	6	rye
B			
B	224.667	6	barley
B			
B	223.333	6	durum

The GLM Procedure

Dependent Variable: minrad

Source	DF	Sum of Squares	Mean Square	F Value	Pr > F
Model	9	2022.800000	224.755556	27.08	<.0001
Error	20	166.000000	8.300000		
Corrected Total	29	2188.800000			

R-Square	Coeff Var	Root MSE	minrad Mean
0.924159	5.903631	2.880972	48.80000

Source	DF	Type I SS	Mean Square	F Value	Pr > F
type	4	10.466667	2.616667	0.32	0.8644
treat	1	1825.200000	1825.200000	219.90	<.0001
type*treat	4	187.133333	46.783333	5.64	0.0033

Source	DF	Type III SS	Mean Square	F Value	Pr > F
type	4	10.466667	2.616667	0.32	0.8644
treat	1	1825.200000	1825.200000	219.90	<.0001
type*treat	4	187.133333	46.783333	5.64	0.0033

The GLM Procedure

Duncan's Multiple Range Test for minrad

NOTE: This test controls the Type I comparisonwise error rate, not the experimentwise error rate.

Alpha	0.05
Error Degrees of Freedom	20
Error Mean Square	8.3

Number of Means	2	3	4	5
Critical Range	3.470	3.642	3.751	3.828

Means with the same letter are not significantly different.

Duncan Grouping	Mean	N	type
A	49.333	6	durum
A			
A	49.167	6	rye
A			
A	49.000	6	barley
A			
A	48.833	6	wheat
A			
A	47.667	6	oats

The GLM Procedure

Dependent Variable: meanrad

Source	DF	Sum of Squares	Mean Square	F Value	Pr > F
Model	9	9469.466667	1052.162963	133.19	<.0001
Error	20	158.000000	7.900000		
Corrected Total	29	9627.466667			

R-Square	Coeff Var	Root MSE	meanrad Mean
0.983589	2.506564	2.810694	112.1333

Source	DF	Type I SS	Mean Square	F Value	Pr > F
type	4	326.800000	81.700000	10.34	0.0001
treat	1	9013.333333	9013.333333	1140.93	<.0001
type*treat	4	129.333333	32.333333	4.09	0.0139

Source	DF	Type III SS	Mean Square	F Value	Pr > F
type	4	326.800000	81.700000	10.34	0.0001
treat	1	9013.333333	9013.333333	1140.93	<.0001
type*treat	4	129.333333	32.333333	4.09	0.0139

Duncan's Multiple Range Test for meanrad

NOTE: This test controls the Type I comparisonwise error rate, not the experimentwise error rate.

Alpha	0.05
Error Degrees of Freedom	20
Error Mean Square	7.9

Number of Means	2	3	4	5
Critical Range	3.385	3.553	3.660	3.735

Means with the same letter are not significantly different.

Duncan Grouping	Mean	N	type
A	116.833	6	wheat
A			
A	115.167	6	durum
B	110.667	6	rye
B			
B	109.833	6	oats
B			
B	108.167	6	barley

The GLM Procedure

Dependent Variable: majax

Source	DF	Sum of Squares	Mean Square	F Value	Pr > F
Model	9	36741.36667	4082.37407	235.07	<.0001
Error	20	347.33333	17.36667		
Corrected Total	29	37088.70000			

R-Square	Coeff Var	Root MSE	majax Mean
0.990635	0.983093	4.167333	423.9000

Source	DF	Type I SS	Mean Square	F Value	Pr > F
type	4	1483.20000	370.80000	21.35	<.0001
treat	1	32604.03333	32604.03333	1877.39	<.0001
type*treat	4	2654.13333	663.53333	38.21	<.0001

Source	DF	Type III SS	Mean Square	F Value	Pr > F
type	4	1483.20000	370.80000	21.35	<.0001
treat	1	32604.03333	32604.03333	1877.39	<.0001
type*treat	4	2654.13333	663.53333	38.21	<.0001

Duncan's Multiple Range Test for majax

NOTE: This test controls the Type I comparisonwise error rate, not the experimentwise error rate.

Alpha	0.05
Error Degrees of Freedom	20
Error Mean Square	17.36667

Number of Means	2	3	4	5
Critical Range	5.019	5.268	5.427	5.537

Means with the same letter are not significantly different.

Duncan Grouping	Mean	N	type
A	432.500	6	wheat
A			
B A	429.500	6	durum
B			
B C	424.500	6	rye
C			
C	420.500	6	oats
D	412.500	6	barley

The GLM Procedure

Dependent Variable: minax

Source	DF	Sum of Squares	Mean Square	F Value	Pr > F
Model	9	2389.466667	265.496296	18.83	<.0001
Error	20	282.000000	14.100000		
Corrected Total	29	2671.466667			

R-Square	Coeff Var	Root MSE	minax Mean
0.894440	2.079946	3.754997	180.5333

Source	DF	Type I SS	Mean Square	F Value	Pr > F
type	4	203.133333	50.783333	3.60	0.0228
treat	1	1702.533333	1702.533333	120.75	<.0001
type*treat	4	483.800000	120.950000	8.58	0.0003

Source	DF	Type III SS	Mean Square	F Value	Pr > F
type	4	203.133333	50.783333	3.60	0.0228
treat	1	1702.533333	1702.533333	120.75	<.0001
type*treat	4	483.800000	120.950000	8.58	0.0003

Duncan's Multiple Range Test for minax

NOTE: This test controls the Type I comparisonwise error rate, not the experimentwise error rate.

Alpha	0.05
Error Degrees of Freedom	20
Error Mean Square	14.1

Number of Means	2	3	4	5
Critical Range	4.522	4.747	4.890	4.989

Means with the same letter are not significantly different.

Duncan Grouping	Mean	N	type
A	183.500	6	oats
A			
A	182.000	6	durum
A			
A	181.667	6	wheat
A			
B A	179.500	6	rye
B			
B	176.000	6	barley